Laboratory Studies of the Multiday Oxidative Aging of Atmospheric Organic Aerosol

by

Christopher Y. Lim

B.S., University of California, Berkeley (2009)

Submitted to the Department of Civil and Environmental Engineering
in Partial Fulfillment of the Requirements for the

Degree of Doctor of Philosophy

at the

MASSACHUSETTS INSTITUTE OF TECHNOLOGY

February 2019

Signature redacted

Signature of Author .....
Department of Civil and Environmental Engineering
January 11, 2019

Signature redacted

Certified by .....
Jesse H. Kroll
Associate Professor of Civil and Environmental Engineering
Thesis Supervisor

Signature redacted

Accepted by .....
Heidi M. Nepf
Donald and Martha Harleman Professor
Chair, Graduate Program Committee

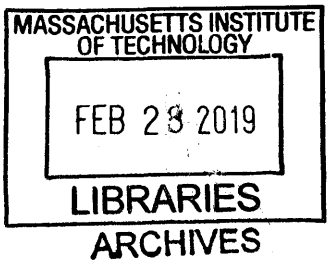

Laboratory Studies of the Multiday Oxidative Aging of Atmospheric Organic Aerosol

by

Christopher Y. Lim

Submitted to the Department of Civil and Environmental Engineering on January 11, 2019 in Partial Fulfillment of the Requirements for the Degree of Doctor of Philosophy in Environmental Chemistry

ABSTRACT

Fine particulate matter (PM, or "aerosol") in the atmosphere affects the Earth's radiative balance and is one of the most important risk factors leading to premature mortality worldwide. Thus, understanding the processes that control the loading and chemical composition of PM in the atmosphere is key to understanding air quality and climate. However, the chemistry of organic aerosol (OA), which comprises a significant fraction of submicron atmospheric PM, is immensely complex due to the vast number of organic compounds in the atmosphere and their numerous reaction pathways. Laboratory experiments have generally focused on the initial formation of OA from volatile organic compounds (VOCs), but have neglected processes that can change the composition and loading of OA over longer timescales ("aging"). This thesis describes several laboratory studies that better constrain the effect of two important aging processes over timescales of several days, the oxidation of gas phase species to form secondary OA (condensation) and the reaction of gas phase radicals with organic molecules in the particle phase (heterogeneous oxidation). First, the oxidation of biomass burning emissions is studied by exposing particles and gases present in smoke to hydroxyl radicals (OH). Increases in organic aerosol mass are observed for all fuels burned, and the amount of OA formed is explained well by the extent of aging and the total concentration of measured organic gases. Second, the effect of particle morphology on the rate of heterogeneous oxidation is examined by comparing the oxidation of particles with thin organic coatings to the oxidation of pure organic particles. Results show that morphology can have a strong impact on oxidation kinetics and that particles with high organic surface area to volume ratios can be rapidly oxidized. Third, the molecular products from the heterogeneous OH oxidation of a single model compound (squalane) are measured. Formation of a range of gas-phase oxygenated VOCs is observed, indicating the importance of fragmentation reactions that decrease OA mass, and providing insight into heterogeneous reaction mechanisms. The results from this work emphasize that the concentration and composition of OA can change dramatically over multiple days of atmospheric oxidation.

Thesis Supervisor: Jesse H. Kroll
Title: Associate Professor of Civil and Environmental Engineering

Acknowledgements

I would like to thank all of the people that have helped me throughout my time at MIT – I could not have done it alone. First, I would like to acknowledge my adviser, Prof. Jesse Kroll. Meeting him was my main reason for choosing to come to MIT to pursue my Ph.D. Graduate school is difficult for nearly everyone, but working with Jesse made the process as enjoyable and seamless as possible. I could not have asked for a better adviser, one that has great ideas, is available for discussion, is motivating, and understanding. I would also like to thank my other thesis committee members as well, Prof. Colette Heald and Prof. Dan Cziczo. Both were instrumental to my thesis work and gave invaluable input, often challenging me to understand the implications of my work and how my research fit in to the field of atmospheric chemistry and climate. I believe all three are not only great scientists, but also true role models in academia.

To all of my fellow Kroll group members, past and present, thanks for being there when I needed help. I would specifically like to thank Anthony Carrasquillo, Kelsey Boulanger, Kelly Daumit, Jon Franklin, James Hunter, Eben Cross, and Eleanor Browne who helped me get started in the lab when I arrived as a first-year graduate student and who I now consider my good friends. Many thanks to postdocs Abigail Koss, Gabriel Isaacman-VanWertz, and Rachel O'Brien for helpful discussions and assistance in lab. Special thanks to Kroll group UROP Rebecca Sugrue who was instrumental to my flow tube oxidation work and graduate student David Hagan who helped with construction of the mini chamber. I would like to thank current group members James Rowe, Mark Goldman, Josh Moss, and Kevin Nihill as well – the group is in good hands going forward. I would also like to thank our group administrative assistant Jacqueline Foster for her work and fun conversation.

Much of this work would not have been possible without contributions from collaborators. Thanks to collaborators Prof. Chris Cappa, Matthew Coggon, Kanako Sekimoto, and other scientists and staff who participated in the FIREX 2016 campaign. I would also like to thank Alex Zaytsev and Martin Breitenlechner for help with the PTR3 instrument and analysis. Special thanks to scientists at Aerodyne, Inc., particularly Tim Onasch, Ed Fortner, Paula Massoli, Manjula Canagaratna, and Leah Williams, for all of the guidance and assistance over the years. I also need to thank funding from the National Science Foundation and MIT which made all of this work possible.

Finally, I need to acknowledge all of the friends I have not yet mentioned and my family. Thanks to my family for being supportive and allowing me to pursue my interests. Thanks to my friends in the Parsons community for keeping me company and making Parsons a great place to come to work every day over the past five and a half years. I also want to thank all of my friends outside of MIT for visiting me in Cambridge and generally being available to talk to or spend time with whenever I needed. I really could not have done this without all of you.

Contents

Chapter 1

Introduction

1.1 Motivation

Understanding the processes that control the loading and chemical composition of fine particulate matter in the atmosphere (i.e., aerosol) is key to understanding air quality and climate. Airborne particles play an important role in the Earth's climate system by scattering or absorbing light and also by acting as cloud condensation nuclei (CCN); however, aerosols also contribute the greatest uncertainty to the total radiative forcing estimate (Boucher et al., 2013). In addition to these climate effects, particulate matter (PM) is a key component of air pollution and studies have shown correlations between the concentration of fine particles and premature mortality (Dockery et al., 1993; Health Effects Institute, 2000; Pope et al., 2002). Recent assessments of the global burden of disease and mortality due to PM exposure ranked ambient air pollution as one of the biggest environmental risks leading to premature mortality, responsible for an estimated 9 million deaths in 2015 (Burnett et al., 2018; Vos et al., 2017).

Understanding the sources, chemistry, and composition of atmospheric aerosol is critically important to predicting its impact on health and climate. Organic aerosol (OA), which comprises a significant fraction (20 – 90%) of submicron atmospheric particulate matter (Kanakidou et al., 2004; Zhang et al., 2007), has consequently been the subject of intense research. Yet, our understanding of OA is incomplete, due to the vast number of organic compounds in the atmosphere, the diverse sources of these compounds (both anthropogenic and biogenic), and their complex reaction pathways. OA can be divided into two major categories: primary organic aerosol (POA) and secondary organic aerosol (SOA). POA is directly emitted to the atmosphere from sources such as biomass burning and fossil fuel combustion, while SOA is formed in the atmosphere from the oxidation of gas phase species and subsequent partitioning to the particle phase. Field and laboratory studies have focused on quantifying OA and the initial formation of SOA from atmospherically relevant volatile organic compounds (VOCs) (Hallquist et al., 2009; Kroll & Seinfeld, 2008). However, the composition of OA is dynamic, subject to additional chemical and physical processes, and continues to evolve over the lifetime of the particles in the

atmosphere (~1 week). An improved understanding of OA chemistry, including its long-term evolution, is critical to inform effective decisions regarding air quality and climate policy.

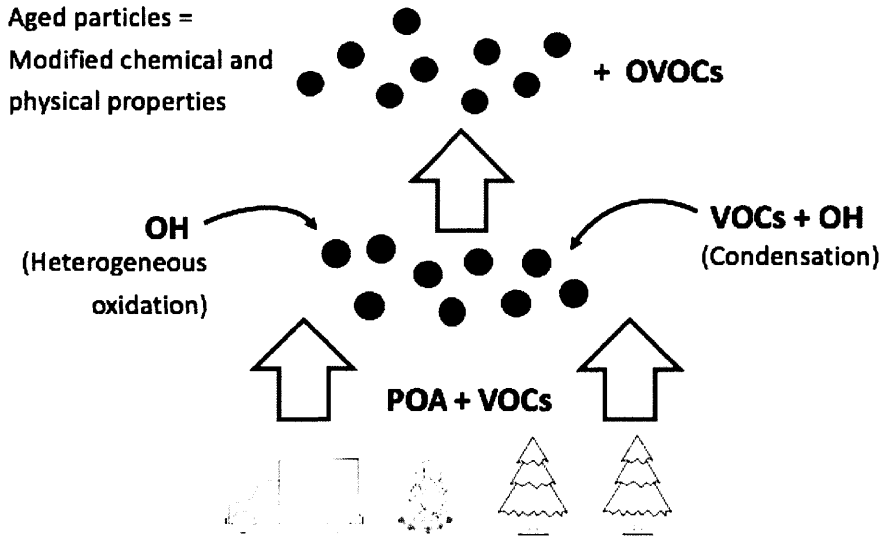

Figure 1-1. Generalized schematic for the aging of OA by condensation and heterogeneous oxidation. Particles (POA) and gases (VOCs) are emitted to the atmosphere and undergo aging. Particles react directly with oxidants (heterogeneous oxidation) and oxidation of VOCs leads to OA growth (condensation). These processes lead to particles with modified loading, composition, and properties and serve as a potential source for oxygenated VOCs (OVOCs) to the atmosphere.

1.2 Background

Laboratory experiments and models often fail to reproduce the oxidation state or loading of ambient OA measurements (Chen et al., 2015; Heald et al., 2011; Kroll et al., 2011; Tsigaridis et al., 2014). Several processes can influence the amount and composition of OA over multiday timescales and potentially bridge the gap between ambient measurements, experiments, and models (Rudich et al., 2007). For example, photolysis of organic material can lead to the breakage of chemical bonds in photolabile species and the volatilization of mass from the particle phase (Hodzic et al., 2015). Dilution of ambient plumes can lead to a decrease in the mass of OA due to the partitioning of semivolatile species from the particle to the gas phase (Robinson et al., 2007). Aqueous processing of organic species in cloud droplets can lead to highly oxidized material and additional SOA mass (Ervens et al., 2011). The work in this thesis will focus on two aging processes in particular, condensation and heterogeneous oxidation. Condensation includes the oxidation of VOCs to form low-volatility compounds that can then partition to pre-existing

particles forming SOA, increasing particle mass and potentially increasing the average carbon oxidation state ($OS_C = 2O/C - H/C$) of the particles. This process has generally been considered important in VOC-rich environments (i.e., near emission sources), where oxidation of reactive organic gases can lead to the substantial growth of particles. Heterogeneous oxidation, on the other hand, is the reaction of gas-phase oxidants such as the hydroxyl radical (OH) and ozone (O_3) directly with organic molecules in the condensed phase. Over multiple days, heterogeneous oxidation is expected to have a significant impact on OA composition (Jimenez et al., 2009; Robinson et al., 2006) and may serve as a source of oxygenated VOCs (OVOCs) to the atmosphere (Heald et al., 2011; Kwan et al., 2006). For particles with longer lifetimes such as those transported in the free troposphere where particles lifetimes with respect to deposition can reach weeks (Balkanski et al., 1993), heterogeneous oxidation might be even more important.

1.3 Key uncertainties

Biomass burning is one of the largest sources of carbonaceous aerosol and organic gases to the atmosphere (Akagi et al., 2011; Bond et al., 2004), but it is not known whether aging of biomass burning emissions leads to SOA formation or not. Despite the recent progress on SOA formation from VOCs, there are many compounds that have unknown SOA yields. For a complex system, such as biomass burning, with many potential SOA precursors, an accurate bottom-up estimate of the effect of condensation is not possible (Hatch et al., 2017). Aircraft measurements show that the composition biomass burning OA (BBOA) consistently becomes more oxidized as photochemical age increases (Capes et al., 2008; Cubison et al., 2011; Forrister et al., 2015; Jolleys et al., 2015; Jolleys et al., 2012). However, field measurements show mixed results on whether or not aging leads to a net increase in SOA formation downwind of fires. Laboratory aging experiments have been similarly inconclusive, with some experiments showing significant amounts of SOA growth and others showing a net loss of OA (Grieshop et al., 2009; Hennigan et al., 2011; Ortega et al., 2013; Tkacik et al., 2017). Thus, the estimated global source of SOA from biomass burning is essentially unconstrained and spans nearly two orders of magnitude (0 – 95 Tg yr^{-1}) (Shrivastava et al., 2017). The evolution of biomass burning emissions likely includes effects from both condensation in the near-field and heterogeneous oxidation farther from the source. Understanding how these processes effect net BBOA and its composition is important for accurately modeling global particulate matter.

The typical time for each molecule to become oxidized by OH, the most important oxidant globally, in a well-mixed particle is on the order of days to weeks (Robinson et al., 2006), which has important implications for OA loadings, properties, and measurements of atmospheric compounds used as source apportionment tracers (e.g., levoglucosan for biomass burning). For OH, heterogeneous reactions are likely to occur at or near the surface of organic particles due to typical diffusion and reaction timescales (Hanson et al., 1994; Worsnop, 2002). Because of the short reacto-diffusive length of OH in organic particles (a few nanometers), heterogeneous oxidation is often considered to be slow since the bulk of the molecules in the condensed phase are essentially shielded from reaction. Although generally considered to be slower than gas-phase oxidation, it is clear that heterogeneous oxidation plays an important role in the evolution of OA. Typically, over the course of one week of heterogeneous OH oxidation, particles will lose approximately 5 to 10% of their carbon mass and OS_C will increase by 0.3 to 0.6 (Kroll et al., 2015). However, most heterogeneous oxidation studies have been done in flow tube reactors using single-component organic particles as proxies for OA and have assumed that the particles are well-mixed (George & Abbatt, 2010; Kroll et al., 2015). This is a major simplification of ambient OA, which has been shown can adopt complex morphologies (e.g., core-shell or fractal) (Fu et al., 2012; Li et al., 2003) and have different phase states (e.g., glassy or semi-solid) (Koop et al., 2011). The morphology and phase of OA could have important effects on the kinetics of aging and the distribution of products within the particle phase (Renbaum & Smith, 2009; Shiraiwa et al., 2011). For example, in mixing-limited particles, the composition of the surface can change rapidly relative to the bulk particle; also, particles with high surface area might be oxidized more rapidly than spherical ones. This has important implications for the health- and climate-relevant properties of OA which depend on composition (Cappa et al., 2011; Harmon et al., 2013; Slade & Knopf, 2014) and in some cases have been shown to be sensitive to the composition of the particle surface (Ruehl et al., 2016; Ruehl & Wilson, 2014).

A detailed understanding of heterogeneous oxidation also depends on the specific reaction mechanisms that are important in particles and at the interface between the condensed and gas phases. As a starting point, previous studies have used reaction mechanisms established in the gas-phase (Atkinson, 1997) and bulk, condensed-phase literature (Bennett & Summers, 1974; Russell,

1957), but it is not clear how applicable these are to heterogeneous OA reactions. Two major reaction pathways describing the effect of heterogeneous reactions include functionalization and fragmentation. Functionalization reactions involve the addition of oxygen-containing functional groups to molecules, leading to increased oxidation and mass. In contrast, fragmentation involves carbon-carbon bond breakage, leading to smaller, more volatile compounds that can potentially partition to the gas phase and result in a loss of OA mass. A key parameter determining the overall effect of heterogeneous oxidation is the branching ratio between functionalization and fragmentation reactions (Kroll et al., 2009). Most studies have only shown modest amounts of carbon loss in laboratory studies and suggest that functionalization reactions dominate the heterogeneous oxidation of OA (George et al., 2008; Hearn & Smith, 2006; McNeill et al., 2008; Smith et al., 2009). However, there are exceptions that show rapid volatilization of carbon (Molina et al., 2004) and fragmentation reactions might be more important for highly oxidized species (Kroll et al., 2009). An integrated analysis of the gas and particle phase products of these reactions can give insight into the detailed reaction pathways; however, most studies have focused on the overall characterization of the particle phase (Kroll et al., 2015). Some studies have identified products in the gas phase, but few have quantified them leading to limited insights into the underlying chemistry (McNeill et al., 2008; Molina et al., 2004; Vlasenko et al., 2008). Identifying the important reaction pathways and the conditions that influence heterogeneous oxidation (e.g., chemical structure, oxidant concentration) is key to interpreting the results from these studies and applying them to ambient conditions.

1.4 Research questions and outline

In this thesis, results from a combination of laboratory flow tube and chamber oxidation experiments are analyzed to better quantify the effects of condensation and heterogeneous oxidation on organic aerosol. This work specifically examines the three following research questions:

1) What is the effect of aging on biomass burning emissions and is this a significant source of secondary organic aerosol?
2) How does the morphology and phase of particles affect the kinetics of heterogeneous oxidation?

3) What are the products (and yields) of heterogeneous oxidation and which reaction pathways are most important?

These questions are addressed in detail in the following chapters:

Chapter 2: Biomass burning emissions are photochemically aged in an environmental chamber as part of the Fire Influence on Regional and Global Environments Experiment (FIREX 2016) at the USDA Fire Sciences Laboratory. Fuels studied are representative of the western U.S and are aged for 1 – 10 days of equivalent OH exposure. An aerosol mass spectrometer (AMS) and proton transfer reaction time-of-flight mass spectrometer (PTR-ToF-MS) are used to characterize the composition of the particle and gas phases. An estimate of SOA yield from biomass burning total non-methane organic gases is calculated enabling a simple parameterization for use in models.

Chapter 3: The role of particle morphology and phase on heterogeneous oxidation kinetics are explored by oxidizing inorganic particles coated with a thin organic layer (squalane) in a flow tube as a proxy for phase-separated of mixing-limited organic particles. Squalane is used as a model compound for chemically reduced organic aerosol. Oxidation of thinly coated particles is compared to the oxidation of pure, well-mixed particles on the basis of OH exposure and oxidation lifetimes. Changes in composition (carbon oxidation state and fraction carbon remaining) are measured with an AMS and related to the measured organic surface area to volume ratio (SA/V).

Chapter 4: The composition and products of heterogeneous squalane oxidation are measured in an environmental chamber. Organic particles are oxidized by OH and monitored with an AMS to measure bulk composition and two state-of-the-art PTR-ToF-MS instruments (PTR3 and CHARON PTR3) to measure speciated products. Gas and particle phase products of oxidation are identified, providing insight into the reaction mechanisms of heterogeneous OH reactions. Major gas phase products are quantified and corrected for OH reaction to give first-generation product yields. This method is also used to calculate the total gas-phase carbon yield from squalane oxidation.

This work will provide detailed knowledge of several aspects of OA chemistry that are poorly understood and not well-constrained in models: SOA from biomass burning, the effect of morphology and phase on aging, and the products from heterogeneous oxidation. The results from this work will be useful for constraining the effect of aging processes (condensation and heterogeneous oxidation) on OA and including these processes into chemical transport models. Ultimately, the goal of this thesis is to gain an improved understanding of multiday aging on OA chemistry and composition, enabling better model predictions of OA loading and properties, ideally resulting in more effective policy decisions concerning public health and climate.

1.5 References

Akagi, S. K., Yokelson, R. J., Wiedinmyer, C., Alvarado, M. J., Reid, J. S., Karl, T., et al. (2011). Emission factors for open and domestic biomass burning for use in atmospheric models. *Atmospheric Chemistry and Physics*, *11*(9), 4039–4072. https://doi.org/10.5194/acp-11-4039-2011

Atkinson, R. (1997). Gas-Phase Tropospheric Chemistry of Volatile Organic Compounds: 1. Alkanes and Alkenes. *Journal of Physical and Chemical Reference Data*, *26*(2), 215–277. Retrieved from http://scitation.aip.org/content/aip/journal/jpcrd/26/2/10.1063/1.556012

Balkanski, Y. J., Jacob, D. J., Gardner, G. M., Graustein, W. C., & Turekian, K. K. (1993). Transport and residence times of tropospheric aerosols inferred from a global three-dimensional simulation of 210Pb. *Journal of Geophysical Research*, *98*(D11), 20573. Retrieved from http://doi.wiley.com/10.1029/93JD02456

Bennett, J. E., & Summers, R. (1974). Product Studies of Mutual Termination Reactions of Sec-Alkylperoxy Radicals - Evidence for Non-Cyclic Termination. *Can. J. Chem.*, *52*, 1377–1379. https://doi.org/10.1139/v74-209

Bond, T. C., Streets, D. G., Yarber, K. F., Nelson, S. M., Woo, J. H., & Klimont, Z. (2004). A technology-based global inventory of black and organic carbon emissions from combustion. *Journal of Geophysical Research: Atmospheres*, *109*(14), 1–43. https://doi.org/10.1029/2003JD003697

Boucher, O., Randall, D., Artaxo, P., Bretherton, C., Feingold, G., Forster, P., et al. (2013). IPCC AR5 Clouds and Aerosols. *Climate Change 2013 - The Physical Science Basis*, 571–658. https://doi.org/10.1017/CBO9781107415324.016

Burnett, R., Chen, H., Szyszkowicz, M., Fann, N., Hubbell, B., Pope, C. A., et al. (2018). Global estimates of mortality associated with long-term exposure to outdoor fine particulate matter. *Proceedings of the National Academy of Sciences*, *115*(38), 201803222. https://doi.org/10.1073/pnas.1803222115

Capes, G., Johnson, B., McFiggans, G., Williams, P. I., Haywood, J., & Coe, H. (2008). Aging of biomass burning aerosols over West Africa: Aircraft measurements of chemical composition, microphysical properties, and emission ratios. *Journal of Geophysical Research Atmospheres*, *113*(23), 1–13. https://doi.org/10.1029/2008JD009845

Cappa, C. D., Che, D. L., Kessler, S. H., Kroll, J. H., & Wilson, K. R. (2011). Variations in organic aerosol optical and hygroscopic properties upon heterogeneous OH oxidation. *Journal of Geophysical Research: Atmospheres*, *116*(15), 1–12. https://doi.org/10.1029/2011JD015918

Chen, Q., Heald, C. L., Jimenez, J. L., Canagaratna, M. R., Zhang, Q., He, L. Y., et al. (2015). Elemental composition of organic aerosol: The gap between ambient and laboratory measurements. *Geophysical Research Letters*, *42*(10), 4182–4189. https://doi.org/10.1002/2015GL063693

Cubison, M. J., Ortega, A. M., Hayes, P. L., Farmer, D. K., Day, D., Lechner, M. J., et al. (2011). Effects of aging on organic aerosol from open biomass burning smoke in aircraft and laboratory studies. *Atmospheric Chemistry and Physics*, *11*(23), 12049–12064. https://doi.org/10.5194/acp-11-12049-2011

Dockery, D. W., Pope, C. A., Xu, X., Spengler, J. D., Ware, J. H., Fay, M. E., et al. (1993). An association between air pollution and mortality in six U.S. cities. *The New England Journal of Medicine*, *329*(24), 1753–1759. Retrieved from http://www.nejm.org/doi/abs/10.1056/NEJM199312093292401

Ervens, B., Turpin, B. J., & Weber, R. J. (2011). Secondary organic aerosol formation in cloud droplets and aqueous particles (aqSOA): a review of laboratory, field and model studies. *Atmospheric Chemistry and Physics Discussions*, *11*(8), 22301–22383. Retrieved from http://www.atmos-chem-phys-discuss.net/11/22301/2011/

Forrister, H., Liu, J., Scheuer, E., Dibb, J., Ziemba, L., Thornhill, K. L., et al. (2015). Evolution of brown carbon in wildfire plumes. *Geophysical Research Letters*, *42*(11), 4623–4630. https://doi.org/10.1002/2015GL063897

Fu, H., Zhang, M., Li, W., Chen, J., Wang, L., Quan, X., & Wang, W. (2012). Morphology, composition and mixing state of individual carbonaceous aerosol in urban Shanghai. *Atmospheric Chemistry and Physics*, *12*(2), 693–707. https://doi.org/10.5194/acp-12-693-2012

George, I. J., & Abbatt, J. P. D. (2010). Heterogeneous oxidation of atmospheric aerosol particles by gas-phase radicals. *Nature Publishing Group*, *2*(9), 713–722. Retrieved from http://dx.doi.org/10.1038/nchem.806

George, I. J., Slowik, J., & Abbatt, J. P. D. (2008). Chemical aging of ambient organic aerosol from heterogeneous reaction with hydroxyl radicals. *Geophysical Research Letters*, *35*(13), 1–5. https://doi.org/10.1029/2008GL033884

Grieshop, A. P., Logue, J. M., Donahue, N. M., & Robinson, A. L. (2009). Laboratory investigation of photochemical oxidation of organic aerosol from wood fires 1: Measurement and simulation of organic aerosol evolution. *Atmospheric Chemistry and Physics*, *9*(4), 1263–1277. https://doi.org/10.5194/acp-9-1263-2009

Hallquist, M., Wenger, J. C., Baltensperger, U., Rudich, Y., Simpson, D., Claeys, M., et al. (2009). The formation, properties and impact of secondary organic aerosol: current and emerging issues. *Atmospheric Chemistry and Physics Discussions*, *9*(1), 3555–3762. Retrieved from http://www.atmos-chem-phys-discuss.net/9/3555/2009/

Hanson, D. R., Ravishankara, a. R., & Solomon, S. (1994). Heterogeneous reactions in sulfuric acid aerosols: A framework for model calculations. *Journal of Geophysical Research*, *99*(D2), 3615–3629. https://doi.org/10.1029/93JD02932

Harmon, C. W., Ruehl, C. R., Cappa, C. D., & Wilson, K. R. (2013). A statistical description of the evolution of cloud condensation nuclei activity during the heterogeneous oxidation of squalane and bis(2-ethylhexyl) sebacate aerosol by hydroxyl radicals. *Physical Chemistry Chemical Physics*, *15*(24), 9615–9679. Retrieved from http://xlink.rsc.org/?DOI=c3cp50347j

Hatch, L. E., Yokelson, R. J., Stockwell, C. E., Veres, P. R., Simpson, I. J., Blake, D. R., et al. (2017). Multi-instrument comparison and compilation of non-methane organic gas emissions from biomass burning and implications for smoke-derived secondary organic aerosol precursors. *Atmospheric Chemistry and Physics*, 1471–1489. https://doi.org/10.5194/acp-17-1471-2017

Heald, C. L., Coe, H., Jimenez, J. L., Weber, R. J., Bahreini, R., Middlebrook, A. M., et al. (2011). Exploring the vertical profile of atmospheric organic aerosol: Comparing 17 aircraft field campaigns with a global model. *Atmospheric Chemistry and Physics*, *11*(24), 12676–12696. https://doi.org/10.5194/acp-11-12673-2011

Health Effects Institute. (2000). Reanalysis of the Harvard Six Cities Study and the American Cancer Society Study of particulate air pollution and mortality. *A Special Report of the Institute's Particle Epidemiology Reanalysis*, (July), 97. Retrieved from http://pubs.healtheffects.org/getfile.php?u=478

Hearn, J. D., & Smith, G. D. (2006). A mixed-phase relative rates technique for measuring aerosol reaction kinetics. *Geophysical Research Letters*, *33*(17), 3–7. https://doi.org/10.1029/2006GL026963

Hennigan, C. J., Miracolo, M. A., Engelhart, G. J., May, A. A., Presto, A. A., Lee, T., & Sullivan, A. P. (2011). and Physics Chemical and physical transformations of organic aerosol from the photo-oxidation of open biomass burning emissions in an environmental chamber, 7669–7686. https://doi.org/10.5194/acp-11-7669-2011

Hodzic, A., Madronich, S., Kasibhatla, P. S., Tyndall, G., Aumont, B., Jimenez, J. L., et al.

(2015). Organic photolysis reactions in tropospheric aerosols: Effect on secondary organic aerosol formation and lifetime. *Atmospheric Chemistry and Physics*, *15*(16), 9253–9269. https://doi.org/10.5194/acp-15-9253-2015

Jimenez, J. L., Canagaratna, M. R., Donahue, N. M., Prevot, A. S. H., Zhang, Q., Kroll, J. H., et al. (2009). Evolution of Organic Aerosols in the Atmosphere. *Science*, *326*(5959), 1525–1529. Retrieved from http://www.sciencemag.org/cgi/doi/10.1126/science.1180353

Jolleys, M. D., Coe, H., McFiggans, G., Capes, G., Allan, J. D., Crosier, J., et al. (2012). Characterizing the aging of biomass burning organic aerosol by use of mixing ratios: A meta-analysis of four regions. *Environmental Science and Technology*, *46*(24), 13093–13102. https://doi.org/10.1021/es302386v

Jolleys, M. D., Coe, H., McFiggans, G., Taylor, J. W., O'Shea, S. J., Le Breton, M., et al. (2015). Properties and evolution of biomass burning organic aerosol from Canadian boreal forest fires. *Atmospheric Chemistry and Physics*, *15*(6), 3077–3095. https://doi.org/10.5194/acp-15-3077-2015

Kanakidou, M., Seinfeld, J. H., Pandis, S. N., Barnes, I., Dentener, F. J., Facchini, M. C., et al. (2004). Organic aerosol and global climate modelling: a review. *Atmospheric Chemistry and Physics Discussions*, *4*(5), 5855–6024. Retrieved from http://www.atmos-chem-phys-discuss.net/4/5855/2004/

Koop, T., Bookhold, J., Shiraiwa, M., & Pöschl, U. (2011). Glass transition and phase state of organic compounds: dependency on molecular properties and implications for secondary organic aerosols in the atmosphere. *Physical Chemistry Chemical Physics*, *13*(43), 19238. https://doi.org/10.1039/c1cp22617g

Kroll, J. H., & Seinfeld, J. H. (2008). Chemistry of secondary organic aerosol: Formation and evolution of low-volatility organics in the atmosphere. *Atmospheric Environment*, *42*(16), 3593–3624. Retrieved from http://linkinghub.elsevier.com/retrieve/pii/S1352231008000253

Kroll, J. H., Smith, J. D., Che, D. L., Kessler, S. H., Worsnop, D. R., & Wilson, K. R. (2009). Measurement of fragmentation and functionalization pathways in the heterogeneous oxidation of oxidized organic aerosol. *Physical Chemistry Chemical Physics*, *11*(36), 8005. Retrieved from http://xlink.rsc.org/?DOI=b905289e

Kroll, J. H., Donahue, N. M., Jimenez, J. L., Kessler, S. H., Canagaratna, M. R., Wilson, K. R., et al. (2011). Carbon oxidation state as a metric for describing the chemistry of atmospheric organic aerosol. *Nature Chemistry*, *3*(2), 133–139. https://doi.org/10.1038/nchem.948

Kroll, J. H., Lim, C. Y., Kessler, S. H., & Wilson, K. R. (2015). Heterogeneous Oxidation of Atmospheric Organic Aerosol: Kinetics of Changes to the Amount and Oxidation State of Particle-Phase Organic Carbon. *Journal of Physical Chemistry A*, *119*(44), 10767–10783. https://doi.org/10.1021/acs.jpca.5b06946

Kwan, A. J., Crounse, J. D., Clarke, A. D., Shinozuka, Y., Anderson, B. E., Crawford, J. H., et al. (2006). On the flux of oxygenated volatile organic compounds from organic aerosol oxidation. *Geophysical Research Letters*, *33*(15), 1–5. https://doi.org/10.1029/2006GL026144

Li, J., Posfai, M., Hobbs, P. V., & Buseck, P. R. (2003). Individual Aerosol Particles from Biomass Burning in Southern Africa: 2. Compositions and Aging of Inorganic Particles. *Journal of Geophysical Research*, *108*, 1–12. https://doi.org/10.1029/2002JD002310

McNeill, V. F., Yatavelli, R. L. N., Thornton, J. a., Stipe, C. B., & Landgrebe, O. (2008, March 17). The heterogeneous OH oxidation of palmitic acid in single component and internally mixed aerosol particles: vaporization, secondary chemistry, and the role of particle phase. *Atmospheric Chemistry and Physics Discussions*. https://doi.org/10.5194/acpd-8-6035-2008

Molina, M. J., Ivanov, A. V, Trakhtenberg, S., & Molina, L. T. (2004). Atmospheric evolution of organic aerosol. *Geophysical Research Letters*, *31*(22), L22104-5. Retrieved from http://doi.wiley.com/10.1029/2004GL020910

Ortega, A. M., Day, D. A., Cubison, M. J., Brune, W. H., Bon, D., Gouw, J. A. De, & Jimenez, J. L. (2013). Secondary organic aerosol formation and primary organic aerosol oxidation from biomass-burning smoke in a flow reactor during, 11551–11571. https://doi.org/10.5194/acp-13-11551-2013

Pope III, C. A., Burnett, R. T., Thun, M. J., Calle, E. E., Krewski, D., & Thurston, G. D. (2002). Lung Cancer, Cardiopulmonary Mortality, and Long-term Exposure to Fine Particulate Air Pollution. *The Journal of the American Medical*, *287*(9).

Renbaum, L. H., & Smith, G. D. (2009). The importance of phase in the radical-initiated oxidation of model organic aerosols: reactions of solid and liquid brassidic acid particles. *Physical Chemistry Chemical Physics*, *11*(14), 2411–2441. Retrieved from http://xlink.rsc.org/?DOI=b816799k

Robinson, A. L., Donahue, N. M., & Rogge, W. F. (2006). Photochemical oxidation and changes in molecular composition of organic aerosol in the regional context. *Journal of Geophysical Research Atmospheres*, *111*(3), 1–15. https://doi.org/10.1029/2005JD006265

Robinson, A. L., Donahue, N. M., Shrivastava, M. K., Weitkamp, E. A., Sage, A. M., Grieshop, A. P., et al. (2007). Rethinking Organic Aerosols: Semivolatile Emissions and Photochemical Aging. *Science*, *315*(5816), 1259–1262. Retrieved from http://www.sciencemag.org/cgi/doi/10.1126/science.1133061

Rudich, Y., Donahue, N. M., & Mentel, T. F. (2007). Aging of Organic Aerosol: Bridging the Gap Between Laboratory and Field Studies. *Annual Review of Physical Chemistry*, *58*(1), 321–352. https://doi.org/10.1146/annurev.physchem.58.032806.104432

Ruehl, C. R., & Wilson, K. R. (2014). Surface organic monolayers control the hygroscopic

growth of submicrometer particles at high relative humidity. *The Journal of Physical Chemistry. A*, *118*(22), 3952–66. https://doi.org/10.1021/jp502844g

Ruehl, C. R., Davies, J. F., & Wilson, K. R. (2016). Droplet Formation on Organic Aerosols, *351*(6280), 1447–1450.

Russell, G. A. (1957). Deuterium-isotope Effects in the Autoxidation of Aralkyl Hydrocarbons. Mechanism of the Interaction of PEroxy Radicals 1. *Journal of the American Chemical Society*, *79*(14), 3871–3877. https://doi.org/10.1021/ja01571a068

Shiraiwa, M., Ammann, M., & Koop, T. (2011). Gas uptake and chemical aging of semisolid organic aerosol particles. In *Proceedings of the* .... Retrieved from http://www.pnas.org/content/108/27/11003.short

Shrivastava, M., Cappa, C. D., Fan, J., Goldstein, A. H., Guenther, A. B., Jimenez, J. L., et al. (2017). Recent advances in understanding secondary organic aerosol: Implications for global climate forcing. *Reviews of Geophysics*, *55*(2), 509–559. https://doi.org/10.1002/2016RG000540

Slade, J. H., & Knopf, D. A. (2014). Multiphase OH oxidation kinetics of organic aerosol: The role of particle phase state and relative humidity. *Geophysical Research Letters*, *41*(14), 5297–5306. https://doi.org/10.1002/2014GL060582

Smith, J. D., Kroll, J. H., Cappa, C. D., Che, D. L., Liu, C. L., Ahmed, M., et al. (2009). The heterogeneous reaction of hydroxyl radicals with sub-micron squalane particles: a model system for understanding the oxidative aging of ambient aerosols. *Atmospheric Chemistry and Physics*, *9*(9), 3209–3222. Retrieved from http://www.atmos-chem-phys.net/9/3209/2009/

Tkacik, D. S., Robinson, E. S., Ahern, A., Saleh, R., Stockwell, C., Veres, P., et al. (2017). A dual-chamber method for quantifying the effects of atmospheric perturbations on secondary organic aerosol formation from biomass burning emissions. *Journal of Geophysical Research*, *122*(11), 6043–6058. https://doi.org/10.1002/2016JD025784

Tsigaridis, K., Daskalakis, N., Kanakidou, M., Adams, P. J., Artaxo, P., Bahadur, R., et al. (2014). The AeroCom evaluation and intercomparison of organic aerosol in global models. *Atmospheric Chemistry and Physics*, *14*(19), 10845–10895. https://doi.org/10.5194/acp-14-10845-2014

Vlasenko, A., George, I. J., & Abbatt, J. P. D. (2008). Formation of volatile organic compounds in the heterogeneous oxidation of condensed-phase organic films by gas-phase OH. *Journal of Physical Chemistry A*, *112*(7), 1552–1560. https://doi.org/10.1021/jp0772979

Vos, T., Abajobir, A. A., Abbafati, C., Abbas, K. M., Abate, K. H., Abd-Allah, F., et al. (2017). Global, regional, and national incidence, prevalence, and years lived with disability for 328 diseases and injuries for 195 countries, 1990-2016: A systematic analysis for the Global

Burden of Disease Study 2016. *The Lancet*, *390*(10100), 1211–1259. https://doi.org/10.1016/S0140-6736(17)32154-2

Worsnop, D. R. (2002). A chemical kinetic model for reactive transformations of aerosol particles. *Geophysical Research Letters*, *29*(20), 19–22. https://doi.org/10.1029/2002GL015542

Zhang, Q., Jimenez, J. L., Canagaratna, M. R., Allan, J. D., Coe, H., Ulbrich, I., et al. (2007). Ubiquity and dominance of oxygenated species in organic aerosols in anthropogenically-influenced Northern Hemisphere midlatitudes. *Geophysical Research Letters*, *34*(13). Retrieved from http://doi.wiley.com/10.1029/2007GL029979

Chapter 2

Secondary organic aerosol formation from biomass burning emissions

2.1 Introduction

Biomass burning is a major source of particulate matter and trace gases to the atmosphere, and strongly effects global air quality and climate (Akagi et al., 2011; Bond et al., 2004; Liu et al., 2017). In fire-prone regions such as the western United States, the frequency and intensity of wildfires have increased over the past several decades, due to fire management practices and climate change (Westerling et al., 2006), and this trend is expected to continue (Dennison et al., 2014; Spracklen et al., 2009). Emissions from fires have been the subject of intense study, but the primary emissions alone do not determine the atmospheric impacts of biomass burning, since smoke plumes can be transported thousands of kilometers and undergo dramatic chemical changes over their lifetime in the atmosphere (Andreae et al., 1988; Cubison et al., 2011). In particular, biomass burning organic aerosol (BBOA) is subject to atmospheric aging processes that could significantly alter the climate- and health-relevant properties of biomass burning emissions (Hennigan et al., 2012; Vakkari et al., 2014). However, despite the potential importance of aging on biomass burning emissions, the effect of aging on BBOA composition and loading over multiday timescales is not well-constrained, and usually is not included in global chemical transport models (Shrivastava et al., 2017).

Field measurements provide strong evidence that the composition of BBOA changes significantly when photochemically aged. In biomass burning plumes, gas-phase organic compounds are oxidized and potentially partition to the particle phase, forming secondary organic aerosol (SOA); molecules in the particle phase are directly subject to oxidation through heterogeneous reactions; and semi-volatile molecules in the particle phase may evaporate as the plume dilutes, potentially undergoing subsequent oxidation in the gas phase. In aircraft measurements of biomass burning plumes, OA consistently becomes more oxidized downwind, relative to the source of emissions (Capes et al., 2008; Cubison et al., 2011; Forrister et al., 2015; Jolleys et al., 2015; Jolleys et al., 2012). Additionally, decreases in reactive tracers from biomass burning, such as levoglucosan

(Cubison et al., 2011), is observed after aging when compared to their contribution to fresh emissions. Despite these consistencies, field measurements show mixed results with regards to whether or not there is an increase in net SOA downwind of fires. Net SOA formation is usually characterized by an OA enhancement ratio, defined as the ratio between fresh and aged $\Delta OA/\Delta CO$ measurements to account for plume dilution. Some studies show that little to no net secondary organic aerosol is formed over the course of several days of aging, or even that a loss of organic mass can occur (Akagi et al., 2012; Capes et al., 2008; Cubison et al., 2011; Hecobian et al., 2011; Jolleys et al., 2015; Jolleys et al., 2012; May et al., 2015). However, other studies show that significant OA enhancement can occur as well (Decarlo et al., 2010; Vakkari et al., 2018; Yokelson et al., 2009).

Laboratory studies intended to constrain the effects of aging on biomass burning emissions have also had variable results. Consistent with field measurements, laboratory experiments in which emissions from open burning and wood stoves were photochemically aged found that BBOA became increasingly oxidized and tracers were depleted with increased aging time (Bertrand et al., 2018; Cubison et al., 2011; Grieshop et al., 2009; Hennigan et al., 2011; Ortega et al., 2013; Tkacik et al., 2017). Most laboratory experiments investigating the aging of biomass burning emissions find that significant amounts of SOA are formed in most, but not all, cases (Bruns et al., 2016; Grieshop et al., 2009; Hennigan et al., 2011; Ortega et al., 2013; Tiitta et al., 2016; Tkacik et al., 2017). Even under constrained laboratory experimental conditions, these studies show significant variability in SOA formation between burns of similar or even identical fuels. This variability is often attributed to differences in burning conditions (e.g., flaming and smoldering) (Hennigan et al., 2011) or the presence of unmeasured SOA precursors (Bruns et al., 2016; Grieshop et al., 2009; Ortega et al., 2013), but good predictors to explain biomass burning SOA across fuel types and burning conditions have not been found.

The high degree of variability in net OA observed from biomass burning studies leads to a large range of estimates of SOA from biomass burning, which span nearly two orders of magnitude. The range of global estimates is thus essentially unconstrained, with some studies ranking biomass burning as an insignificant source of SOA and others ranking it as the major source of global SOA (Shrivastava et al., 2015, 2017). Understanding the evolution of biomass burning emissions is

necessary to better evaluate the effects of biomass burning and inform effective policy decisions. To this end, we describe the results from a set of laboratory aging experiments on a variety of fuels, employing an oxidation reactor coupled with real-time measurements of the composition of both the particle phase and gas phase emissions, to better constrain the effects of aging on biomass burning emissions.

2.2 Methods

2.2.1 Experimental setup and emissions sampling

Experiments were carried out as part of the Fire Influence on Regional and Global Environments Experiment (FIREX 2016) at the USDA Fire Sciences Laboratory (FSL) in Missoula, MT, with the goal of better understanding the evolution of biomass burning emissions within a controlled environment. Experiments took place during the "stack burn" portion of FIREX, in which fuels were burned beneath a 1.6 m diameter, 17 m tall exhaust stack, and were well mixed before being characterized at the top of the stack. Fuels burned were characteristic of the western U.S. and included Engelmann spruce, lodgepole pine, subalpine fire, chamise, manzanita, Douglas fir, ponderosa pine, and sagebrush (Selimovic et al., 2018). For each of these fuels, components of each fuel (e.g. canopy, litter, duff) were burned individually, to determine differences between components, and in combination, as they would in natural wildfires and prescribed burns. In addition to these fuels, several other fuel types were included, such as peat, dung, excelsior (wood shavings), rice straw, loblolly pine, and bear grass. The weight of fuel used for each experiment was between 250 – 6000 g.

Aging experiments were conducted in a 150 L PFA environmental chamber (the "mini-chamber"), an oxidation reactor of intermediate size between standard flow tube reactors and large environmental chambers. The mini-chamber was located in the wind tunnel room in the FSL; smoke from the top of the stack was transported to the wind-tunnel room with a 30 m long community inlet (see Appendix, Figure A2-1). The community inlet was constructed out of 8 in. diameter aluminum ducting and an inline fan at the ducting exhaust (giving a transport time from top of stack to chamber of < 2 s) and was designed to minimize interaction of the smoke with the walls of the inlet. Smoke from the community inlet was sub-sampled using an ejector diluter pressurized with clean air, then passed through 1 m of passivated stainless-steel tubing and a PM1

cyclone, and injected into the chamber. Comparisons of fresh emissions between direct measurements from the top of the stack and measurements in the mini-chamber indicated some loss of gases and particles along the community inlet and transfer line, but these were relatively minor and are not expected to affect results significantly (Figure A2-2).

Prior to sampling, the chamber was flushed with clean air from a zero-air generator (Teledyne 701H) and humidified air (total 15 slpm) for approximately 45 minutes, leading to initial particle concentrations 10^3 – 10^4 times smaller than the peak concentrations during filling. Relative humidity remained in the range of 25 – 40 % throughout the entire experiment. Emissions sampling generally lasted for a significant fraction of each fire (5 – 20 minutes sampling time, while fires burned for 5 – 40 minutes) and initial dilution factors were approximately 7 relative to concentrations in the stack. Once the fuel was completely burned or the chamber particle concentration notably declined from the maximum concentration, sampling was stopped and the chamber was allowed to mix for 5 – 10 minutes while the fresh emissions were characterized. The chamber was operated in semi-batch mode, meaning that after sampling, the chamber was continuously diluted with clean air while the smoke was oxidized and monitored. Chemical aging was initiated by OH, generated from both ozone photolysis and reaction of the resulting $O(^1D)$ with water vapor and the photolysis of other OH precursors present in the smoke (e.g., HONO). A mercury pen-ray lamp (Jelight Model 600 ozone generator) was used to generate ozone (50 - 100 ppb in dilution air), which was added to the chamber starting just after the sampling period and continually added over the course of the experiment. The O_3 concentration in the chamber was typically lower at the start of each experiment and higher toward the end and ranged from 10 – 80 ppb throughout. OH oxidation was initiated by exposing the chamber to 254 nm UV light (UVP, LLC. XX-40S). Use of low-wavelength UV light can introduce non-OH chemistry (Peng et al., 2016); however, loss rates of common compounds from biomass burning such as toluene, phenol, and naphthalene agree well with predicted loss rates from OH reaction alone (average [OH] $\approx 2 \times 10^8$ molec cm^{-3}, photon flux $\approx 3 \times 10^{15}$ photons cm^{-2} s^{-1}). Under these conditions, photolysis can be competitive with OH reactions for compounds with a low ratio between their OH reaction rate constant to absorption cross section ($k_{OH} / \sigma_{254nm} < 1.5 \times 10^7$ cm/s), and high quantum yields (e.g., conjugated carbonyls). Oxidation lasted 30 – 60 minutes, then the chamber was flushed with clean air before the next experiment. At the end of each day, the chamber was left to flush with clean air

and with the UV lamps on overnight. In addition to the aging experiments, control runs were conducted without UV light and used to characterize the evolution of the smoke in the absence of OH oxidation.

Particles and gases exiting the reactor were monitored with a suite of analytical instrumentation. Particle composition measurements were made with an aerosol mass spectrometer with a standard tungsten vaporizer (AMS, Aerodyne Research, Inc.) which measures the mass and composition of non-refractory particles with diameters between 70 nm and 1 μm. Black carbon mass was measured with a Single Particle Soot Photometer (SP2, Droplet Measurement Technologies) and SP-AMS (Aerodyne Research Inc.). Particle size distributions were measured with a Scanning Electrical Mobility Spectrometer (SEMS, Brechtel). All particle phase measurements were made alternating between a two-stage thermal denuder (150 °C and 250 °C) and a room-temperature bypass line. From these measurements, particle organic mass fraction remaining (MFR) was calculated by comparing the thermally denuded particle organic mass to the mass after the bypass line. Non-methane organic gases (NMOGs) were measured with a proton-transfer-reaction time-of-flight mass spectrometer (NOAA PTR-ToF-MS); these measurements are described in detail elsewhere (Koss et al., 2018, Sekimoto et al., 2018). Auxiliary measurements of inorganic gases included O_3 (2B Technologies, Model 202), CO (Teledyne, Model T300), CO_2 (LI-COR, LI-840A), and SO_4/SO_2 (Thermo Fisher 5020i). Particle optical properties were monitored with a three-wavelength photoacoustic spectrometer (PASS-3), a two-wavelength cavity ring down photoacoustic spectrometer (CRD-PAS), and a cavity attenuated phase shift spectrometer (CAPS). Optical measurements from these instruments are not used in the present study, and instead will be discussed in a future publication (Cappa et al., in preparation). 20 aging experiments with both AMS and PTR-ToF-MS data are considered in this work out of a total of 56 burns sampled.

2.2.2 Data analysis

Particle mass and composition data from the AMS were analyzed using the ToF-AMS analysis toolkits (Squirrel version 1.57I, Pika version 1.16I) using the "improved-ambient" method for calculating oxygen-to-carbon (O/C) and hydrogen-to-carbon (H/C) elemental ratios (Canagaratna et al., 2015). Particle density and collection efficiency were calculated by comparing AMS particle time-of-flight (PToF) and SEMS size distributions (Bahreini et al., 2005) for a subset of data points

with sufficient PToF signal. An AMS collection efficiency (CE) correction was then applied to the entire data set by parameterizing the exponential relationship between AMS CE with the particle MFR (Figure A2-3). Generally, particle MFR increases with increased oxidation, indicating that particles are becoming less volatile and more likely to be (semi-)solid, and therefore likely to have a lower CE (due to increased bounce off of the AMS vaporizer). Calculated AMS collection efficiencies range from 0.35 to 0.64, with the average CE of fresh emissions equal to 0.54 and average CE of aged (i.e., end of oxidation) emissions equal to 0.40.

Acetonitrile, an inert tracer species, was used to correct all data for chamber dilution. An exponential function was fitted to the decay of acetonitrile for each experiment ($\tau_{dilution} \sim 20$ minutes). All gas- and particle-phase species concentrations are corrected for dilution using an experiment-specific dilution rate. Dilution rates calculated from the fitted decay of acetonitrile agree well with estimates based on chamber volume and flow rates; this is in contrast with dilution rates derived from CO, which is produced in the chamber during oxidation. Particle mass concentrations were also corrected for loss to the chamber walls, by fitting an exponential equation to the particle organic mass concentration during a control experiment in which the UV lamps were not turned on ($\tau_{wall} = 35$ min; Figure A2-4). Comparison of wall loss rates calculated between two dark experiments and size dependent wall loss rates calculated from SEMS data yield similar results. All particle concentrations presented, unless otherwise noted, are corrected for collection efficiency, dilution, and wall loss. Gases were corrected for dilution only; control runs showed that wall loss was not a major loss pathway for most primary intermediate volatility organic compounds (IVOCs; Figure A2-5).

OH exposures in the chamber were estimated by measuring the decay of an OH tracer, deuterated n-butanol (D9, 98%, Cambridge Isotope Laboratories), added at the beginning of each experiment (10 μL, 2% in water). OH exposure was then calculated from the dilution-corrected concentration of deuterated butanol and its reaction rate coefficient with OH ($k = 3.4 \times 10^{-12}$ cm^3 molec^{-1} s^{-1}) (Barmet et al., 2012). Differences in the initial concentration of OH precursors (e.g., O_3 and HONO) in the chamber, OH sinks, and experiment duration resulted in variations in total OH exposure from experiment to experiment, with end-of-experiment OH exposures (calculated at the point when UV lamps are turned off) ranging from 1 – 10 days of atmospheric aging. Throughout

this work, OH exposure is converted to equivalent atmospheric aging time (in days) by assuming an average OH concentration of 1.5 x 10^6 molec cm^{-3}.

2.3 Results and discussion

2.3.1 Loading and composition of fresh and aged biomass burning particles

The total aerosol mass in the chamber varied widely from experiment to experiment, averaging 130 ± 103 μg m^{-3} (mean ± 1σ), depending on the amount of fuel burned, fuel type, sampling time, and dilution factor prior to oxidation (Appendix Table T2-1). For all experiments considered here, the organic fraction dominated the composition of the primary particle mass (as measured by the sum total of the AMS and SP2, with initial primary OA (POA) concentrations accounting for 70 – 99 % of the total aerosol mass. The initial fraction of black carbon (BC) mass also varied significantly (0 – 30 % of total aerosol mass) and was highly dependent on fuel type, with the highest BC mass fractions observed for chaparral and Excelsior fuels. Fires with the lowest initial AMS OA to SP-AMS BC ratios (OA/rBC < 3.4) showed enhanced wall loss rates with UV light and are excluded from this analysis. Concentrations of non-BC inorganic components (AMS measured nitrate, sulfate, ammonium, and chloride) were variable, but low for all experiments (≤ 8 % of total aerosol mass). After initiation of oxidation, organic aerosol loadings grew substantially for all experiments (Fig. 2-1a). The average mass loading of SOA formed (corrected OA mass at the end of the experiment, minus the OA mass prior to OH oxidation) was 260 ± 250 μg m^{-3}. Alternatively, the amount of SOA at the end of experiment can be expressed as an OA enhancement ratio, defined as the final OA mass (secondary + primary) divided by the initial (primary) OA mass. The average OA enhancement ratio was 3.5 ± 1.7, and is considerably higher than previous studies (Hennigan et al., 2011; Ortega et al., 2016; Tkacik et al., 2017); however, these results are consistent with previous studies once OH exposure and AMS CE are taken into account (Figure A2-6). Discussion of the relationship between SOA formation and gas phase composition will be discussed further in Section 3.2.

The chemical composition of the primary organic particulate matter varied significantly between experiments. The initial O/C ranged from 0.20 to 0.60 (0.35 ± 0.09) and initial H/C ranged from 1.72 to 1.85 (1.77 ± 0.04), indicating significant variation in POA elemental composition.

Elemental ratios stayed constant in the chamber for each given experiment until the lights were turned on. Similarly, control experiments (with no oxidation) showed constant OA/BC, O/C, and H/C over the course of the run, indicating that OA mass and overall oxidation state of biomass burning POA is stable in the chamber without exposure to UV light, despite the potential for semi-volatile compounds to partition between the gas and particle phase and/or be lost to the chamber walls (Grieshop et al., 2009; May et al., 2015).

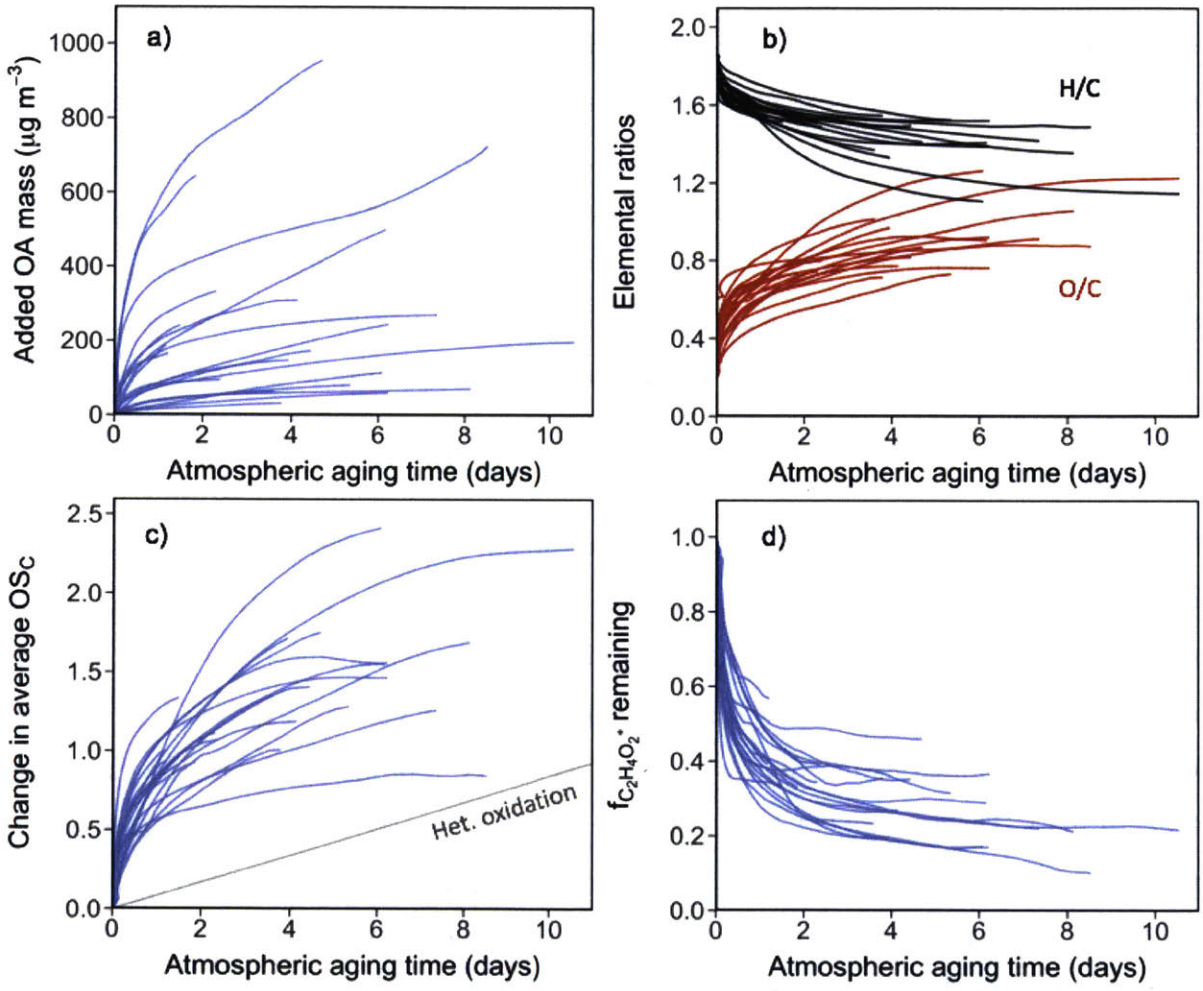

Figure 2-1. Changes in OA mass and composition as a function of aging time, assuming an atmospheric [OH] of 1.5 x 10^6 molec cm^{-3}. Each line represents a separate aging experiment. (a) Increase in OA mass with oxidation, showing variable SOA across all experiments. (b) Elemental ratios (red: O/C, black: H/C). (c) Change in average OS_C; reference line shows average change due to heterogeneous oxidation of laboratory flow tube experiments for comparison (Kroll et al., 2015). (d) Normalized fraction of AMS organic signal due to fragment $C_2H_4O_2^+$, a common primary biomass burning OA tracer, indicative of levoglucosan and related compounds.

OH oxidation, initiated in the chamber by exposure to UV light, rapidly changes the composition of OA, as shown in Figure 2-1b, c, d. Gas phase chemistry in the mini-chamber will be discussed in detail in a forthcoming publication (Coggon et al., in preparation). Despite differences in initial composition between experiments, OA in all experiments undergoes a large increase in O/C and decrease in H/C (Figure 2-1b), and a corresponding increase in average carbon oxidation state (OS_C, equal to 2 O/C – H/C) (Figure 2-1c). OS_C for all fuels increases with increasing OH exposure, with the average, end-of-experiment increase in OS_C of 1.33 ± 0.50. Most of this change occurs during the initial period of oxidation (equivalent timescales of just 1 – 2 days); after this, changes in OS_C still occur, but over much longer timescales. Both condensation of SOA and heterogeneous oxidation (direct reactions between gas-phase oxidants and particle-phase organic molecules) can contribute to the observed increases in oxidation state. However, the initial rate of change for aging of biomass burning emissions (gases and particles combined) is much faster than the average rate of OS_C change measured in laboratory heterogeneous OH-oxidation experiments (Kroll et al., 2015) (shown as the grey line in Figure 2-1c), implying that condensation of highly oxidized secondary mass is the main driver for the changes in composition observed.

Similar to the elemental ratios, the initial fraction of the primary organic signal from the AMS fragment ion $C_2H_4O_2^+$ ($f_{C2H4O2+}$) varies from burn to burn (mean 2.2 ± 1.2 %). This fragment is a small contributor to the overall OA mass (< 6%), but is known to correlate with levoglucosan (and related molecules) and is commonly used as a tracer for biomass burning POA (Simoneit et al., 1999). Figure 2-1d shows the evolution of $f_{C2H4O2+}$, normalized to its value at the start of each experiment. This ion is known to correspond to semi-volatile species (Grieshop et al., 2009), and changes to $f_{C2H4O2+}$ (~ 25 % loss) are observed even in the absence of oxidation; however, oxidation greatly enhances the rate and magnitude of its decrease. Under oxidative conditions, the contribution of this fragment to the total organic mass decreases dramatically over the course of 1 – 2 days of equivalent OH exposure, then stabilizes after that. This is in agreement with previous aircraft studies, which show that even in highly aged airmasses, a small amount of this tracer remains elevated relative to the atmospheric background level (Cubison et al., 2011), potentially due to contribution of other molecules to this tracer. Overall, the chemical changes observed here are likely dominated by the formation of SOA, although heterogeneous oxidation, dilution-driven evaporation, and wall loss will also contribute.

2.3.2 Secondary organic aerosol formation

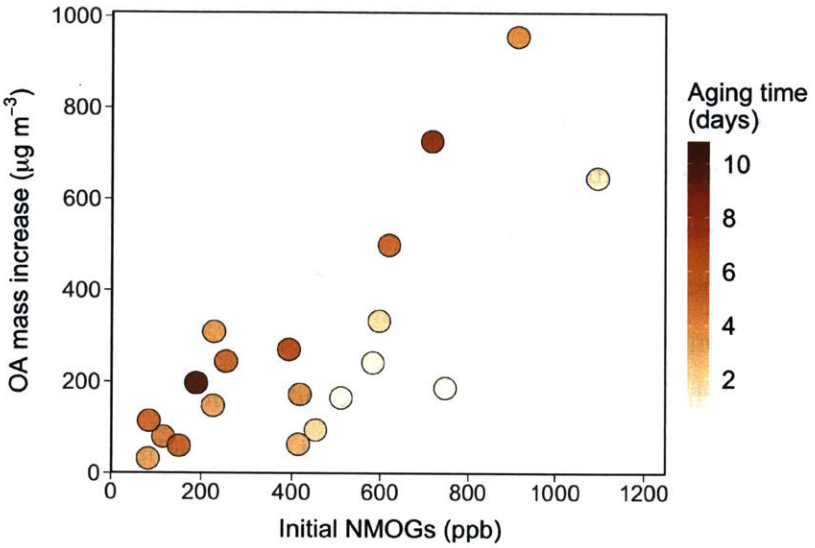

Figure 2-2. End-of-experiment SOA formation vs. total NMOG concentration in the chamber before OH oxidation. Points are colored by the atmospheric equivalent aging time corresponding to the end of each experiment.

All aging experiments show substantial SOA formation, with OA mass continuing to increase with extended aging time (Fig. 2-1a). Consistent with previous studies, the correlations between OA mass enhancement ratio and various parameters that could affect SOA production (e.g., OH exposure, POA, common SOA precursors, total NMOG concentration) are weak at best (Figure A2-7). However, the absolute amount of SOA formed does appear to correlate with some of these. Figure 2-2 shows the relationship between SOA formed by the end of each experiment ($\mu g\ m^{-3}$) and the initial concentration of total NMOGs in the chamber (ppb) measured by the PTR-ToF-MS. A positive correlation is seen between the two variables, but the correlation is not especially strong ($r^2 = 0.51$). A confounding variable in this relationship is the difference in total OH exposure between experiments, as shown in the color scale. To account for the differences in OH exposure, Figure 2-3 shows the same relationship between SOA and NMOG concentration, but now compared at equal OH exposures (0.25, 0.5, 1, 2, 3, and 4 days of atmospheric aging) and with both axes converted to carbon mass. Although there is still significant scatter, possibly due to differences in initial POA levels (Figure A2-8), there is an improved correlation ($r^2 = 0.64$ to 0.83) between SOA and NMOG carbon mass at each OH exposure. Subplots in Figure 2-3 contain different numbers of data points, due to the differences in final OH exposure achieved in each experiment. As such, the r^2 values are not strictly comparable, but are labeled to show the

correlation in all cases. Additionally, the slopes of these plots exhibit a clear trend, increasing with OH exposure. This indicates that a greater fraction of carbon from NMOGs is converted to SOA as aging time increases, consistent with continual SOA formation over long aging timescales. Total PTR-ToF-MS measured NMOGs also correlates well with POA concentration; as such, POA shows a similarly strong relationship with SOA (Figure A2-9).

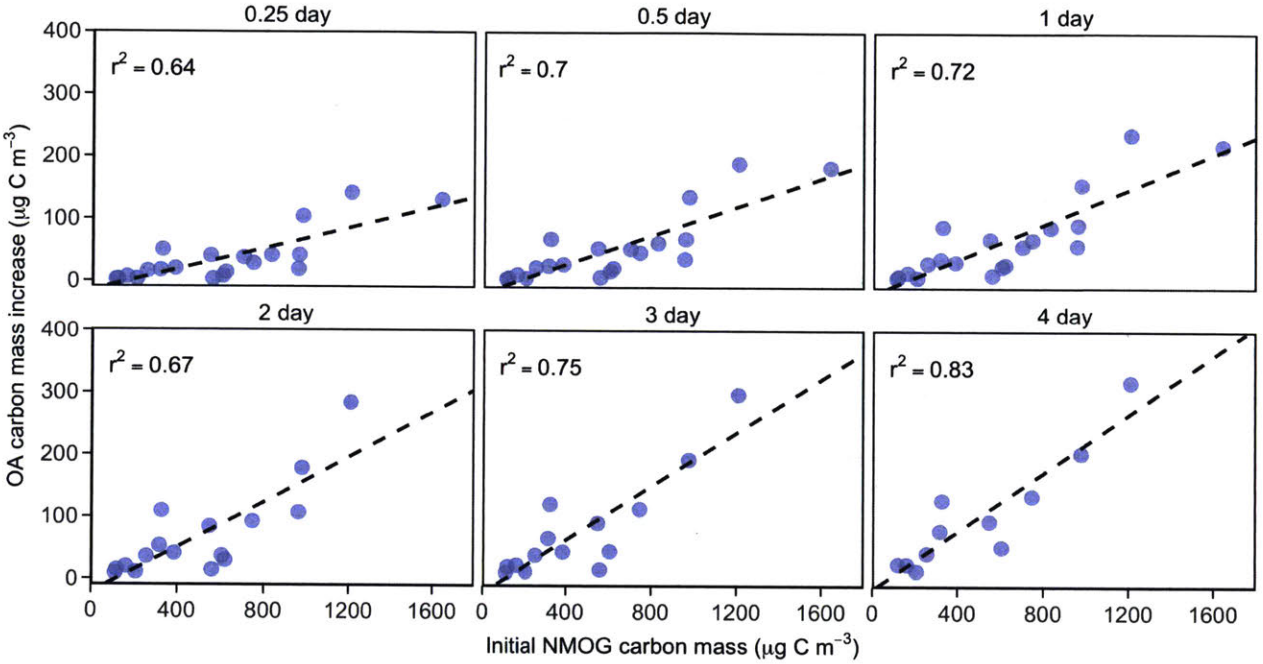

Figure 2-3. OA carbon mass added vs. initial NMOG carbon mass from PTR-ToF-MS measurements at various OH exposures (0.25 – 4 days of equivalent atmospheric aging). All subplots show correlation coefficients (r^2) of 0.64 or higher, and the linear relationships at longer aging times show larger slopes (i.e., more SOA; see Figure 2-5).

The correlation between SOA formation and the initial chamber concentration of NMOGs is reasonable, since NMOGs provide the carbon that drive SOA growth. However, the PTR-ToF-MS measures many compounds that likely do not contribute to SOA formation (e.g., small compounds such as methanol and acetonitrile). In addition to comparing SOA to the initial NMOG concentration, we can examine how SOA formation correlates with the concentration of NMOGs above some molecular weight cutoff. Figure 2-4 shows the correlation coefficient for the linear fit between SOA carbon mass and summed NMOG carbon mass at each molecular weight cutoff for 1 day of equivalent aging. While low molecular weight NMOGs are not expected to contribute to SOA mass, the correlation coefficient between SOA carbon mass and initial NMOG carbon mass does not improve substantially when these are excluded (left side of Fig. 2-4). In fact, the

correlation between SOA is relatively insensitive to the *m/z* cutoff point, until only compounds with molecular weight greater than monoterpenes (*m/z* > 137) are considered. After this point the correlation drops rapidly to zero, likely because the PTR-ToF-MS signal is very low in this mass range and compounds with 10 or fewer carbon atoms are major contributors to SOA formation or correlate with some unmeasured SOA forming species. This suggests that the ratio of SOA precursors to the total concentration of measured NMOGs is relatively constant between experiments. Additionally, we do not observe strong correlations between SOA and any single SOA precursor (e.g., monoterpenes) or any subset or class of compounds measured by the PTR-ToF-MS (e.g., IVOCs). PTR-ToF-MS measurements taken directly from the FSL exhaust stack show that although the NMOG emissions are incredibly complex, much of the variability in emissions (~85%) can be described by just two factors (derived using positive matrix factorization, or PMF), one high-temperature combustion factor and one low-temperature combustion factor (Sekimoto et al., 2018). We do not see improved correlations between NMOGs and SOA when splitting the NMOGs by factor type, indicating that both factors contain compounds that contribute to SOA formation.

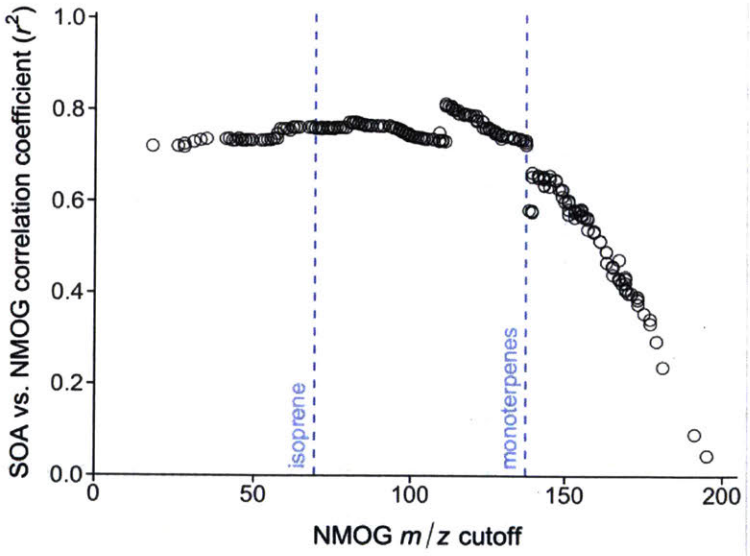

Figure 2-4. Correlation coefficients (r^2) between OA carbon mass added and the summed NMOG carbon mass above some ion mass (*m/z*) cutoff. For example, the point labeled "isoprene" shows the correlation between SOA carbon mass and initial NMOG carbon mass for all measured ions with mass-to-charge ratio equal to or greater than that of isoprene (i.e., species of molecular weight 68 g/mol or higher). Initial NMOG carbon mass is calculated prior to oxidation and data points all correspond to r^2 values at 1 day of atmospheric aging time. Correlation coefficients are high for all cutoff points below monoterpenes, then drop off due to loss of signal and the importance of compounds with lower molecular weight to SOA formation.

Previous biomass burning aging experiments with both aerosol and NMOG measurements have not observed this relationship between SOA and total NMOGs (Ortega et al., 2013) or known SOA precursors (Bruns et al., 2016; Grieshop et al., 2009; Ortega et al., 2013; Tkacik et al., 2017). In this analysis, we have included both identified and calibrated PTR-ToF-MS ions (~90% of the signal, approximately 150 ions) as well as an additional 370 unidentified ions (Koss et al., 2018). Unidentified ions use a calibration factor based on their molecular formula and are typically larger, more oxygenated compounds, potentially important for SOA formation. Recent work has pointed to the importance of "non-traditional" SOA precursors to SOA formation for residential wood combustion of a single fuel type (beech wood) (Bruns et al., 2016). These precursors include semivolatile and intermediate-volatility volatile organic compounds (S/IVOCs) such as phenols and naphthalenes (Bruns et al., 2016). For many of these compounds, SOA yields are unknown or highly uncertain, complicating a bottom-up estimate of SOA from biomass burning organic gases (Hatch et al., 2017). The initial total NMOG concentration measured by the PTR-ToF-MS, in conjunction with OH exposure, in the present dataset provides a reasonable predictor for the amount of SOA formation without the need for speciated aerosol yields. Compared to previous similar studies, the NMOG data presented here are more extensive in terms of the number of experiments, as well as the fraction of emissions that have been identified and calibrated for (Koss et al., 2018). Additionally, it is estimated that the PTR-ToF-MS measures somewhere between 50 – 80% of reactive gas-phase carbon from biomass burning, making it a good tool for characterizing the total organic, gas-phase emissions from fires (Hatch et al., 2017). Previous aging studies with both aerosol and VOC data typically have identified only half or less of the NMOG signal and/or are limited to a small number of experiments (Grieshop et al., 2009; Ortega et al., 2013; Tkacik et al., 2017); this could potentially explain why similar correlations between total VOCs and SOA have not been observed before. The majority of gas-phase carbon observed by the PTR-ToF-MS is in compounds with low carbon number ($n_C < 7$), with corresponding volatilities, as estimated in Koss et al. (2018), that are weighted towards volatile compounds ($c_0 > 10^7$ μg m^{-3}) rather than S/IVOCs (Fig. 2-5). This means that SOA from biomass burning is strongly influenced by the oxidation of relatively smaller, volatile species; alternatively, this could mean that the PTR-ToF-MS does not measure all important SOA precursors, but measures compounds that are co-emitted and correlate well with them.

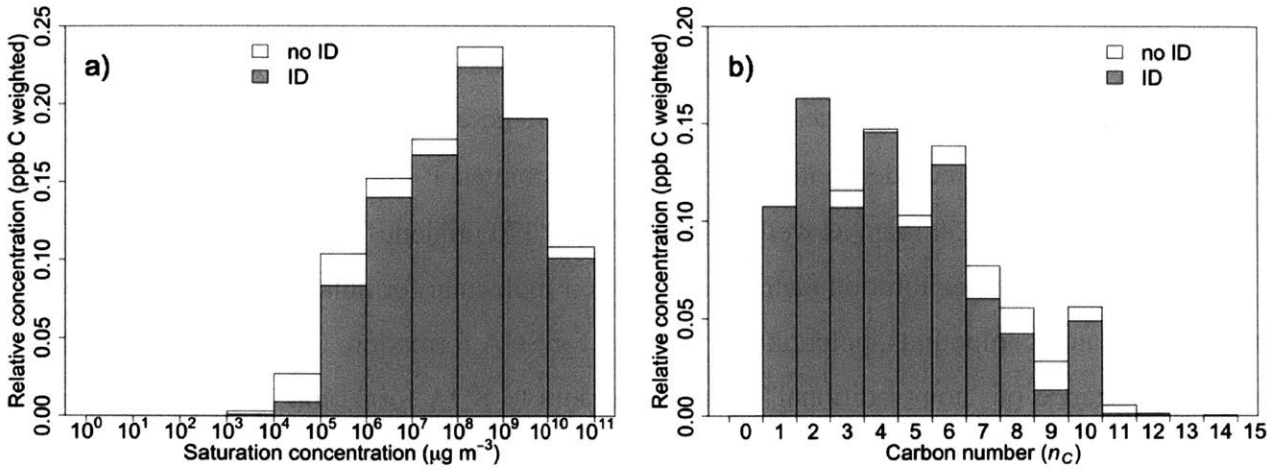

Figure 2-5. Estimated saturation vapor concentration (c_0) distribution (a) and carbon number (n_C) distribution (b) for compounds (NMOGs) measured by the PTR-ToF-MS (Koss et al., 2018) in the chamber prior to oxidation, averaged over all burns. Distributions are separated into identified and unidentified ions and are weighted by ppb C.

From each of the relationships between SOA carbon mass and initial NMOG carbon mass (linear fits in Figure 2-3), an effective carbon yield can be calculated. Carbon yield is defined here as the SOA formed at a given OH exposure divided by the total NMOG carbon reacted at each respective OH exposure ($\Delta[C]_{OA}/\Delta[C]_{NMOG}$). The amount of gas phase carbon reacted ($\Delta[C]_{NMOG}$) is estimated from the initial concentration of PTR-ToF-MS measured gas-phase organic carbon in the chamber before oxidation, experiment specific dilution rates, and speciated OH reaction rates for identified compounds present in each fire (Koss et al., 2018). Carbon yields as a function of atmospheric age are shown in Figure 2-6, and range from 24 ± 4% at 0.25 days of equivalent atmospheric oxidation to 56 ± 9% after 4 days of equivalent atmospheric oxidation. Since the PTR-ToF-MS doesn't measure the true total NMOG concentration (e.g., some missing alkanes and alkenes), these carbon yields are likely to be upper bounds. The calculated yields use our best estimate of OA carbon mass, using the AMS CE correction described previously. The gray points in Figure 2-6 show the carbon yields assuming a constant AMS CE equal to 1 (a common assumption in previous studies). In both cases, the amount of SOA formed increases with increasing aging time. Accounting for changes in collection efficiency that occur with aging leads to an approximate factor of 4 increase in yields; better constraints on estimates of AMS collection efficiency are needed for improved estimates of SOA formation from biomass burning. Nonetheless, this carbon yield, combined with laboratory- or field-based estimates of NMOG

emissions, provides a means for including SOA formation from biomass burning sources within chemical transport models.

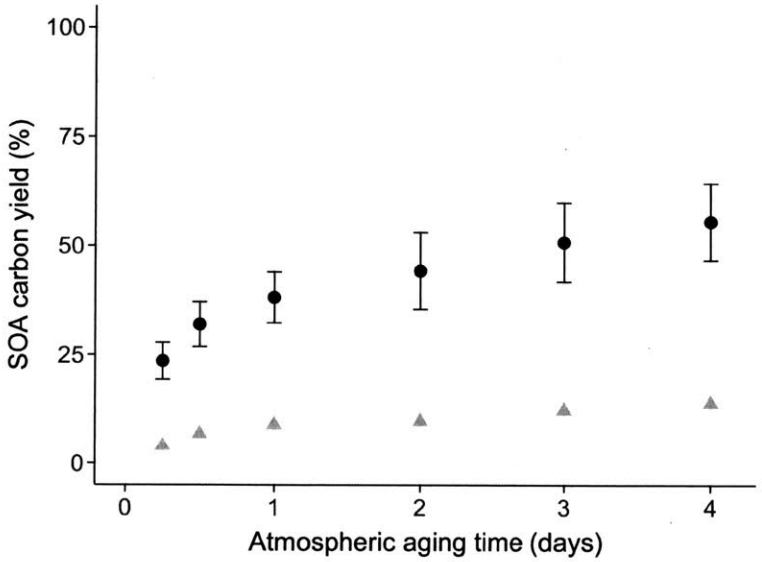

Figure 2-6. SOA carbon yield from aging of biomass burning emissions. Black points are carbon yields using our best estimate of OA carbon mass. Yields are calculated from the slopes of the linear relationships between SOA and initial NMOG by estimating the amount of measured NMOG carbon reacted at each respective time point using the average carbon-weighted OH rate coefficient for identified compounds and accounting for chamber dilution. Error bars are +/- 1σ in the slope of the linear fit between SOA and NMOG carbon mass. Gray triangles are estimated yields using AMS CE = 1 for all OA, both before and after aging, and is a common assumption made in previous studies on the aging of biomass burning. See Appendix (Table T2-2) for tabulated yields.

The variability in findings from previous lab and field studies on the effect aging has on net SOA from biomass burning can be potentially explained by the effects of dilution on the evolution of BBOA mass. Some fraction of BBOA is semi-volatile, and dilution (in chambers or ambient smoke plumes) will cause volatile OA components to partition from the particle phase to the gas phase (May et al., 2013). Recent modeling work has shown that even in plumes that show no net SOA formation, significant condensation of secondary organic mass may occur (Bian et al., 2017), but net growth is low (or even negligible) due to dilution-driven evaporation of OA. In ambient plumes, dilution drives semi-volatile species from the particle to gas phase; although this causes a loss in OA mass, it also serves as a source of SVOCs that can condense back onto particles after oxidation, leading to little to no net change in OA. Related to this point, calculated net OA values are also sensitive to the choice of starting point (i.e., t_0). Initial dilution in chamber experiments

may result in substantial POA evaporation, which provide high concentrations of SVOCs that are efficiently converted to SOA upon oxidation. However, some laboratory experiments find a net loss of OA mass during aging (Hennigan et al., 2011; Ortega et al., 2013; Tkacik et al., 2017), which we do not observe in the present experiments. The reason for this is unclear, but could be due to some combination of dilution and wall losses (gas and particle) in chambers and flow tubes. On the other hand, smaller chambers such as the mini-chamber have lower initial dilution factors, but much higher OH concentrations, potentially favoring condensation from VOC oxidation over evaporation. With the potential preference for condensation over evaporation, this present study may be effectively measuring the potential SOA formation while excluding evaporation from the extensive dilution that occurs in biomass burning plumes; therefore, it is primarily accessing the "chemistry" component of OA evolution (Bian et al., 2017). Thus, the carbon yields shown in Figure 2-6 need to be combined with a realistic treatment of BBOA partitioning for effective model inputs to describe BBOA evolution in the atmosphere.

2.4 Conclusions

We show that the OH-initiated aging of biomass burning emissions exhibit significant changes in BBOA composition and loading. These changes are dependent on OH exposure, and are especially large over the first few days after emission. Significant amounts of SOA are formed from all fuels studied here, but SOA formation is highly variable. Despite large differences in fuel type and burning conditions, much of this variability can be explained by differences in the initial total NMOG concentration and OH exposure. Correlations between SOA formation and the concentration of initial measured NMOGs in the chamber at given OH exposures are good, with r^2 values between 0.64 and 0.83, and indicate SOA carbon yields between 24% (after 6 hours of equivalent atmospheric oxidation) to 56% (after 4 days). Given total NMOG measurements from future field campaigns, the calculated SOA carbon yields can be used to estimate gross SOA formation from biomass burning in chemical transport models. However, these estimates would likely need to be used in conjunction with good estimates of BBOA evaporation rates to calculate the *net* effect of aging on OA concentrations. Future work investigating the evolution of biomass burning emissions should attempt to further constrain the rates of BBOA evaporation and compare the relative rates of oxidation and dilution from field and laboratory studies. In addition to this, laboratory studies on a wider range of fuels (i.e., those found in areas other than the western U.S.),

and under a wider range of reaction conditions, will help improve ability to predict the loadings, properties, and impacts of biomass burning emissions globally.

2.5 Acknowledgements

This work was supported by NOAA award NA16OAR4310111. CYL and ARK were supported by the NSF graduate research fellowship program. The authors would like to thank Ed Fortner, Tim Onasch, Berk Knighton, Bob Yokelson, and the rest of the FIREX science team, and Missoula Fire Sciences Lab staff for support during the project.

2.6 References

Akagi, S. K., Yokelson, R. J., Wiedinmyer, C., Alvarado, M. J., Reid, J. S., Karl, T., et al. (2011). Emission factors for open and domestic biomass burning for use in atmospheric models. *Atmospheric Chemistry and Physics*, *11*(9), 4039–4072. https://doi.org/10.5194/acp-11-4039-2011

Akagi, S. K., Craven, J. S., Taylor, J. W., McMeeking, G. R., Yokelson, R. J., Burling, I. R., et al. (2012). Evolution of trace gases and particles emitted by a chaparral fire in California. *Atmospheric Chemistry and Physics*, *12*(3), 1397–1421. https://doi.org/10.5194/acp-12-1397-2012

Andreae, M. O., Browell, E. V., Garstang, M., Gregory, G. L., Harriss, R. C., Hill, G. F., et al. (1988). Biomass-burning emissions and associated haze layers over Amazonia. *Journal of Geophysical Research*, *93*(D2), 1509–1527. https://doi.org/10.1029/JD093iD02p01509

Bahreini, R., Keywood, M. D., Ng, N. L., Varutbangkul, V., Gao, S., Flagan, R. C., et al. (2005). Measurements of secondary organic aerosol from oxidation of cycloalkenes, terpenes, and m-xylene using an aerodyne aerosol mass spectrometer. *Environmental Science and Technology*, *39*(15), 5674–5688. https://doi.org/10.1021/es048061a

Barmet, P., Dommen, J., DeCarlo, P. F., Tritscher, T., Praplan, A. P., Platt, S. M., et al. (2012). OH clock determination by proton transfer reaction mass spectrometry at an environmental chamber. *Atmospheric Measurement Techniques*, *5*(3), 647–656. https://doi.org/10.5194/amt-5-647-2012

Bertrand, A., Stefenelli, G., Jen, C. N., Pieber, S. M., Bruns, E. A., Ni, H., et al. (2018). Evolution of the chemical fingerprint of biomass burning organic aerosol during aging. *Atmospheric Chemistry and Physics*, 7607–7624. Retrieved from https://www.atmos-chem-phys.net/18/7607/2018/acp-18-7607-2018.pdf

Bian, Q., Jathar, S. H., Kodros, J. K., Barsanti, K. C., Hatch, L. E., May, A. A., et al. (2017). Secondary organic aerosol formation in biomass-burning plumes: Theoretical analysis of lab studies and ambient plumes. *Atmospheric Chemistry and Physics*, *17*(8), 5459–5475.

https://doi.org/10.5194/acp-17-5459-2017

Bond, T. C., Streets, D. G., Yarber, K. F., Nelson, S. M., Woo, J. H., & Klimont, Z. (2004). A technology-based global inventory of black and organic carbon emissions from combustion. *Journal of Geophysical Research: Atmospheres*, *109*(14), 1–43. https://doi.org/10.1029/2003JD003697

Bruns, E. A., El Haddad, I., Slowik, J. G., Kilic, D., Klein, F., Baltensperger, U., & Prévôt, A. S. H. (2016). Identification of significant precursor gases of secondary organic aerosols from residential wood combustion. *Scientific Reports*, *6*(May), 1–9. https://doi.org/10.1038/srep27881

Canagaratna, M. R., Jimenez, J. L., Kroll, J. H., Chen, Q., Kessler, S. H., Massoli, P., et al. (2015). Elemental ratio measurements of organic compounds using aerosol mass spectrometry: characterization, improved calibration, and implications. *Atmospheric Chemistry and Physics*, *15*(1), 253–272. Retrieved from http://www.atmos-chem-phys.net/15/253/2015/

Capes, G., Johnson, B., McFiggans, G., Williams, P. I., Haywood, J., & Coe, H. (2008). Aging of biomass burning aerosols over West Africa: Aircraft measurements of chemical composition, microphysical properties, and emission ratios. *Journal of Geophysical Research Atmospheres*, *113*(23), 1–13. https://doi.org/10.1029/2008JD009845

Cubison, M. J., Ortega, A. M., Hayes, P. L., Farmer, D. K., Day, D., Lechner, M. J., et al. (2011). Effects of aging on organic aerosol from open biomass burning smoke in aircraft and laboratory studies. *Atmospheric Chemistry and Physics*, *11*(23), 12049–12064. https://doi.org/10.5194/acp-11-12049-2011

Decarlo, P. F., Ulbrich, I. M., Crounse, J., De Foy, B., Dunlea, E. J., Aiken, A. C., et al. (2010). Investigation of the sources and processing of organic aerosol over the Central Mexican Plateau from aircraft measurements during MILAGRO. *Atmospheric Chemistry and Physics*, *10*(12), 5257–5280. https://doi.org/10.5194/acp-10-5257-2010

Dennison, P. E., Brewer, S. C., Arnold, J. D., & Moritz, M. a. (2014). Geophysical Research Letters. *Geophysical Prospecting*, *41*, 2928–2933. https://doi.org/10.1002/2014GL061184.Received

Forrister, H., Liu, J., Scheuer, E., Dibb, J., Ziemba, L., Thornhill, K. L., et al. (2015). Evolution of brown carbon in wildfire plumes. *Geophysical Research Letters*, *42*(11), 4623–4630. https://doi.org/10.1002/2015GL063897

Grieshop, A. P., Logue, J. M., Donahue, N. M., & Robinson, A. L. (2009). Laboratory investigation of photochemical oxidation of organic aerosol from wood fires 1: Measurement and simulation of organic aerosol evolution. *Atmospheric Chemistry and Physics*, *9*(4), 1263–1277. https://doi.org/10.5194/acp-9-1263-2009

Grieshop, A. P., Donahue, N. M., & Robinson, A. L. (2009). Laboratory investigation of photochemical oxidation of organic aerosol from wood fires 2: analysis of aerosol mass

spectrometer data. *Atmospheric Chemistry and Physics*, *9*, 2227–2240. https://doi.org/10.5194/acp-9-2227-2009

Hatch, L. E., Yokelson, R. J., Stockwell, C. E., Veres, P. R., Simpson, I. J., Blake, D. R., et al. (2017). Multi-instrument comparison and compilation of non-methane organic gas emissions from biomass burning and implications for smoke-derived secondary organic aerosol precursors. *Atmospheric Chemistry and Physics*, 1471–1489. https://doi.org/10.5194/acp-17-1471-2017

Hecobian, A., Liu, Z., Hennigan, C. J., Huey, L. G., Jimenez, J. L., Cubison, M. J., et al. (2011). Comparison of chemical characteristics of 495 biomass burning plumes intercepted by the NASA DC-8 aircraft during the ARCTAS/CARB-2008 field campaign. *Atmospheric Chemistry and Physics*, *11*(24), 13325–13337. https://doi.org/10.5194/acp-11-13325-2011

Hennigan, C. J., Miracolo, M. A., Engelhart, G. J., May, A. A., Presto, A. A., Lee, T., & Sullivan, A. P. (2011). and Physics Chemical and physical transformations of organic aerosol from the photo-oxidation of open biomass burning emissions in an environmental chamber, 7669–7686. https://doi.org/10.5194/acp-11-7669-2011

Hennigan, C. J., Westervelt, D. M., Riipinen, I., Engelhart, G. J., Lee, T., Collett, J. L., et al. (2012). New particle formation and growth in biomass burning plumes: An important source of cloud condensation nuclei. *Geophysical Research Letters*, *39*(9), 1–5. https://doi.org/10.1029/2012GL050930

Jolleys, M. D., Coe, H., McFiggans, G., Capes, G., Allan, J. D., Crosier, J., et al. (2012). Characterizing the aging of biomass burning organic aerosol by use of mixing ratios: A meta-analysis of four regions. *Environmental Science and Technology*, *46*(24), 13093–13102. https://doi.org/10.1021/es302386v

Jolleys, M. D., Coe, H., McFiggans, G., Taylor, J. W., O'Shea, S. J., Le Breton, M., et al. (2015). Properties and evolution of biomass burning organic aerosol from Canadian boreal forest fires. *Atmospheric Chemistry and Physics*, *15*(6), 3077–3095. https://doi.org/10.5194/acp-15-3077-2015

Koss, A. R., Sekimoto, K., Gilman, J. B., Selimovic, V., Coggon, M. M., Zarzana, K. J., et al. (2018). Non-methane organic gas emissions from biomass burning: Identification, quantification, and emission factors from PTR-ToF during the FIREX 2016 laboratory experiment. *Atmospheric Chemistry and Physics*, *18*(5), 3299–3319. https://doi.org/10.5194/acp-18-3299-2018

Kroll, J. H., Lim, C. Y., Kessler, S. H., & Wilson, K. R. (2015). Heterogeneous Oxidation of Atmospheric Organic Aerosol: Kinetics of Changes to the Amount and Oxidation State of Particle-Phase Organic Carbon. *The Journal of Physical Chemistry A*, *119*(44), 10767–10783. Retrieved from http://pubs.acs.org/doi/10.1021/acs.jpca.5b06946

Liu, X., Huey, L. G., Yokelson, R. J., Selimovic, V., Simpson, I. J., Müller, M., et al. (2017). Airborne measurements of western U.S. wildfire emissions: Comparison with prescribed burning and air quality implications. *Journal of Geophysical Research*, *122*(11), 6108–

6129. https://doi.org/10.1002/2016JD026315

May, A. A., Levin, E. J. T., Hennigan, C. J., Riipinen, I., Lee, T., Collett, J. L., et al. (2013). Gas-particle partitioning of primary organic aerosol emissions: 3. Biomass burning. *Journal of Geophysical Research Atmospheres*, *118*(19), 11327–11338. https://doi.org/10.1002/jgrd.50828

May, A. A., Lee, T., McMeeking, G. R., Akagi, S., Sullivan, A. P., Urbanski, S., et al. (2015). Observations and analysis of organic aerosol evolution in some prescribed fire smoke plumes. *Atmospheric Chemistry and Physics*, *15*(11), 6323–6335. https://doi.org/10.5194/acp-15-6323-2015

Ortega, A. M., Day, D. A., Cubison, M. J., Brune, W. H., Bon, D., Gouw, J. A. De, & Jimenez, J. L. (2013). Secondary organic aerosol formation and primary organic aerosol oxidation from biomass-burning smoke in a flow reactor during, 11551–11571. https://doi.org/10.5194/acp-13-11551-2013

Ortega, A. M., Hayes, P. L., Peng, Z., Palm, B. B., Hu, W., Day, D. A., et al. (2016). Real-time measurements of secondary organic aerosol formation and aging from ambient air in an oxidation flow reactor in the Los Angeles area. *Atmospheric Chemistry and Physics*, *16*(11), 7411–7433. https://doi.org/10.5194/acp-16-7411-2016

Peng, Z., Day, D. A., Ortega, A. M., Palm, B. B., Hu, W., Stark, H., et al. (2016). Non-OH chemistry in oxidation flow reactors for the study of atmospheric chemistry systematically examined by modeling. *Atmospheric Chemistry and Physics*, *16*(7), 4283–4305. https://doi.org/10.5194/acp-16-4283-2016

Sekimoto, K., Koss, A. R., Gilman, J. B., Selimovic, V., Coggon, M. M., Zarzana, K. J., et al. (2018). High- and low-temperature pyrolysis profiles describe volatile organic compound emissions from western US wildfire fuels. *Atmospheric Chemistry and Physics Discussions*, (February), 1–39. https://doi.org/10.5194/acp-2018-52

Selimovic, V., Yokelson, R. J., Warneke, C., Roberts, J. M., De Gouw, J., Reardon, J., & Griffith, D. W. T. (2018). Aerosol optical properties and trace gas emissions by PAX and OP-FTIR for laboratory-simulated western US wildfires during FIREX. *Atmospheric Chemistry and Physics*, *18*(4), 2929–2948. https://doi.org/10.5194/acp-18-2929-2018

Shrivastava, M., Easter, R. C., Liu, X., Zelenyuk, A., Singh, B., Zhang, K., et al. (2015). Global transformation and fate of SOA: Implications of low-volatility SOA and gas-phase fragmentation reactions. *Journal of Geophysical Research: Atmospheres*, *120*(9), 4169–4195. https://doi.org/10.1002/2014JD022563

Shrivastava, M., Cappa, C. D., Fan, J., Goldstein, A. H., Guenther, A. B., Jimenez, J. L., et al. (2017). Recent advances in understanding secondary organic aerosol: Implications for global climate forcing. *Reviews of Geophysics*, *55*(2), 509–559. https://doi.org/10.1002/2016RG000540

Simoneit, B. R. T., Schauer, J. J., Nolte, C. G., Oros, D. R., Elias, V. O., Fraser, M. P., et al.

(1999). Levoglucosan, a tracer for cellulose in biomass burning and atmospheric particles. *Atmospheric Environment*, *33*(2), 173–182. https://doi.org/10.1016/S1352-2310(98)00145-9

Spracklen, D. V., Mickley, L. J., Logan, J. A., Hudman, R. C., Yevich, R., Flannigan, M. D., & Westerling, A. L. (2009). Impacts of climate change from 2000 to 2050 on wildfire activity and carbonaceous aerosol concentrations in the western United States. *Journal of Geophysical Research Atmospheres*, *114*(20), 1–17. https://doi.org/10.1029/2008JDO10966

Tiitta, P., Leskinen, A., Hao, L., Yli-Pirilä, P., Kortelainen, M., Grigonyte, J., et al. (2016). Transformation of logwood combustion emissions in a smog chamber: Formation of secondary organic aerosol and changes in the primary organic aerosol upon daytime and nighttime aging. *Atmospheric Chemistry and Physics*, *16*(20), 13251–13269. https://doi.org/10.5194/acp-16-13251-2016

Tkacik, D. S., Robinson, E. S., Ahern, A., Saleh, R., Stockwell, C., Veres, P., et al. (2017). A dual-chamber method for quantifying the effects of atmospheric perturbations on secondary organic aerosol formation from biomass burning emissions. *Journal of Geophysical Research*, *122*(11), 6043–6058. https://doi.org/10.1002/2016JD025784

Vakkari, V., Kerminen, V.-M., Beukes, J. P., Titta, P., Zyl, P. G. van, Josipovic, M., et al. (2014). Geophysical Research Letters. *Geophysical Research Letter*, 2644–2651. https://doi.org/10.1002/2014GL059396.Received

Vakkari, V., Beukes, J. P., Jaars, K., Josipovic, M., Venter, A. D., & Zyl, P. G. Van. (2018). Major secondary aerosol formation in southern African open biomass burning plumes. *Nature Geoscience*, *11*, 580–583. https://doi.org/10.1038/s41561-018-0170-0

Westerling, A. L., Hidalgo, H. G., Cayan, D. R., & Swetnam, T. W. (2006). Warming and earlier spring increase Western U.S. forest wildfire activity. *Science*, *313*(5789), 940–943. https://doi.org/10.1126/science.1128834

Yokelson, R. J., Crounse, J. D., DeCarlo, P. F., Karl, T., Urbanski, S., Atlas, E., et al. (2009). Emissions from biomass burning in the Yucatan. *Atmospheric Chemistry and Physics*, *9*(15), 5785–5812. https://doi.org/10.5194/acp-9-5785-2009

Yuan, B., Koss, A. R., Warneke, C., Coggon, M., Sekimoto, K., & De Gouw, J. A. (2017). Proton-Transfer-Reaction Mass Spectrometry: Applications in Atmospheric Sciences. *Chemical Reviews*, *117*(21), 13187–13229. https://doi.org/10.1021/acs.chemrev.7b00325

2.7 Appendix

T2-1. Initial PM composition

		PTR total initial signal		AMS initial composition			
Fire	Fuel	ppb	µg C m-3	POA (µg m-3)	BC (µg m-3)	O/C	H/C
Fire08	Engelmann spruce(PIEN)	250.06	369.75	51.80	0.76	0.33	1.79
Fire21	lodgepole pine (PICO) - Litter	167.14	261.53	28.83	2.29	0.25	1.84
Fire25	Engelmann spruce (PIEN) - Canopy	113.52	172.47	9.66	2.75	0.34	1.80
Fire26	Engelmann spruce (PIEN) - Duff	295.42	397.01	20.14	0.00	0.20	1.86
Fire28	chaparral (manzanita) - Uncontaminated (M-NM),	456.18	680.61	46.14	24.00	0.27	1.79
Fire30	chaparral (manzanita) - Contaminated (M-SD),	797.37	1055.01	68.13	43.74	0.32	1.75
Fire31	Douglas-fir (PSME), Rotten Log	768.22	1078.06	152.92	0.04	0.60	1.79
Fire33	chaparral (manzanita) - Contaminated (M-SD),	666.90	839.08	54.33	30.04	0.31	1.77
Fire38	ponderosa pine (PIPO) - Litter	196.89	297.53	19.12	5.00	0.34	1.78
Fire39	ponderosa pine (PIPO) - Canopy	635.94	1035.87	139.41	5.82	0.31	1.75
Fire41	lodgepole (PICO) - Litter	151.83	251.55	14.55	0.36	0.38	1.76
Fire50	Dung	955.79	1293.72	200.81	0.77	0.21	1.84
Fire52	Engelmann spruce (PIEN)	227.36	331.91	24.82	4.14	0.38	1.73
Fire53	loblolly pine (PITA) - Litter	265.07	461.89	41.58	9.39	0.33	1.78
Fire56	Subalpine fir (ABLA), Fish Lake - Duff	632.51	927.77	28.70	0.02	0.24	1.80
Fire57	Douglas-fir (PSME)	445.64	651.54	68.33	8.09	0.44	1.74
Fire61	Excelsior	480.06	687.78	33.90	26.87	0.52	1.73
Fire62	Bear Grass	546.89	771.58	67.12	3.93	0.32	1.74
Fire63	lodgepole (PICO)	590.09	883.59	96.97	9.57	0.37	1.75
Fire64	Douglas-fir (PSME) - Canopy	1139.78	1731.36	194.96	6.04	0.37	1.72
Fire66	Sage	502.32	715.94	37.72	7.19	0.38	1.73

Table T2-1. Initial conditions for experiments before start of oxidation. Fire 63 is a dark, control experiment (no oxidation).

A2-1. Experimental setup

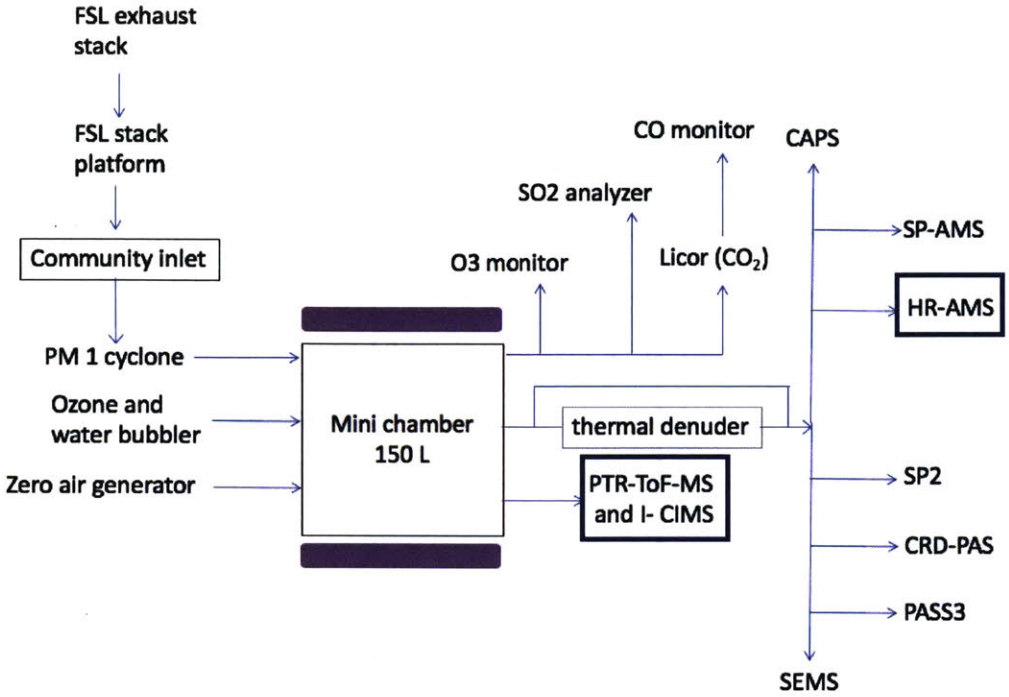

Figure A2-1. Experimental setup. Emissions from fires entered the exhaust stack and were drawn through a community inlet to the mini chamber. Chamber was run in semi-batch mode. Full suite of measurements is shown.

A2-2. Comparison between stack and chamber

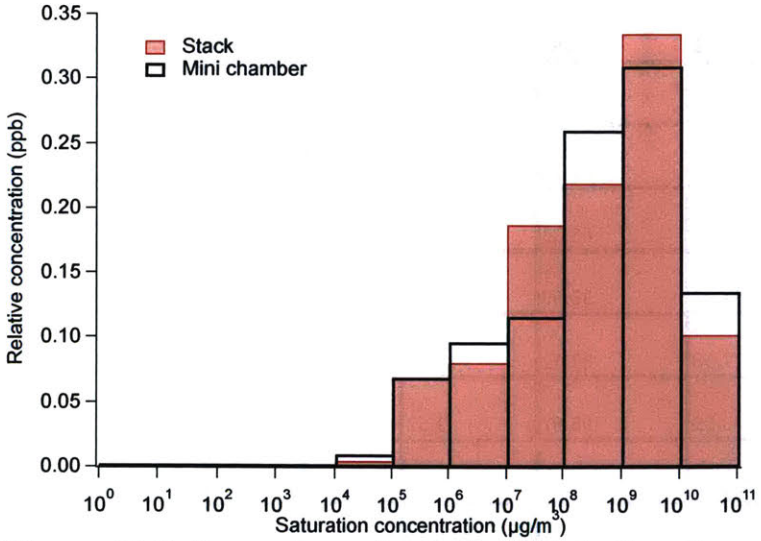

Figure A2-2. Comparison of volatility distributions for gas phase compounds measured in the mini chamber (black) and measured directly from the FSL stack in red (Koss et al., 2017). Distribution of compounds measured is roughly the same indicating that vapor losses from the community inlet or other transfer lines did not significantly affect the mixture of gas phase compounds entering the mini chamber.

A2-3. Collection efficiency parameterization

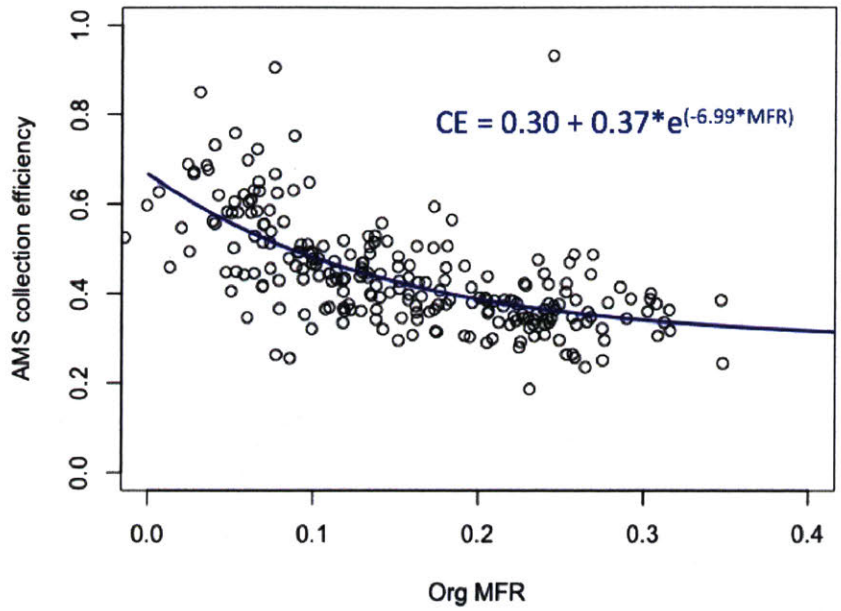

Figure A2-3. Calculated AMS collection efficiency vs. Org MFR (mass fraction remaining after passing through thermal denuder). Blue exponential fit (CE_{best}) was used to parameterize AMS collection efficiency correction for all data points. Red exponential fit (CE_{max}) was used to constrain the range of reasonable carbon yields in Fig. 6.

A2-4. OA wall loss fit

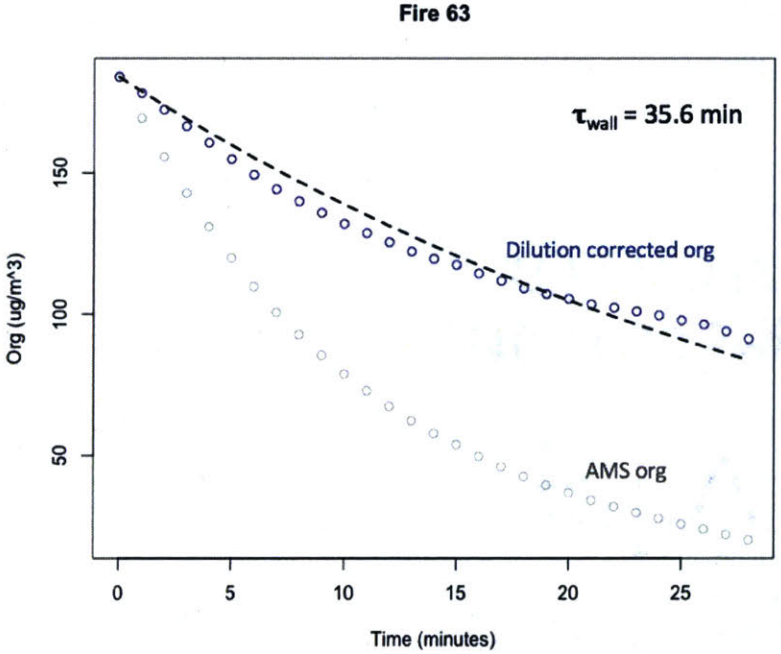

Figure A2-4. Wall loss fit for dark experiment (Fire 63). Wall loss time constant equals 35 minutes, based on fit of dilution corrected OA mass.

A2-5. Dilution corrected primary IVOCs

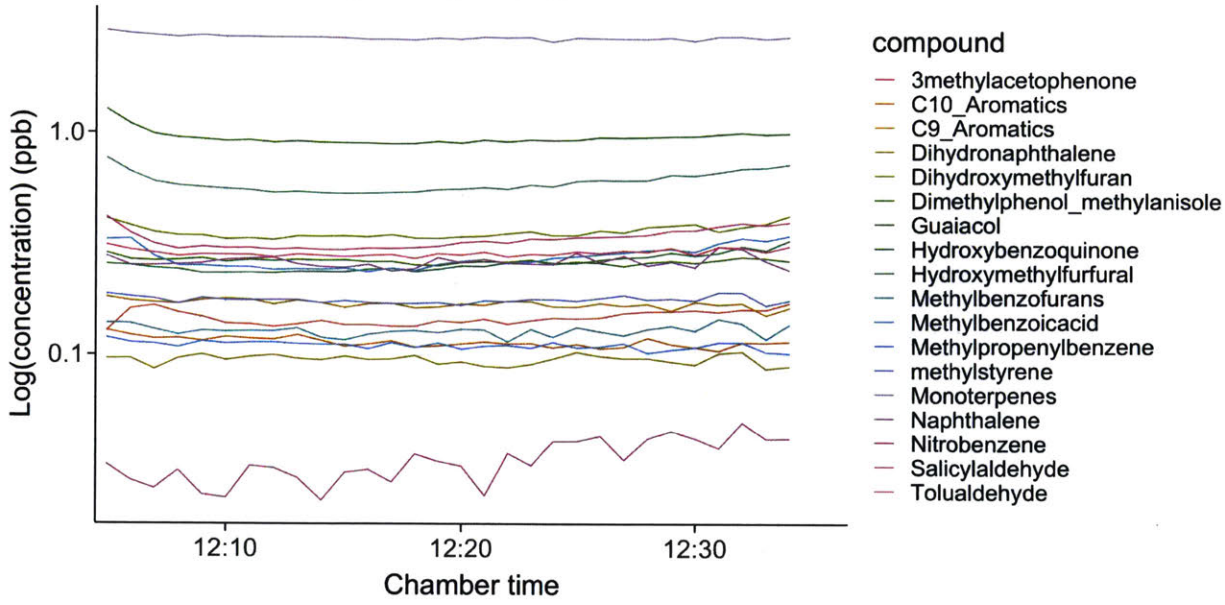

Figure A2-5. Time series for dilution-corrected, high molecular weight gas phase compounds measured by PTR-ToF-MS. Dilution corrected concentrations are stable, indicating the impact of vapor wall loss for these compounds is not important.

A2-6. Comparison between previous FSL aging studies

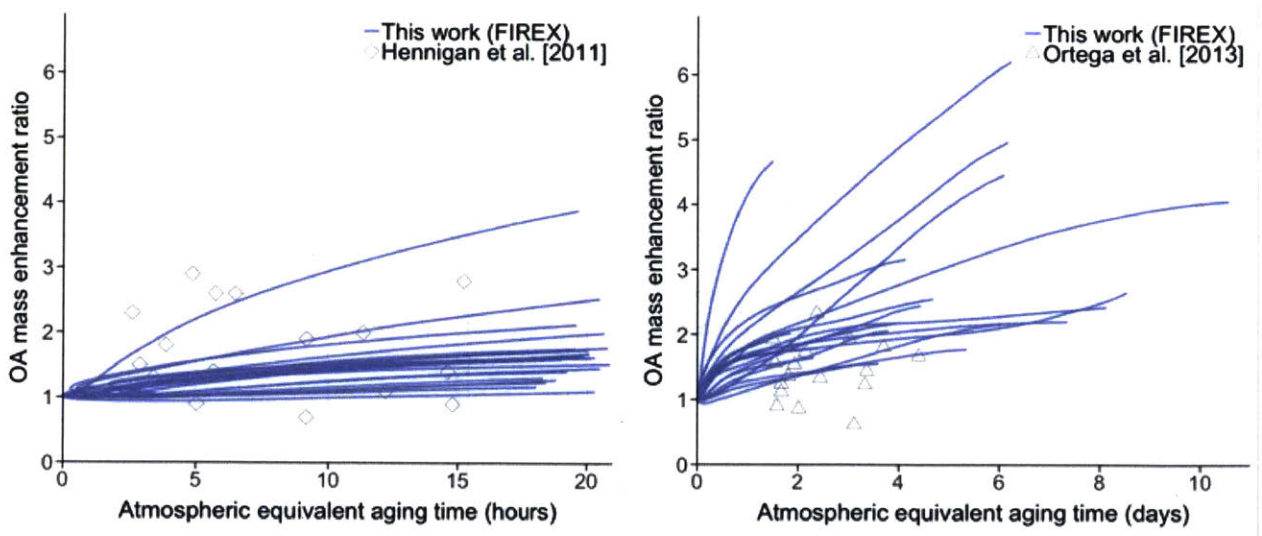

Figure A2-6. Comparison between OA enhancement ratios for this work and previous Fire Lab aging studies. Panel on left is comparison to room-burn, large chamber oxidation from Hennigan et al. (2011). Panel on right is comparison to room-burn, flow tube oxidation from Ortega et al. (2013). Data are not corrected for AMS collection efficiency in order to compare with published work (CE = 1).

A2-7. OA enhancement ratio scatterplots

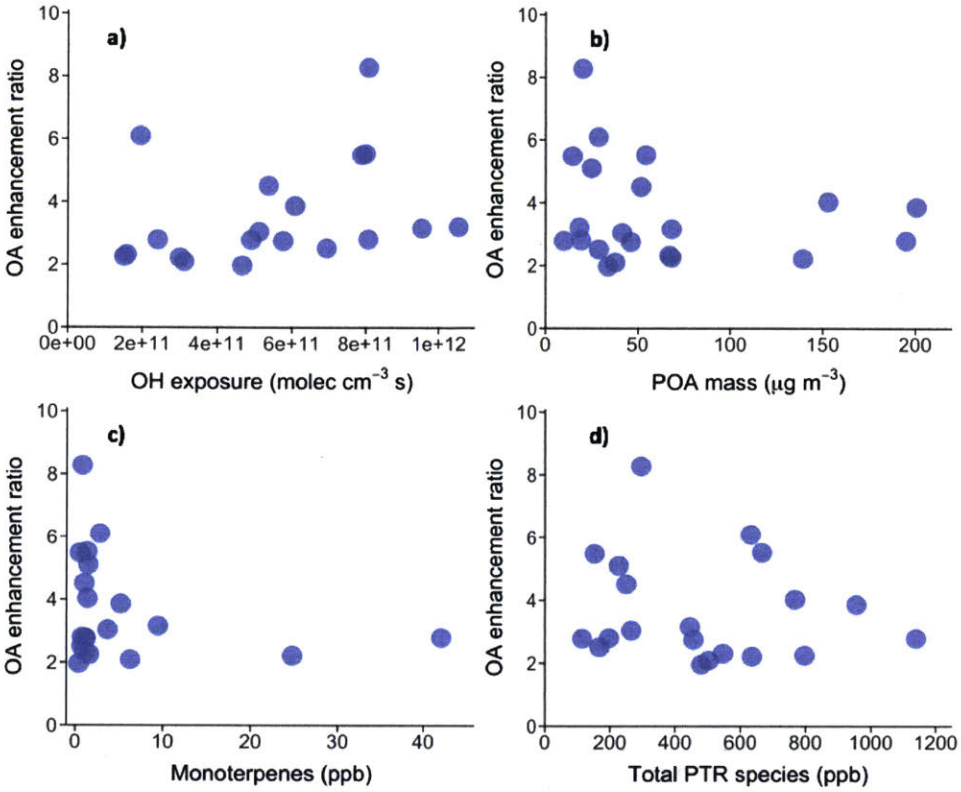

Figure A2-7. Scatterplots of OA enhancement ratio vs. various parameters: (a) OH exposure, (b) POA mass, (c) monoterpene concentration, (d) total PTR species. No single parameter shows a strong relationship with OA enhancement ratio.

A2-8. Effect of aerosol loading on carbon yield

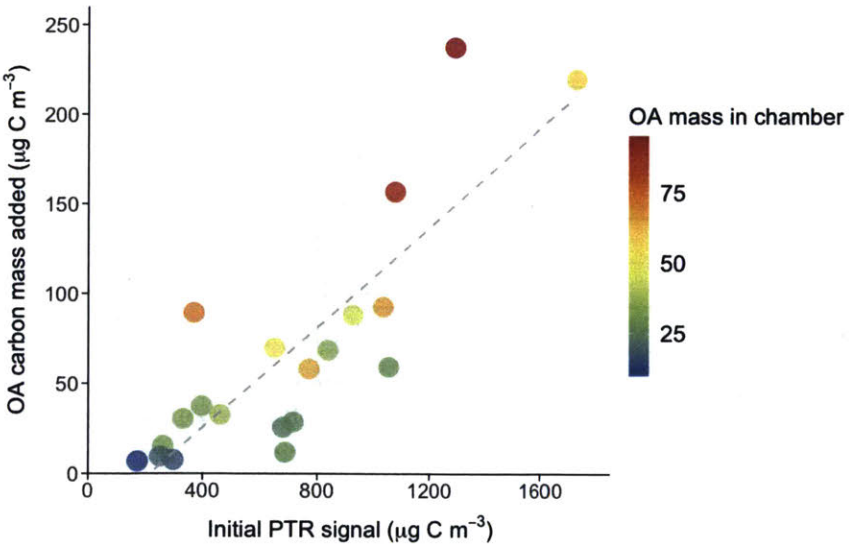

Figure A2-8. OA carbon mass added as a function of initial PTR signal and colored by OA mass in suspended in the chamber (1 day of equivalent exposure). Higher aerosol mass in the chamber contributes to higher conversion of gas-phase carbon to SOA.

A2-9. POA vs. SOA scatterplots

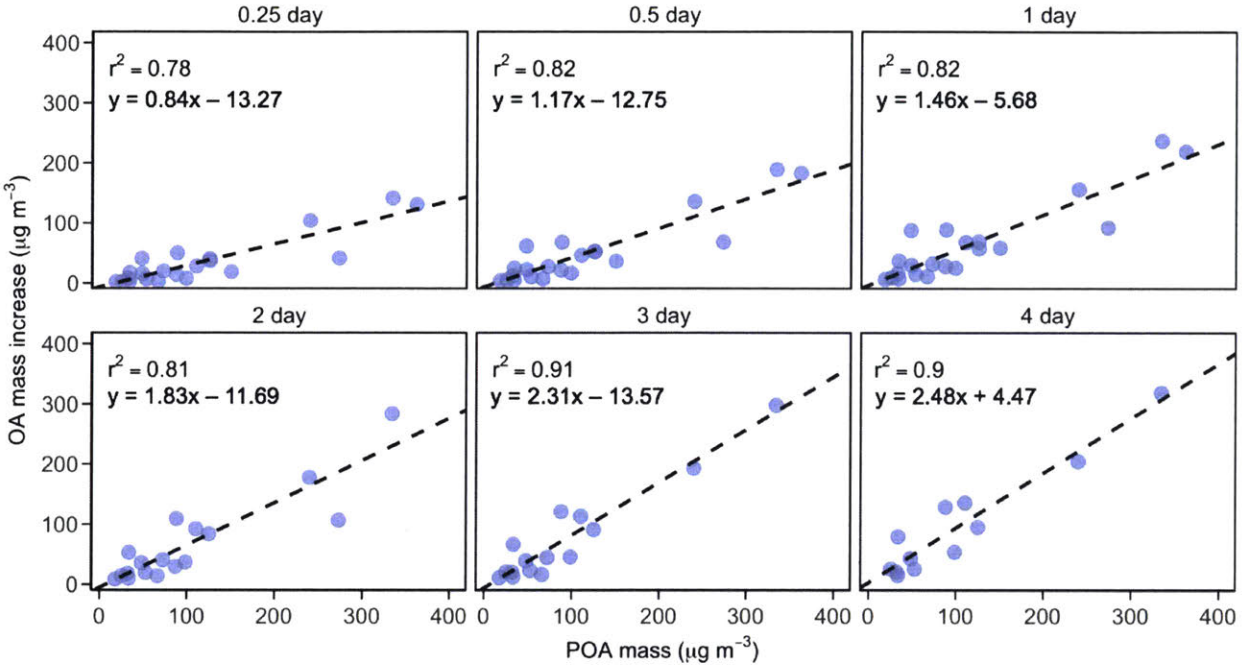

Figure A2-9. Scatterplots of SOA mass vs. POA mass at OH exposures equivalent to 0.25 days of atmospheric aging to 4 days of aging. Dashed lines are linear regressions described by the fit equations.

T2-2. SOA carbon yields

	CE corrected		CE = 1
Days	Yield	Standard error (1σ)	Yield
0.25	0.24	0.04	0.04
0.5	0.32	0.05	0.07
1	0.38	0.06	0.09
2	0.44	0.09	0.10
3	0.51	0.09	0.12
4	0.56	0.09	0.14

Table 2-2. Table of SOA carbon yields from NMOG carbon reacted. NMOG carbon reacted is calculated based on initial NMOG concentration, OH exposure, and an average OH reaction rate constant based on identified NMOGs.

Chapter 3

Rapid heterogeneous oxidation of organic coatings on submicron aerosols

Lim, C. Y., E. C. Browne, R. A. Sugrue, and J. H. Kroll (2017), Rapid heterogeneous oxidation of organic coatings on submicron aerosols, *Geophys. Res. Lett.*, 44, 2949–2957, doi:10.1002/2017GL072585.

3.1 Introduction

Organic aerosol (OA) makes up a significant fraction of fine particulate matter in the atmosphere (Zhang et al., 2007). Over the course of its atmospheric lifetime (approximately five to ten days Balkanski et al., 1993), OA mass and composition can be affected by chemical aging processes, which in turn can alter the climate- and health-relevant properties of the OA. Heterogeneous oxidation, the reaction of gas-phase oxidants (primarily the hydroxyl radical, OH) with organic molecules in the condensed phase, is one important type of aging, with the potential to affect the optical properties, hygroscopicity, and cloud condensation nuclei (CCN) activity of particulate matter (Cappa et al., 2011; Harmon et al., 2013; Slade & Knopf, 2014). Heterogeneous oxidation experiments using a variety of OA proxies, from reduced organic species (alkanes) to highly oxidized organic compounds, generally show increasing average particle carbon oxidation state and loss of particle-phase carbon mass with increasing photochemical age (i.e., OH exposure) (Chan et al., 2014; Kessler et al., 2010, 2012, Kroll et al., 2009, 2011, Nah et al., 2013, 2014; Smith et al., 2009). Recently, from a re-analysis of a series of flow tube OH oxidation experiments, Kroll et al. (2015) estimated that over the course of one week, heterogeneous oxidation causes organic particles to lose on average 3 – 13% of particle-phase carbon, and undergo an increase in average carbon oxidation state of 0.2 – 0.7. These changes are in qualitative agreement with other flow tube heterogeneous oxidation studies on laboratory-generated particles (George et al., 2007; Lambe et al., 2011; McNeill et al., 2008), but are in contrast to results from experiments performed on monolayer films, which showed extremely rapid mass loss with oxidation (Molina et al., 2004).

In order to quantify the importance of heterogeneous oxidation, previous studies have focused on the reactive OH uptake coefficient (γ_{OH}), defined as the fraction of OH-particle collisions that results in reaction. Most studies have found values of γ_{OH} spanning 0.1 to 1 (in the absence of secondary chemistry), indicating efficient oxidation of organic species at particle surfaces (George & Abbatt, 2010). However, the rate at which the composition of an entire organic particle changes depends not only on the rate of reaction at the particle surface, but also on the total amount of organic material within the particle (since the material in the interior of the particle must also undergo reaction if the bulk composition of the OA is to change). Assuming mixing within the particle (i.e., the diffusion of material from the particle interior to the surface) is rapid, the second-order reaction rate constant (k^{II}) of a parent organic compound in the particle phase is equal to the oxidant flux to the particle surface divided by the number of parent molecules present in the particle:

$$k^{II} = \frac{\gamma_{OH} \cdot \bar{c} \cdot M_w \cdot SA}{4 \cdot N_A \cdot \rho_0 \cdot V} \quad (1)$$

in which γ_{OH} is the reactive uptake coefficient, $\bar{c}$ is the mean molecular speed of the gas-phase oxidant, N_A is Avogadro's number, ρ_0 and M_W are the density and molecular weight, respectively, of the reactive organic compound, SA is the surface area of the organic component available for reaction on the particle surface, and V is the volume of the organic component of the particle. This rate constant refers not to the elementary OH-organic reaction at the molecular level, but instead to the reaction between gas-phase OH and generic organic species within the particle (Smith et al., 2009). Assuming a well-mixed spherical particle, this simplifies to:

$$k^{II} = \frac{3 \cdot \gamma_{OH} \cdot \bar{c} \cdot M_w}{2 \cdot N_A \cdot \rho_0 \cdot D_S} \quad (2)$$

Estimates of particle oxidation lifetimes with respect to OH ($\tau_{OH} = 1/(k^{II}[OH])$) using this relationship are on the order of days to weeks – significant for the composition of particles during long-term aging, but unlikely to affect the composition or mass of OA on shorter timescales (Kroll et al., 2015; Robinson et al., 2006).

However, the assumption that OA particles are spherical and well-mixed is a major simplification; field observations and laboratory experiments have shown that atmospheric particles are often

composed of multiple components and adopt complex morphologies and shapes, such as core-shell, lensed, and fractal (Fu et al., 2012; Li et al., 2003). These more complex morphologies may have a significant impact on the rates of chemical aging. For example, organic material that condenses and forms a coating on a pre-existing particle (e.g., black carbon or dust) can have an organic SA/V much higher than the SA/V of the total particle. In addition, glassy or diffusion-limited particles (Koop et al., 2011) can have a much higher effective SA/V compared to the particle as a whole, because only the organic species at or near the particle surface are exposed to OH (which has a short reacto-diffusive length in organic phases, Hanson et al., 1994; Lee & Wilson, 2016; Worsnop, 2002), while the species within the particles, which cannot diffuse rapidly to the surface, are essentially shielded from reaction. Despite the likely importance of such morphologically complex OA particles in the atmosphere, there have been no systematic studies of organic SA/V on the rates and products of heterogeneous oxidation.

Here we present a flow tube study of the OH-initiated heterogeneous reaction of particles composed of a thin layer of hydrocarbon condensed onto an inorganic seed. This system serves as a model for OA coated on primary particles (e.g., black carbon and dust), and can also serve as a proxy for diffusion-limited particles where oxidation is limited to a thin surface layer. These results are compared to the oxidation of pure organic particles, in order to probe how organic SA/V controls the kinetics and products of heterogeneous oxidation, and providing insight into how this effect impacts predictions of OA mass and composition upon aging.

3.2 Methods

3.2.1 Oxidation flow reactor experiments

Experiments involve the heterogeneous oxidation of two types of particles: (1) pure, liquid organic aerosol particles and (2) mixed-composition aerosol, composed of a thin organic coating on solid, inorganic seed particles. For both particle types, the organic compound used is squalane ($C_{30}H_{62}$, Sigma-Aldrich 99%), which has been used as a model system in previous heterogeneous oxidation studies (Kroll et al., 2009; Smith et al., 2009). Pure squalane particles were homogeneously nucleated in a tube furnace (Smith et al., 2009), producing nearly lognormal particle distributions (170 nm at 130°C and 215 nm at 145°C). Coated particles were generated by atomizing a solution of ammonium sulfate, drying, then coating the seed particles (~200 nm surface-weighted diameter)

with squalane following a similar approach to those found in Kwamena et al. (2004) and Lee and Wilson (2016). The amount of squalane condensed onto the seed was controlled by varying the coating temperature between 80 °C and 88 °C. This produced an increase in measured organic mass but not particle number, indicating squalane was condensing onto the seed particles with no new particle formation. Additional details on the particle generation techniques are provided in the Appendix.

Oxidation experiments were performed in a type-219 quartz flow tube reactor (130 cm long, 2.5 cm inner diameter); the experimental setup is shown in Fig. A3-1. The flow tube was run under atmospheric pressure and steady-state conditions, with a calculated residence time of 23 s. Dry air (0.5 slpm) was combined with flow containing particles (0.3 slpm), ozone (0.3 slpm) from an ozone generator (Jelight Model 600), humidified air (0.6 slpm), and the OH-tracer isopentane (150 ppb). Two UV lamps (254 nm, UVP, LLC. XX-40S) were used to photolyze ozone and produce $O(^1D)$, which reacts with water vapor to generate OH radicals and initiate oxidation chemistry. OH exposure was varied by changing the concentration of ozone in the flow tube. Photolysis by 254 nm light and oxidation by other species, such as $O^1(D)$ and $O(^3P)$, is likely minor under the reaction conditions used here (Peng et al., 2016). Temperature in the flow tube enclosure was regulated by rapid airflow and remained within a few degrees of ambient temperature (20 °C); relative humidity within the flow tube was ~30%, ensuring that the ammonium sulfate cores were always solid.

Size distributions of the particles exiting the reactor were measured by a scanning mobility particle sizer (TSI SMPS 3936). A high-resolution time-of-flight aerosol mass spectrometer (AMS, Aerodyne Research Inc.) was used to calculate the particle organic fraction, oxygen-to-carbon ratio (O/C), and hydrogen-to-carbon ratio (H/C) of the aerosol after application of measured relative ionization efficiencies (RIEs) for squalane (5.5), ammonium (3.6), and sulfate (1.0), as well as correction factors for elemental analysis (Aiken et al., 2007, 2008). Revised elemental analysis corrections (Canagaratna et al., 2015) give somewhat higher H/C and O/C; however, the results of this study are largely unaffected by the choice of correction factors. These data enable the calculation of two key quantities, the average carbon oxidation state (OS_C) and the fraction of the original carbon mass remaining per particle (f_C) (Kroll et al., 2015).

The organic SA/V was determined from combining size-resolved composition measurements, from the AMS operating in particle time-of-flight (PToF) mode, with mobility size distributions, measured with the SMPS. These estimates assume that the pure organic particles and ammonium sulfate cores were spherical (Zelenyuk et al., 2006), and that squalane formed uniform coatings on the surface of the ammonium sulfate particles. Details on the SA/V calculation are provided in the Supporting Information. Calculated average organic SA/V ratios for the pure squalane experiments are 0.039 nm^{-1} for the 130 °C nucleation and 0.031 nm^{-1} for the 145 °C nucleation. Calculated average organic SA/V ratios for the coated experiments are substantially higher, 0.42 nm^{-1}, 0.32 nm^{-1}, 0.26 nm^{-1} for the 80 °C, 83 °C, and 88 °C experiments, respectively. These correspond to average equivalent coating thicknesses of 2 nm, 3 nm, and 4 nm (assuming a 200 nm core); coating thickness thus increases with temperature, as expected. If the particles have a morphology other than core-shell (e.g., squalane partially engulfing the core or existing as small "islands" on the surface), organic SA/V will be somewhat lower than calculated here, but will still be substantially higher than for the pure squalane particles.

OH exposure ([OH] × t) was determined by using the mixed-phase relative rates technique described in Hearn and Smith (2006). Isopentane (C_5H_{12}, Airgas) was used as a gas-phase OH-tracer, with concentrations determined by filtering a fraction of the outlet flow through a potassium iodide filter, pre-concentrating it on an adsorbent trap (Carbotrap 300, Supelco) for 60 s, and measuring using a gas chromatograph with flame ionization detector (SRI 8610C). OH exposure, calculated using the 298 K reaction rate coefficient k_{iP+OH} of 3.65×10^{-12} cm^3 $molec^{-1}$ s^{-1} (Wilson et al., 2006), varied in the reactor from zero to 4.5×10^{11} molec cm^{-3} s; assuming an average atmospheric OH concentration of 1.5×10^6 molec cm^{-3}, this corresponds to 0-80 hours of equivalent atmospheric aging.

3.3 Results

3.3.1 Kinetics of squalane loss by heterogeneous oxidation

The kinetics of the oxidative loss of squalane are shown in Fig. 3-1. Measurement of $C_8H_{17}^+$ was used to monitor the reactive loss of squalane, as this fragment ion has been shown to be an excellent

squalane tracer, with no apparent interferences by product species (Smith et al., 2009). The measured rate constant is significantly faster for the coated particles. Exponential fits to the concentration of squalane as a function of OH exposure, shown in Fig. 3-1a, give the second-order squalane rate constant due to reaction with OH (k_{Sq}, equivalent to k^{II} in Eqn. 1):

$$\frac{[Sq]}{[Sq]_0} = \exp(-k_{Sq}\langle OH \rangle \cdot t) \tag{4}$$

Measured values of k_{Sq} as a function of organic SA/V are shown in Fig. 3-1b. Compared to the pure squalane experiments, the coated squalane rate constants are enhanced by factors of 7-10. The lowest-temperature (i.e., highest organic SA/V) coating corresponds to the greatest enhancement in k_{Sq}. In the coated experiments, k_{Sq} at the lowest OH exposures is somewhat more rapid than at higher OH levels. This may be due to changes in the density, viscosity, or AMS RIE of the particulate organic species upon oxidation, similar to the "leveling off" effect seen in other heterogeneous oxidation experiments (Kroll et al., 2015). This deviation from the exponential fit is not seen for pure squalane particles until much higher OH exposures not accessed in this experiment, likely due to the much larger reservoir of squalane molecules in the pure organic case.

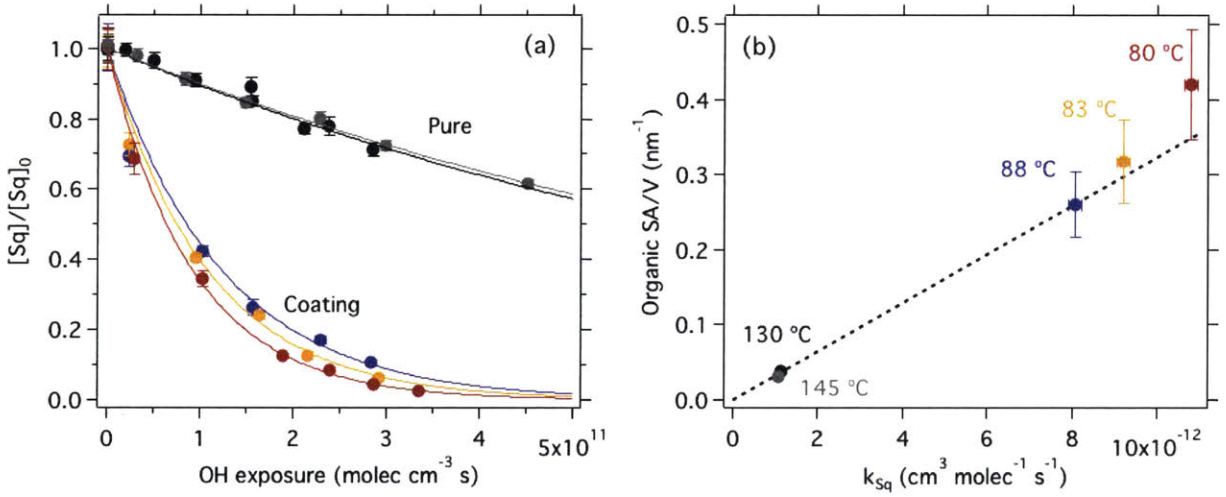

Figure 3-1. (a) Fraction of squalane remaining as a function of OH exposure. Error bars are 1 sigma variation in the measurements; curves are error-weighted exponential fits to the data. Coated particles (80 °C, 83 °C, and 88 °C) show a dramatic increase in the squalane rate constant compared to pure squalane particles (130 °C and 145 °C). **(b)** Organic surface area to volume ratio (nm^{-1}) plotted against squalane rate constant (k_{sq}, determined from the exponential decay of squalane) for both pure and coated experiments. Dashed line denotes the error-weighted fit to the data, forced through zero.

As shown in Fig. 3-1b, the measured squalane rate constant is proportional (within error) to the organic SA/V of the particles, as predicted by Eqn. 1. We conservatively estimate that the average organic SA/V for the coating experiments to be accurate to within ± 20% due to uncertainties in the measured relative ionization efficiency for squalane, ammonium, and sulfate, assuming a core-shell morphology. As noted above, it is possible that the particles may be of different shapes, and hence have somewhat different organic SA/V, than the spherical core-shell morphologies assumed here. However, regardless of their exact configuration, the coated particles certainly have higher organic SA/V than the pure particles, which leads to the observed enhancement in the squalane rate constant.

3.3.2 Changes to aerosol chemical composition

Consistent with the squalane rate constants in Fig. 3-1, the rates of change in the ensemble properties of the particles are also strongly dependent on organic SA/V. Changes to the ensemble chemical composition of OA are quantified in terms of their average carbon oxidation state (OS_C = 2 O/C – H/C) and the fraction of carbon mass remaining (f_C) (Kessler et al., 2012; Kroll et al., 2015) and are shown as a function of OH exposure in Fig. 3-2a and 3-2b. Changes to OS_C and f_C are the result of the competition between the addition of oxygenated functional groups (functionalization) and the cleavage of carbon-carbon bonds and potential loss of volatile compounds to the gas-phase (fragmentation). The relative importance between these two pathways depends on the molecular makeup of the OA, with fragmentation increasing in importance as molecules become more oxidized (Kroll et al., 2009). At the highest OH exposures studied, the pure squalane particles show a +0.2 change in OS_C and a 10% ± 3% loss of carbon mass. These changes are somewhat faster than those observed by Smith et al. (2009), although we calculate identical uptake coefficients (within error); the reason for this is unclear, but possibly due to differences in reaction conditions (e.g., temperature, relative humidity, and OH concentration). For coated particles, the rate of change in OS_C is greatly enhanced compared to the pure experiments, with coatings undergoing up to a +1.3 change in OS_C. The rate of carbon loss for coated particles is also enhanced, with losses up to 60% ± 10% of carbon mass. This amount of carbon loss occurs over a relatively short timescale, equivalent to just 2.7 days of atmospheric OH aging (assuming [OH] of 1.5×10^6 molec cm^{-3}). For comparison, for pure squalane particles to be oxidized to the

extent observed for the coated particles, OH exposures equivalent to roughly 30 days of atmospheric processing would be required.

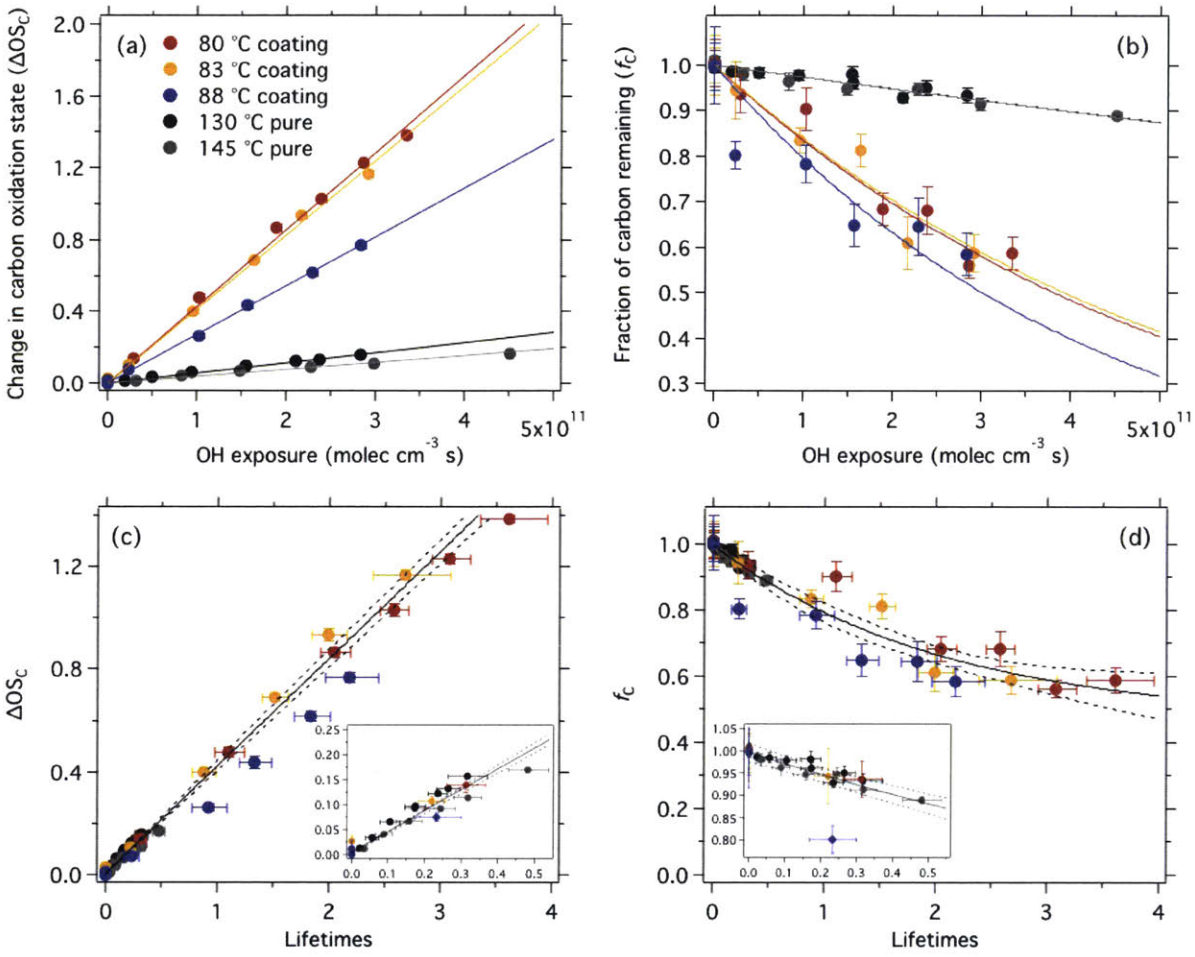

Figure 3-2. Changes to ensemble chemical properties of the particles upon heterogeneous oxidation. **(a)** Change in average carbon oxidation state (ΔOS_C) as a function of OH exposure. **(b)** Fraction carbon remaining (f_C) vs. OH exposure. Error bars (1σ) are from variability in O/C, H/C, and organic mass measurements Curves shown are error-weighted fits (linear in panel a, exponential in panel b) to the measurements for each particle type. **(c)** ΔOS_C and **(d)** f_C vs. squalane lifetimes. Solid lines are error-weighted fits and dashed lines represent 95% confidence intervals. Insets show data from 0 – 0.5 lifetimes. Data from all experiments fall on the same line (within experimental error), indicating that changes in ensemble aerosol properties are driven by organic SA/V, rather than differences in chemistry.

While changes to the ensemble properties of the coated particles are dramatically faster than the changes seen for the pure particles, a linear dependence of ΔOS_C and f_C on organic SA/V is less clear. For example, the rate of change in OS_C for the 88 °C (thickest) coating is the slowest among

the coated experiments, as expected; however, the 80 °C and 83 °C coatings look very similar. Fluctuations in the organic mass measurements introduce relatively large errors to f_C, possibly masking subtle changes in the rate of carbon mass loss. In order to assess whether the differences in the rates of change for ensemble properties are consistent with the differences in reaction rate constants (k_{Sq}), ΔOS_C and f_C are shown as a function of oxidation lifetimes (calculated from squalane rate constants, as in Kroll et al. (2015)) rather than OH exposure (Fig. 3-2c and 3-2d). Describing the ensemble chemical composition in this way allows for chemical changes to be compared on a per-OH reaction basis, independent of differences in physical properties (e.g., SA/V, density, viscosity, etc.). In all experiments (coated and pure), ΔOS_C and f_C exhibit the same dependence on squalane lifetimes (within error). This indicates that the product formation (as described by the ensemble properties ΔOS_C and f_C) is essentially the same in all cases, and that the observed differences between the squalane coatings and pure squalane particles are driven by differences in organic SA/V, rather than differences in the underlying kinetics or mechanism of the oxidation reactions themselves.

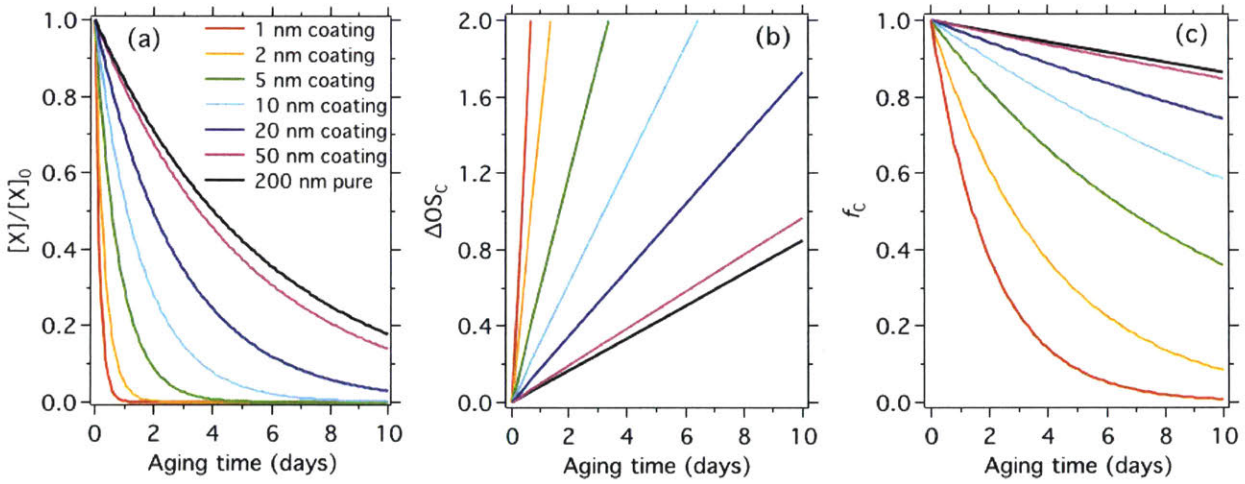

Figure 3-3. Changes to particle composition due to heterogeneous oxidation for 200 nm particles of different compositions. **(a)** Fractional loss of an OA component ($[X]/[X]_0$) based on Eqn. 1, **(b)** change in average carbon oxidation state (ΔOS_C), and **(c)** fractional loss of particle-phase carbon mass (f_C), over 10 days of atmospheric exposure. Fig. 3-3a requires an assumption of the average carbon chain length for the OA component (X), and is assumed to be 10 in this case. Figures 3-3b and 3-3c use the heterogeneous oxidation parameterizations from Kroll et al. (2015), modified for use with organic coatings.

3.4 Discussion and conclusions

We have shown that the heterogeneous transformation of thin organic coatings on particles can be dramatically faster than that of pure organic particles, which are typically used as model systems in laboratory studies of heterogeneous oxidation. This enhancement in the reaction rate constant is driven by differences in the SA/V of the organic fraction of the particle, as expected from Eqn. 1. Such an enhancement is not unique to coated particles, but is simply a result of the high organic SA/V; this is in agreement with the trend seen for oxidation of pure palmitic acid particles of varying sizes by McNeill et al. (2009). This means that a small, pure particle will be chemically transformed at the same rate as a thinly coated one (with an inert core), assuming an equivalent organic SA/V. For example, a 2 nm organic coating on a 200 nm core (80 °C coating case) has an organic SA/V of 0.42 nm and would be oxidized at the same rate as a pure organic particle with a diameter of 14 nm. Changes in key chemical properties of the OA (ΔOS_C and f_C) show similarly dramatic enhancements for coatings relative to the pure particles, reaching high oxidation states and losing a substantial amount of carbon over OH exposures equivalent to days of atmospheric oxidation, rather than weeks to months required for pure particles. This comparison of coated and pure particle oxidation highlights the importance of particle morphology (organic SA/V) in heterogeneous oxidation kinetics and product formation. Moreover, it may explain the discrepancy in estimated OA volatilization lifetime seen for heterogeneous oxidation experiments on aerosol particles that showed relatively little mass loss (George et al., 2007; McNeill et al., 2008; Smith et al., 2009), and experiments performed on monolayer films that showed dramatic loss of mass over relatively short timescales (Molina et al., 2004).

In order to assess the importance of this effect on the rate of chemical aging in the atmosphere, we apply our results to a particle with physical properties and composition representative of ambient organic particles. We apply the linear organic SA/V relationship observed in this study (and predicted in Eqn. 1) to the chemical aging parameterizations made in Kroll et al. (2015) (10% particle-phase carbon lost and ΔOS_C of +0.59 after 1 week of atmospheric aging) for a typical pure, organic particle, (200 nm diameter, O/C = 0.8, H/C = 1.5, ρ = 1.5 g cm^{-3}, and γ_{OH} = 1) and an average [OH] of 1.5×10^6 molec cm^{-3}. Plots of the reaction kinetics and changes to the ensemble chemical properties of the particles are shown in Fig. 3-3 for both pure particles and particles made up of inert cores with a range of organic coating thicknesses (1 to 50 nm), all with diameters of

200 nm. Fig. 3-3a shows the reactive loss of a hypothetical well-mixed compound in the particle phase (e.g., a tracer molecule or pollutant of interest) as a function of aging time in the atmosphere. The 50 nm coating exhibits only a minor enhancement in loss rate over the pure particle case. The importance of the organic SA/V becomes more pronounced for the thinner coatings, which show dramatically faster loss compared to the pure or thickly coated particles. This effect on the heterogeneous oxidation rate constant may have implications for the measurement of tracer species used for source apportionment, such as levoglucosan for biomass burning (Schauer et al., 2001; Simoneit et al., 1999) and hopanes for motor vehicle emissions (Rogge et al., 1993). Such species present in thin (1-10 nm) coatings will essentially be completely lost within a week or less, assuming no subsequent coatings of secondary aerosol.

The change in average carbon oxidation state (ΔOS_C) and fraction of particle-phase carbon remaining (f_C) show similar trends, with the 1-20 nm coatings exhibiting markedly faster rates than the pure and 50 nm coated particles. In terms of OS_C (Fig. 3-3b), the predicted rate of change is accelerated for coated particles, which exhibit slopes up to +2.8/day, whereas the slope for pure particles is much more modest, at +0.08/day. Particle-phase carbon displays a wide range of lifetimes (Fig. 3-3c), ranging from 2 days for 1 nm coatings to 69 days for pure 200 nm particles. So while heterogeneous oxidation plays a relatively minor role in OA lifetime for pure organic particles, it may play a large part in controlling the particle-phase lifetime of OA with high organic SA/V (i.e., thin coatings), or species preferentially present near the surface (Browne et al., 2015). Over the atmospherically relevant timescale shown here, heterogeneous oxidation may thus potentially be an important OA mass sink and a route toward highly oxidized materials on particle surfaces. Additionally, the rapid modification of surface properties may lead to efficient formation of CCN, given that CCN activity of OA can be critically sensitive to surface composition (Ruehl et al., 2016; Ruehl & Wilson, 2014).

Global chemical transport models generally do not include reactions that take into account the heterogeneous oxidation of OA, or they include highly simplified representations of the process (Heald et al., 2011; Hodzic et al., 2016; Murphy et al., 2012). This is largely due to the absence of laboratory-based parameterizations that can be easily implemented in atmospheric models. The results from this study show that heterogeneous oxidation can be important for the evolution of

aerosol composition (Kroll et al., 2015), but also that organic SA/V is critical to the effective rate and products of such oxidation processes in the atmosphere. Thus in order to accurately simulate the timescales over which OA particles evolve as a result of heterogeneous oxidation, it may be necessary for chemical transport models to track organic SA/V or some similar parameter (e.g., average coating thickness).

Though this work focuses on phase-separated particles and organic coatings, it also has implications for some purely organic particles. For instance, for diffusion-limited particles in which the characteristic particle mixing time is long relative to oxidation, the chemical composition near the surface will change much more rapidly than the bulk of the particle. Thus the heterogeneous oxidation of such particles may lead to rapid chemical modification of their surfaces, similar to the coated-particle case described above, which could in turn affect their CCN activity and other surface-related properties. This work adds to an increasing number of studies that have emphasized the dependency of chemical aging on the physical properties of particles, as well as environmental conditions such as relative humidity and temperature (Shiraiwa et al., 2011; Slade & Knopf, 2014). Ultimately, understanding the rates, products, and impacts of heterogeneous oxidation relies critically on an improved understanding of the key physical properties (phase, viscosity, morphology, etc.) of ambient particles under a range of atmospheric conditions.

3.5 Acknowledgments

The data for this paper are available upon request from the authors. This was supported by the National Science Foundation under Grant No. CHE-1307664 and the Environmental Protection Agency under Grant No. RD-8350331. This work was carried out under Assistance Agreement No. D-8350331 awarded by the U.S. Environmental Protection Agency to MIT. It has not been formally reviewed by EPA. The views expressed in this document are solely those of the authors and do not necessarily reflect those of the Agency. EPA does not endorse any products or commercial services mentioned in this publication. CYL is also supported by the NSF Graduate Research Fellowship Program and RAS is supported by the MIT Undergraduate Research Opportunities Program. The authors would like to thank T. Onasch and Aerodyne, Inc. for supplying the tube furnace used in this work, and K. Wilson and C. Heald for helpful discussions.

3.6 References

Aiken, A. C., DeCarlo, P. F., & Jimenez, J. L. (2007). Elemental Analysis of Organic Species with Electron Ionization High-Resolution Mass Spectrometry. *Analytical Chemistry*, *79*(21), 8350–8358. Retrieved from http://pubs.acs.org/doi/abs/10.1021/ac071150w

Aiken, A. C., DeCarlo, P. F., Kroll, J. H., Worsnop, D. R., Huffman, J. A., Docherty, K. S., et al. (2008). O/C and OM/OC Ratios of Primary, Secondary, and Ambient Organic Aerosols with High-Resolution Time-of-Flight Aerosol Mass Spectrometry. *Environmental Science & Technology*, *42*(12), 4478–4485. Retrieved from http://pubs.acs.org/doi/abs/10.1021/es703009q

Balkanski, Y. J., Jacob, D. J., Gardner, G. M., Graustein, W. C., & Turekian, K. K. (1993). Transport and residence times of tropospheric aerosols inferred from a global three-dimensional simulation of 210Pb. *Journal of Geophysical Research*, *98*(D11), 20573. Retrieved from http://doi.wiley.com/10.1029/93JD02456

Browne, E. C., Franklin, J. P., Canagaratna, M. R., Massoli, P., Kirchstetter, T. W., Worsnop, D. R., et al. (2015). Changes to the chemical composition of soot from heterogeneous oxidation reactions. *Journal of Physical Chemistry A*, *119*(7), 1154–1163. https://doi.org/10.1021/jp511507d

Canagaratna, M. R., Jimenez, J. L., Kroll, J. H., Chen, Q., Kessler, S. H., Massoli, P., et al. (2015). Elemental ratio measurements of organic compounds using aerosol mass spectrometry: characterization, improved calibration, and implications. *Atmospheric Chemistry and Physics*, *15*(1), 253–272. Retrieved from http://www.atmos-chem-phys.net/15/253/2015/

Cappa, C. D., Che, D. L., Kessler, S. H., Kroll, J. H., & Wilson, K. R. (2011). Variations in organic aerosol optical and hygroscopic properties upon heterogeneous OH oxidation. *Journal of Geophysical Research: Atmospheres*, *116*(15), 1–12. https://doi.org/10.1029/2011JD015918

Chan, M. N., Zhang, H., Goldstein, A. H., & Wilson, K. R. (2014). Role of Water and Phase in the Heterogeneous Oxidation of Solid and Aqueous Succinic Acid Aerosol by Hydroxyl Radicals. *The Journal of Physical Chemistry C*, *118*(50), 28978–28992. Retrieved from http://pubs.acs.org/doi/abs/10.1021/jp5012022

Fu, H., Zhang, M., Li, W., Chen, J., Wang, L., Quan, X., & Wang, W. (2012). Morphology, composition and mixing state of individual carbonaceous aerosol in urban Shanghai. *Atmospheric Chemistry and Physics*, *12*(2), 693–707. https://doi.org/10.5194/acp-12-693-2012

George, I. J., & Abbatt, J. P. D. (2010). Heterogeneous oxidation of atmospheric aerosol particles by gas-phase radicals. *Nature Publishing Group*, *2*(9), 713–722. Retrieved from http://dx.doi.org/10.1038/nchem.806

George, I. J., Vlasenko, A., Slowik, J. G., Broekhuizen, K., & Abbatt, J. P. D. (2007).

Heterogeneous oxidation of saturated organic aerosols by hydroxyl radicals: uptake kinetics, condensed-phase products, and particle size change. *Atmospheric Chemistry and Physics*, *7*(16), 4187–4201. Retrieved from http://www.atmos-chem-phys.net/7/4187/2007/

Hanson, D. R., Ravishankara, a. R., & Solomon, S. (1994). Heterogeneous reactions in sulfuric acid aerosols: A framework for model calculations. *Journal of Geophysical Research*, *99*(D2), 3615–3629. https://doi.org/10.1029/93JD02932

Harmon, C. W., Ruehl, C. R., Cappa, C. D., & Wilson, K. R. (2013). A statistical description of the evolution of cloud condensation nuclei activity during the heterogeneous oxidation of squalane and bis(2-ethylhexyl) sebacate aerosol by hydroxyl radicals. *Physical Chemistry Chemical Physics*, *15*(24), 9615–9679. Retrieved from http://xlink.rsc.org/?DOI=c3cp50347j

Heald, C. L., Coe, H., Jimenez, J. L., Weber, R. J., Bahreini, R., Middlebrook, A. M., et al. (2011). Exploring the vertical profile of atmospheric organic aerosol: Comparing 17 aircraft field campaigns with a global model. *Atmospheric Chemistry and Physics*, *11*(24), 12676–12696. https://doi.org/10.5194/acp-11-12673-2011

Hearn, J. D., & Smith, G. D. (2006). A mixed-phase relative rates technique for measuring aerosol reaction kinetics. *Geophysical Research Letters*, *33*(17), 3–7. https://doi.org/10.1029/2006GL026963

Hodzic, A., Kasibhatla, P. S., Jo, D. S., Cappa, C. D., Jimenez, J. L., Madronich, S., & Park, R. J. (2016). Rethinking the global secondary organic aerosol (SOA) budget: Stronger production, faster removal, shorter lifetime. *Atmospheric Chemistry and Physics*, *16*(12), 7917–7941. https://doi.org/10.5194/acp-16-7917-2016

Kessler, S. H., Smith, J. D., Che, D. L., Worsnop, D. R., Wilson, K. R., & Kroll, J. H. (2010). Chemical Sinks of Organic Aerosol: Kinetics and Products of the Heterogeneous Oxidation of Erythritol and Levoglucosan. *Environmental Science & Technology*, *44*(18), 7005–7010. Retrieved from http://pubs.acs.org/doi/abs/10.1021/es101465m

Kessler, S. H., Nah, T., Daumit, K. E., Smith, J. D., Leone, S. R., Kolb, C. E., et al. (2012). OH-Initiated Heterogeneous Aging of Highly Oxidized Organic Aerosol. *The Journal of Physical Chemistry A*, *116*(24), 6358–6365. Retrieved from http://pubs.acs.org/doi/abs/10.1021/jp212131m

Koop, T., Bookhold, J., Shiraiwa, M., & Pöschl, U. (2011). Glass transition and phase state of organic compounds: dependency on molecular properties and implications for secondary organic aerosols in the atmosphere. *Physical Chemistry Chemical Physics*, *13*(43), 19238. https://doi.org/10.1039/c1cp22617g

Kroll, J. H., Smith, J. D., Che, D. L., Kessler, S. H., Worsnop, D. R., & Wilson, K. R. (2009). Measurement of fragmentation and functionalization pathways in the heterogeneous oxidation of oxidized organic aerosol. *Physical Chemistry Chemical Physics*, *11*(36), 8005. Retrieved from http://xlink.rsc.org/?DOI=b905289e

Kroll, J. H., Donahue, N. M., Jimenez, J. L., Kessler, S. H., Canagaratna, M. R., Wilson, K. R., et al. (2011). Carbon oxidation state as a metric for describing the chemistry of atmospheric organic aerosol. *Nature Chemistry*, *3*(2), 133–139. https://doi.org/10.1038/nchem.948

Kroll, J. H., Lim, C. Y., Kessler, S. H., & Wilson, K. R. (2015). Heterogeneous Oxidation of Atmospheric Organic Aerosol: Kinetics of Changes to the Amount and Oxidation State of Particle-Phase Organic Carbon. *The Journal of Physical Chemistry A*, *119*(44), 10767–10783. Retrieved from http://pubs.acs.org/doi/10.1021/acs.jpca.5b06946

Kwamena, N. O. A., Thornton, J. A., & Abbatt, J. P. D. (2004). Kinetics of surface-bound benzo[a]pyrene and ozone on solid organic and salt aerosols. *Journal of Physical Chemistry A*, *108*(52), 11626–11634. https://doi.org/10.1021/jp046161x

Lambe, A. T., Ahern, A. T., Williams, L. R., Slowik, J. G., Wong, J. P. S., Abbatt, J. P. D., et al. (2011). Characterization of aerosol photooxidation flow reactors: heterogeneous oxidation, secondary organic aerosol formation and cloud condensation nuclei activity measurements. *Atmospheric Measurement Techniques*, *4*(3), 445–461. Retrieved from http://www.atmos-meas-tech.net/4/445/2011/

Lee, L., & Wilson, K. (2016). The Reactive-Diffusive Length of OH and Ozone in Model Organic Aerosols. *Journal of Physical Chemistry A*, *120*(34), 6800–6812. https://doi.org/10.1021/acs.jpca.6b05285

Li, J., Posfai, M., Hobbs, P. V., & Buseck, P. R. (2003). Individual Aerosol Particles from Biomass Burning in Southern Africa: 2. Compositions and Aging of Inorganic Particles. *Journal of Geophysical Research*, *108*, 1–12. https://doi.org/10.1029/2002JD002310

McNeill, V. F., Yatavelli, R. L. N., Thornton, J. a., Stipe, C. B., & Landgrebe, O. (2008, March 17). The heterogeneous OH oxidation of palmitic acid in single component and internally mixed aerosol particles: vaporization, secondary chemistry, and the role of particle phase. *Atmospheric Chemistry and Physics Discussions*. https://doi.org/10.5194/acpd-8-6035-2008

Molina, M. J., Ivanov, A. V, Trakhtenberg, S., & Molina, L. T. (2004). Atmospheric evolution of organic aerosol. *Geophysical Research Letters*, *31*(22), L22104-5. Retrieved from http://doi.wiley.com/10.1029/2004GL020910

Murphy, B. N., Donahue, N. M., Fountoukis, C., Dall'Osto, M., O'Dowd, C., Kiendler-Scharr, A., & Pandis, S. N. (2012). Functionalization and fragmentation during ambient organic aerosol aging: Application of the 2-D volatility basis set to field studies. *Atmospheric Chemistry and Physics*, *12*(22), 10797–10816. https://doi.org/10.5194/acp-12-10797-2012

Nah, T., Kessler, S. H., Daumit, K. E., Kroll, J. H., Leone, S. R., & Wilson, K. R. (2013). OH-initiated oxidation of sub-micron unsaturated fatty acid particles. *Physical Chemistry Chemical Physics*, *15*(42), 18615–18649. Retrieved from http://xlink.rsc.org/?DOI=c3cp52655k

Nah, T., Kessler, S. H., Daumit, K. E., Kroll, J. H., Leone, S. R., & Wilson, K. R. (2014). Influence of Molecular Structure and Chemical Functionality on the Heterogeneous OH-

Initiated Oxidation of Unsaturated Organic Particles. *The Journal of Physical Chemistry A*, *118*(23), 4106–4119. Retrieved from http://pubs.acs.org/doi/abs/10.1021/jp502666g

Peng, Z., Day, D. A., Ortega, A. M., Palm, B. B., Hu, W., Stark, H., et al. (2016). Non-OH chemistry in oxidation flow reactors for the study of atmospheric chemistry systematically examined by modeling. *Atmospheric Chemistry and Physics*, *16*(7), 4283–4305. https://doi.org/10.5194/acp-16-4283-2016

Robinson, A. L., Donahue, N. M., & Rogge, W. F. (2006). Photochemical oxidation and changes in molecular composition of organic aerosol in the regional context. *Journal of Geophysical Research*, *111*(D3), D03302-15. Retrieved from http://doi.wiley.com/10.1029/2005JD006265

Rogge, W. F., Hildemann, L. M., Mazurek, M. a., Cass, G. R., & Simoneit, B. R. T. (1993). Sources of fine organic aerosol. 2. Noncatalyst and catalyst-equipped automobiles and heavy-duty diesel trucks. *Environmental Science & Technology*, *27*(4), 636–651. https://doi.org/10.1021/es00041a007

Ruehl, C. R., & Wilson, K. R. (2014). Surface organic monolayers control the hygroscopic growth of submicrometer particles at high relative humidity. *The Journal of Physical Chemistry. A*, *118*(22), 3952–66. https://doi.org/10.1021/jp502844g

Ruehl, C. R., Davies, J. F., & Wilson, K. R. (2016). Droplet Formation on Organic Aerosols, *351*(6280), 1447–1450.

Schauer, J. J., Kleeman, M. J., Cass, G. R., & Simoneit, B. R. T. (2001). Measurement of emissions from air pollution sources. 3. C1-C29 organic compounds from fireplace combustion of wood. *Environmental Science and Technology*, *35*(9), 1716–1728. https://doi.org/10.1021/es001331e

Shiraiwa, M., Ammann, M., & Koop, T. (2011). Gas uptake and chemical aging of semisolid organic aerosol particles. In *Proceedings of the* .... Retrieved from http://www.pnas.org/content/108/27/11003.short

Simoneit, B. R. T., Schauer, J. J., Nolte, C. G., Oros, D. R., Elias, V. O., Fraser, M. P., et al. (1999). Levoglucosan, a tracer for cellulose in biomass burning and atmospheric particles. *Atmospheric Environment*, *33*(2), 173–182. https://doi.org/10.1016/S1352-2310(98)00145-9

Slade, J. H., & Knopf, D. A. (2014). Multiphase OH oxidation kinetics of organic aerosol: The role of particle phase state and relative humidity. *Geophysical Research Letters*, *41*(14), 5297–5306. https://doi.org/10.1002/2014GL060582

Smith, J. D., Kroll, J. H., Cappa, C. D., Che, D. L., Liu, C. L., Ahmed, M., et al. (2009). The heterogeneous reaction of hydroxyl radicals with sub-micron squalane particles: a model system for understanding the oxidative aging of ambient aerosols. *Atmospheric Chemistry and Physics*, *9*(9), 3209–3222. Retrieved from http://www.atmos-chem-phys.net/9/3209/2009/

Wilson, E. W., Hamilton, W. A., Kennington, H. R., Evans, B., Scott, N. W., & DeMore, W. B. (2006). Measurement and Estimation of Rate Constants for the Reactions of Hydroxyl Radical with Several Alkanes and Cycloalkanes. *The Journal of Physical Chemistry A*, *110*(10), 3593–3604. Retrieved from http://pubs.acs.org/doi/abs/10.1021/jp055841c

Worsnop, D. R. (2002). A chemical kinetic model for reactive transformations of aerosol particles. *Geophysical Research Letters*, *29*(20), 19–22. https://doi.org/10.1029/2002GL015542

Zelenyuk, A., Cai, Y., & Imre, D. (2006). From Agglomerates of Spheres to Irregularly Shaped Particles: Determination of Dynamic Shape Factors from Measurements of Mobility and Vacuum Aerodynamic Diameters. *Aerosol Science and Technology*, *40*(3), 197–217. https://doi.org/10.1080/02786820500529406

Zhang, Q., Jimenez, J. L., Canagaratna, M. R., Allan, J. D., Coe, H., Ulbrich, I., et al. (2007). Ubiquity and dominance of oxygenated species in organic aerosols in anthropogenically-influenced Northern Hemisphere midlatitudes. *Geophysical Research Letters*, *34*(13). Retrieved from http://doi.wiley.com/10.1029/2007GL029979

3.7 Appendix

Text A3-1.

The organic SA/V distribution (104 size bins between 15.7 nm and 637.8 nm) is determined by dividing the SA/V of each size bin ($6/D_p$) by the organic volume fraction ($f_{org} = V_{org}/V_{total}$). The organic SA/V distribution is then weighted by the particle surface area distribution to give the surface-weighted average organic SA/V:

$$\left\langle \frac{SA}{V_{org}} \right\rangle = \frac{1}{S} \sum_i \left[\frac{6}{f_{org} \cdot D_p} \right]_i s_i \tag{3}$$

where D_p is the particle diameter of bin i, s_i is the particle surface area within the size bin, and S is the integrated surface area of the entire distribution. Organic SA/V calculated from Eqn. 3 for pure particles ($f_{org} = 1$) gave values within ~10% of that calculated by simple geometry for a spherical particle (SA/V = $6/D_S$, where D_S is the average surface-weighted diameter), giving us confidence in this approach. Size dependent measurements of organic, ammonium, and sulfate were used to calculate the average organic SA/V of the particle distributions. For coated particles, AMS PToF organic, ammonium, and sulfate distributions are needed to calculate the f_{org} distribution for a given coating temperature. The chemically speciated organic, ammonium, and sulfate size distributions are then applied to the SMPS measured particle size distributions to base all calculations on the electrical mobility diameter, rather than vacuum aerodynamic diameter. Coated particles do not appear to show size-dependent collection efficiency. As evidence for this, after accounting for density factors and the conversion between vacuum aerodynamic and electrical mobility diameters, there is very little difference between the shape of the AMS PToF measured distribution and the SMPS volume distribution (Fig. A3-2).

Based on the surface area available for condensation, the fraction of the particle that is organic should decrease monotonically with particle diameter; however, the calculated f_{org} values at the edges of the distributions had poor signal to noise (see Fig. A3-3), so data were fit (from diameters 100 nm to 500 nm) to an exponential function and the fit was used to calculate the average organic SA/V in Eqn. 3. Average organic SA/V for the unoxidized particles at both the beginning and end of the experiment (no oxidation) gave identical values (within error), indicating negligible drift in the unoxidized particle size distribution or coating thickness over the course of each experiment.

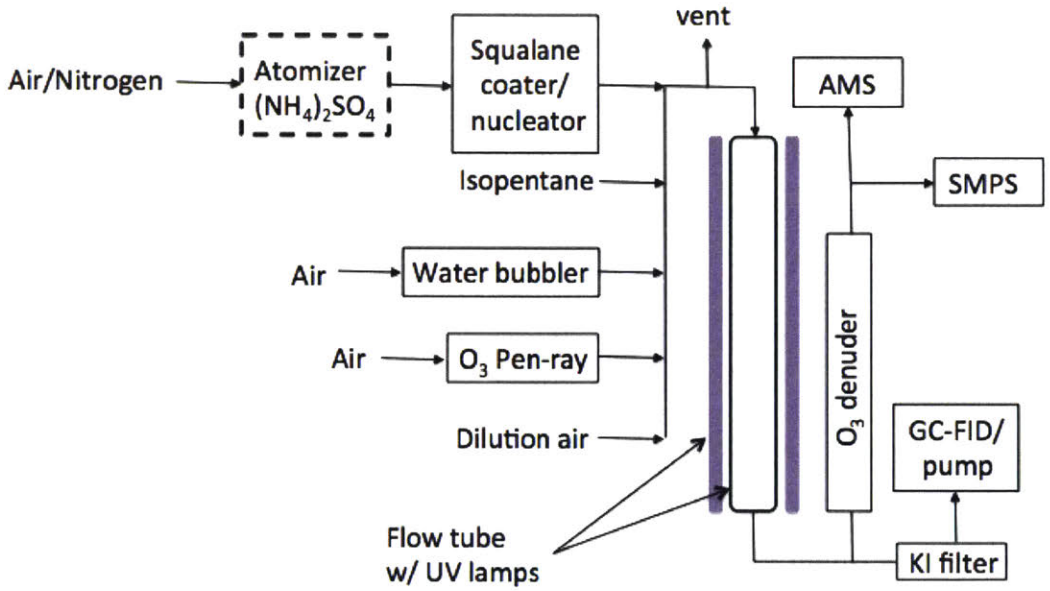

Figure A3-1. Experimental setup. Pure squalane experiments used a tube furnace to homogeneously nucleate squalane particles in nitrogen. Coated particles were made up of dry ammonium sulfate seed particles passed through a squalane coater.

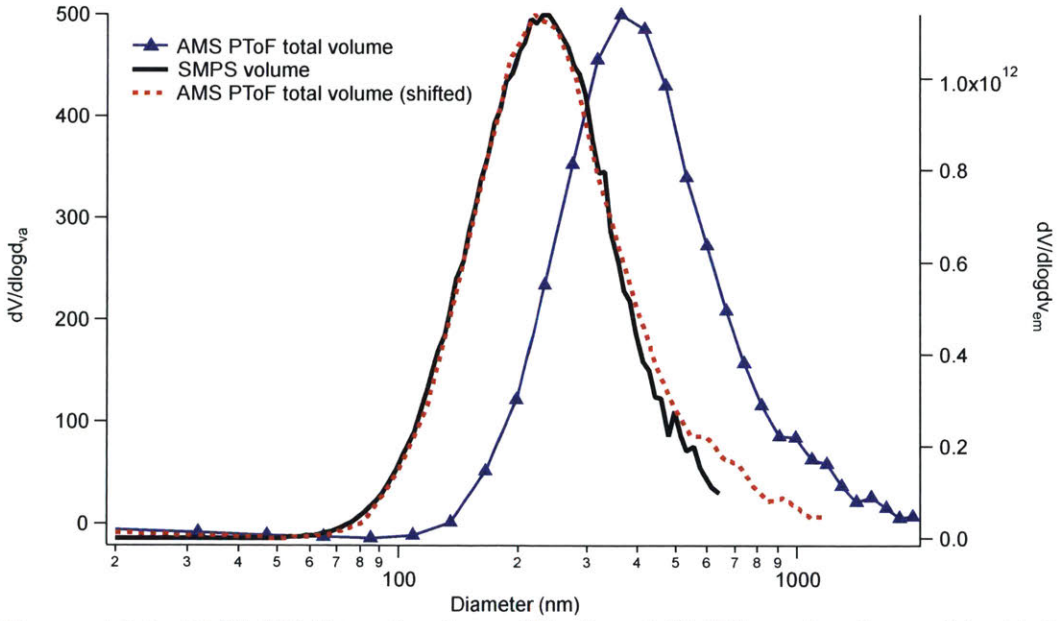

Figure A3-2. AMS PToF total volume (blue) and SMPS total volume (black) for 88 °C coating experiment. Dotted red line shows AMS PToF volume shifted over to match SMPS electric mobility diameter.

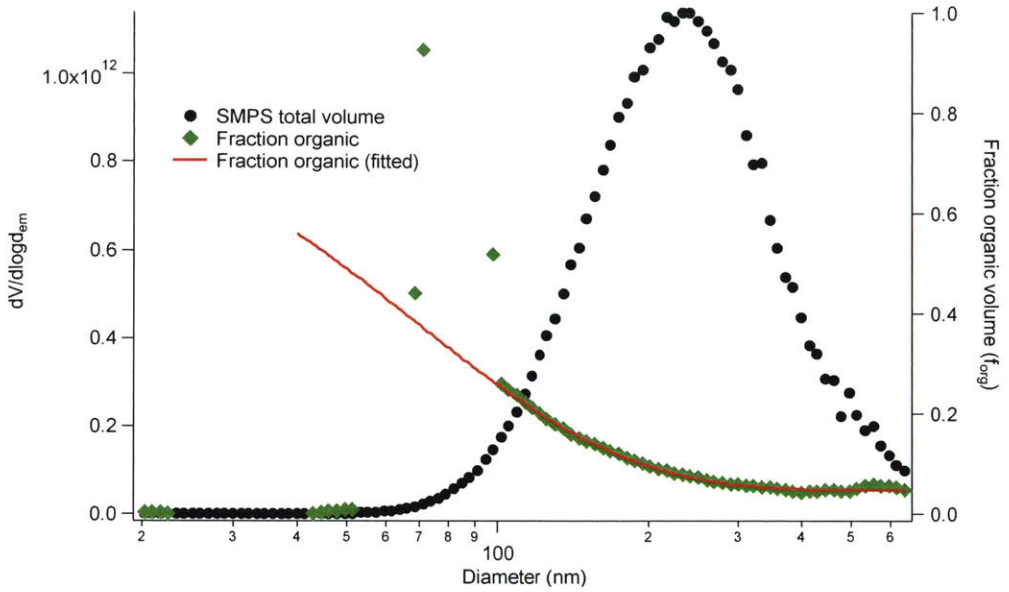

Figure A3-3. SMPS total volume (black circles) and organic volume fraction measurements (green triangles). Organic volume fraction from ca. 100 – 500 nm were fit to an exponential function (red line) for each experiment in order to calculate the average organic SA/V (see Eqn. 3).

Chapter 4

Fragmentation products and gas phase carbon yield from the heterogeneous oxidation of squalane

4.1 Introduction

Organic aerosol (OA) makes up a significant fraction of fine particulate matter (PM) in the atmosphere (Zhang et al., 2007). In addition to the direct emission of primary organic aerosol (POA) from sources such as biomass burning and fossil fuel combustion, the oxidation of gas-phase volatile organic compounds (VOCs) can form lower volatility compounds which can subsequently partition to the particle phase forming secondary organic aerosol (SOA) (Hallquist et al., 2009; Kroll & Seinfeld, 2008). However, the composition of OA after emission or formation in the atmosphere is not static, but rather continues to chemically change over its lifetime due to oxidative processes (George & Abbatt, 2010; Kroll et al., 2011). More specifically, OA is subject to heterogeneous oxidation, defined as the reaction of gas-phase oxidants such as the hydroxyl radical (OH) directly with organic molecules in the particle phase. Over typical atmospheric OA lifetimes, which span from days to weeks (Balkanski et al., 1993), the composition of OA can change dramatically, altering the climate and health impacts of atmospheric particulate matter (Kroll et al., 2015).

Laboratory studies have found that the heterogeneous reaction of oxidants with organic particles is generally very efficient. OH uptake coefficients (γ_{OH}), the fraction of OH-particle collisions that results in reaction, has been measured for a variety of organic model compounds to be between 0.1 and 1 (George et al., 2007; Kessler et al., 2010, 2012; Kroll et al., 2009; Lambe et al., 2007; McNeill et al., 2008; Smith et al., 2009a). Several studies have measured γ_{OH} greater than 1, potentially indicating a radical chain mechanism and secondary chemistry, leading to more rapid oxidation (Chan et al., 2014; Hearn et al., 2007; Hearn & Smith, 2006; Lambe et al., 2009; Nah et al., 2014). Although heterogeneous reaction rates tend to be slower than reactions in the gas phase – only molecules near the surface of particles are available for reaction (Worsnop, 2002) – it is clear that heterogeneous oxidation can play an important role in the multiday aging of OA. A recent review of flow tube heterogeneous oxidation studies found that over the course of one week

of atmospheric processing, 10% of the particle carbon mass is lost to the gas phase and the average carbon oxidation state (OS_C) of the particles increases by 0.6 (Kroll et al., 2015). The rate of these changes depends critically on the organic surface area to volume ratio of the particles and organic coatings or surfaces can be oxidized even more rapidly than pure, well-mixed particles *(Chapter 3)*.

Despite the strong evidence that heterogeneous oxidation can change the loading and composition of OA significantly over atmospherically relevant timescales and serve as a source of gas phase carbon, there is relatively little work describing underlying reaction mechanisms. The two general reaction pathways by which heterogeneous oxidation acts on OA are functionalization and fragmentation (Kroll et al., 2009). Functionalization reactions add oxygen-containing functional groups to the organic molecule, leading to higher molecular weight products and an increase in oxidation state. These reactions will increase the overall mass of OA and lead to lower volatility. On the other hand, fragmentation reactions result in molecules with lower carbon number that have the potential to volatilize, leading to a decrease in OA mass. This pathway for volatilization has been proposed as a potentially important mechanism to explain the concentrations of OA and VOCs aloft (Heald et al., 2011; Kwan et al., 2006). The relative importance of functionalization versus fragmentation depends critically on the fate of the organic peroxy radicals (RO_2) formed from OH reaction.

Identification of products from heterogeneous oxidation can be used to help identify specific reaction mechanisms and branching ratios between pathways; however, only a few studies have attempted to identify and/or quantify the products of heterogeneous oxidation. Carbonyls and alcohols have been identified as the major products formed in the particle phase (George et al., 2007; Hearn et al., 2007; McNeill et al., 2008; Renbaum & Smith, 2009; Ruehl et al., 2013). In the gas phase, small, oxygenated VOCs (OVOCs) such as carbonyls and carboxylic acids have been observed (McNeill et al., 2008; Molina et al., 2004; Slade & Knopf, 2013; Vlasenko et al., 2008). However, a detailed mechanistic understanding of these reactions and quantitative product yields from multiday aging of organic particles still lacking. In this work, we examine the heterogeneous oxidation of squalane, a saturated hydrocarbon, simultaneously monitoring the evolution of the

bulk particle phase composition while measuring speciated products in both the gas and particle phases using a pair of state-of-the-art proton transfer reaction mass spectrometers.

4.2 Methods

4.2.1 Experimental setup

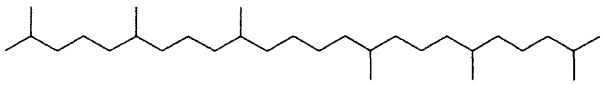

Figure 4-1. Squalane ($C_{30}H_{62}$). Model organic compound used to generate OA particles in this work. Commonly used as a proxy for reduced, primary OA.

Particles were heterogeneously oxidized in a 150 L environmental chamber constructed out of PFA (full setup shown in Fig. 4-2). A polydisperse distribution of inorganic seed particles was generated from a solution of ammonium sulfate (1.5 g/L in MilliQ water, washed with dichloromethane to remove organic contaminants) using a constant output atomizer (TSI aerosol generator 3076). The seed particles were dried (mean diameter = 140 nm) then passed over bed of liquid squalane ($C_{30}H_{62}$, Sigma Aldrich > 98%) contained in a Pyrex tube and heated to 100 °C (Thermo Scientific, TF55035A-1) to coat the particles with a layer of organic material. At this temperature, squalane is not expected to homogeneously nucleate; measured size distributions show a single mode, indicating squalane was indeed coated onto the seed particles rather than forming new particles.

Prior to the experiment, the chamber was flushed with clean air for one hour to remove any residual particulate matter and VOCs. Once the chamber was clean (OA < 0.1 $\mu g/m^3$), the furnace was heated and the coated particles were injected into the chamber over the course of 10 minutes, resulting in a maximum squalane concentration of 150 $\mu g/m^3$. The chamber was then allowed to equilibrate for an additional 10 minutes to characterize the unreacted particles and background chamber air. OH was generated by the photolysis of ozone (O_3), produced with a mercury pen-ray lamp (185 nm, Jelight Model 600 ozone generator) and continuously added to the chamber over the course of the experiment. 254 nm UV light was used to photolyze O_3 to $O(^1D)$, which subsequently reacts with water vapor (chamber RH = 40%) to form OH. After addition of particles and ozone to the chamber ($[O_3]$ = 1 ppm), a 254 nm UV lamp (UVP, LLC., XX-40S) outside the

chamber was turned on to initiate oxidation. During oxidation, the chamber was continuously diluted with clean air (semi-batch operation) while the particle composition, particle mass, and gas-phase composition were monitored.

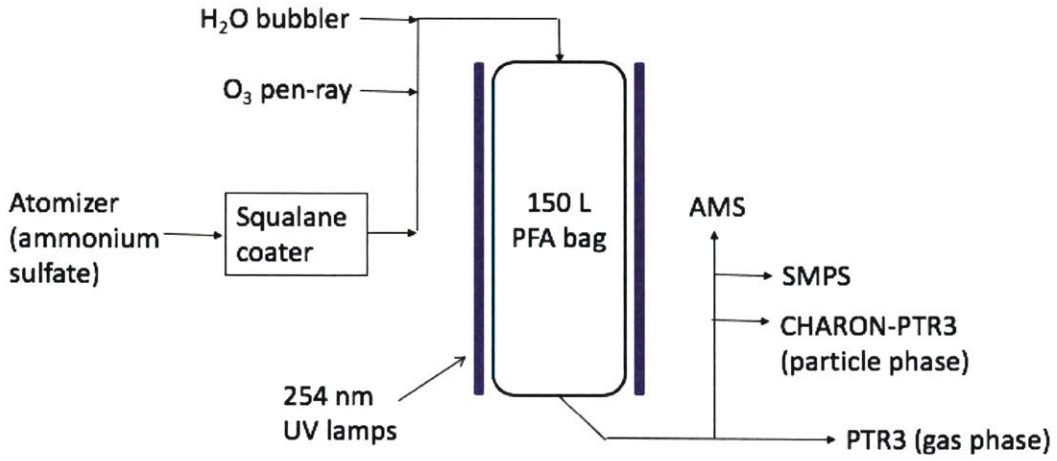

Figure 4-2. Experimental setup. Dry ammonium sulfate particles were coated with squalane then injected into the chamber. Particles were aged via heterogeneous oxidation by OH (ozone photolysis + water) and the composition was measured with an AMS, PTR3 (gas), and CHARON PTR3 (particle).

Gas phase products from heterogeneous oxidation were characterized by a PTR3, a recently developed proton transfer reaction time-of-flight mass spectrometer (PTR-MS) that shows high sensitivities over 10,000 cps $ppbv^{-1}$ (counts per second/parts per billion) for select compounds (Breitenlechner et al., 2017). Molecular products in the particle phase were measured with an additional PTR3 equipped with a CHARON (chemical analysis of aerosol online) inlet. Briefly, the CHARON inlet consists of a denuder to remove gas phase organics, and a heater that thermally vaporizes the particles for detection by PTR-MS (Müller et al., 2017). The loading and average composition of the particles were measured with an aerosol mass spectrometer (AMS, Aerodyne Research, Inc.). The AMS gives information on total organic mass and bulk elemental ratios such as oxygen-to-carbon (O/C) and hydrogen-to-carbon (H/C) for non-refractory particles with vacuum aerodynamic diameters between 70 nm and 1 μm (DeCarlo et al., 2006).

4.2.2 Data analysis

Data are presented in terms of OH exposure ([OH] x time), quantified through the measurement of an OH tracer, deuterated *n*-butanol (D9, 98%, Cambridge Isotope Laboratories). 40 μL of

deuterated butanol solution (1% in water) was added to the chamber during particle injection. During the period between tracer injection and oxidation, the decay of the tracer was used to quantify the dilution rate in the chamber. The dilution time constant was calculated to be 18 minutes, which is consistent with the estimated dilution rate based on the chamber volume and flow rates (Fig. A4-1). All gas phase species were then corrected for dilution using this time constant. The dilution corrected decay of deuterated butanol and its reaction rate coefficient with OH (k_{OH} = 3.4 x 10^{-12} cm^3 $molec^{-1}$ s^{-1}, Barmet et al., 2012) were then used to calculate the OH exposure up to 2 x 10^{12} molec cm^{-3} s. After this exposure, the tracer was essentially fully consumed and OH exposures beyond this were extrapolated up to 5 x 10^{12} molec cm^{-3} s with an exponential fit to the initial data (Fig. A4-2). The maximum OH exposure corresponds to 38 days of equivalent ambient OH exposure ([OH] = 1.5 x 10^6 molec cm^{-3}); this is longer than the typical residence time of most particles in the atmosphere, but useful for elucidating the products and lifecycle of particulate carbon in the atmosphere. OH concentrations in the chamber were on the order of 10^9 molecules cm^{-3}.

PTR3 peak fits were automatically generated by custom analysis software (PTRwid, IDL). 1659 peaks were fit in the gas phase and 1788 peaks were fit in the particle phase and were automatically assigned elemental formulas if a molecular formula match was found within 10 ppm (C, H, and O only). Peak-fit identifications were manually verified and additional peaks were identified during the manual inspection, resulting in 233 identified ions in the gas phase and 376 identified ions in the particle phase. All identified species detected by the PTR3 (gas and particle) were corrected for the mass-dependent efficiency of the mass spectrometer ($dcps(i) = cps(i) \cdot \sqrt{100/m_i}$). Duty-cycle corrected counts (dcps) were then normalized to the primary ion signal (H_3O^+) to yield normalized dcps (ndcps), then converted to concentration (ppb) by applying the measured acetone sensitivity (2.0 x 10^4 ndcps/ppb) for all species. Background concentrations were subtracted from all species by subtracting the concentration before oxidation – for species whose background concentrations change over the course of the experiment, the background concentration was interpolated over time then subtracted (Fig. A4-3).

Organic particle phase data from the AMS were analyzed using the ToF-AMS analysis toolkits (Squirrel version 1.57I, Pika version 1.16I). AMS data were corrected for dilution, wall loss, and

AMS collection efficiency by calculating the organic-to-sulfate ratio (Org/SO_4) scaled to the OA concentration at the start of the experiment (i.e., lights on) (Hildebrandt et al., 2009). OA concentrations were also corrected for squalane's unusually high relative ionization efficiency (RIE = 5.5), which was assumed to remain constant throughout the experiment. Bulk organic elemental ratios (O/C and H/C) were calculated using the "improved-ambient" method (Canagaratna et al., 2015). O/C ratio of unreacted particles matched the oxygen content of squalane (O/C = 0) and were used as calculated; H/C ratios were scaled (0.83x) so that the measured, unreacted particle H/C matched that the known H/C of squalane (H/C = 2.07).

4.3 Results and discussion

4.3.1 Evolution of bulk particle composition

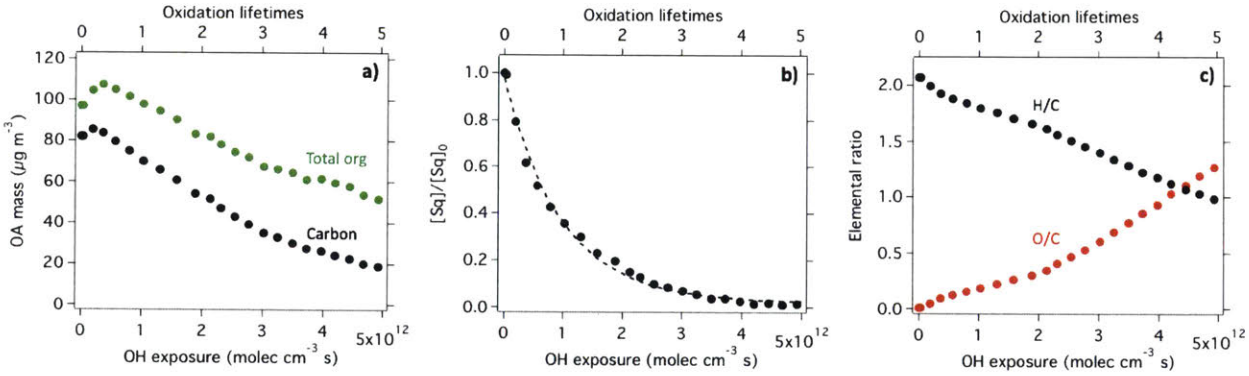

Figure 4-3. Changes to mass and composition of the squalane particles measured as a function of OH exposure (bottom axis) and oxidation lifetimes (top axis). **(a)** Change in total organic mass in green and carbon in black. **(b)** Change in squalane concentration normalized to initial squalane concentration ($[Sq]/[Sq]_0$). Dashed line is an exponential fit to the data, where the rate of decay (k) equals the second-order rate coefficient between particle phase squalane and OH (k^{II} = 1.02 x 10^{-12} cm^3 $molec^{-1}$ s^{-1}). **(c)** Calculated elemental ratios, H/C in black and O/C in red.

Figure 4-3 shows the changes in mass loading and composition of the squalane particles with oxidation. Initial (i.e., lights on) organic mass loading (m_{OA}) in the chamber was 97 μg m^{-3}. Total organic mass and elemental ratios, O/C and H/C, were used to calculate the mass of carbon using equation 1.

$$m_C = m_{OA} \times \frac{12}{12+16(O/C)+H/C} \quad (1)$$

Unreacted squalane is composed of 85% carbon and the thus the initial carbon mass in the chamber is 82 μg m^{-3}. When oxidation is initiated, initial organic mass and carbon mass increase slightly, likely due to condensation from squalane gas-phase oxidation forming a small amount of secondary organic aerosol. After this initial growth, both the organic and carbon mass decrease exponentially to final concentrations of 52 μg m^{-3} (46% organic loss) and 19 μg m^{-3} (77% carbon loss), respectively (Fig. 4-3a). The carbon lifetime with respect to loss from volatilization is 24 days. The unreacted squalane concentration (Fig. 4-3b), measured by tracking AMS fragment $C_8H_{17}^+$ (Smith et al., 2009), decreases exponentially over the course of the reaction and is essentially fully reacted away by the end of the experiment (99% reacted). Over the course of oxidation, O/C increases from 0 to 1.26 and H/C decreases from 2.07 to 0.98 (Fig. 4-3c). These changes in composition (mass and elemental ratios) are much greater than previously observed for the oxidation of pure squalane particles. For example, oxidation of pure squalane particles showed approximately 50% carbon loss and O/C up to 0.5 at very high OH exposures (Kroll et al., 2009); however, it is difficult to compare these sets of experiments based on OH exposure alone, since coated particles with higher organic surface area to volume ratios (SA/V) than pure particles are expected to react more rapidly (*Chapter 2*).

To compare the changes observed in this experiment with previous work, particle composition is compared on the basis of squalane oxidation lifetimes rather than OH exposure to remove the kinetic dependence on organic SA/V. Squalane oxidation lifetime is a measure of the number of reactions each squalane molecule has undergone (i.e., $[Sq]/[Sq]_0 = 1/e$ at 1 oxidation lifetime) and can be calculated as ([OH] x t) / τ, where τ is the kinetic lifetime of squalane ($1/k^{II}$). k^{II} is the second-order rate coefficient of squalane with OH and calculated in this experiment to be 1.02 x 10^{-12} cm^3 $molec^{-1}$ s^{-1} by fitting the normalized $C_8H_{17}^+$ signal ($[Sq]/[Sq]_0$) vs. OH exposure to an exponential function (Smith et al., 2009). In this experiment, 1 oxidation lifetime is thus equivalent to an OH exposure of 1.02 x 10^{12} molec cm^{-3} s and oxidation lifetimes calculated range from 0 to 5 (top axes in Fig. 4-3). After converting the x-axis to lifetimes, the data presented in this work can be compared to data from previous flow tube studies (Kroll et al., 2009; Smith et al., 2009) over lifetimes from 0 to 2 where a significant fraction of squalane still remains in the particles (Fig 4-4). The current study still shows enhanced changes in composition with significant carbon loss (35% loss, compared with no carbon loss in previous work) and O/C ratio approximately 3 times

greater after 2 oxidation lifetimes. Flow tube studies showed that a single oxygen was added per squalane + OH reaction; the more rapid increase in O/C observed here suggests that secondary condensed phase chemistry may be playing a role. OH concentration is also expected to have an effect on rates of oxidation. Lower radical and radical precursor (i.e., ozone) concentrations have been proposed to lead to greater oxidant uptake and faster oxidation kinetics (Chim et al., 2018; Renbaum & Smith, 2011; Slade & Knopf, 2014); however, the radical concentrations used here are unlikely fully account for the differences observed since previous experiments have used OH concentrations lower than this but did not see equivalent enhancements in oxidation (Che et al., 2009). The more rapid composition changes in this work could be due to differences in experimental setup, for example, the difference between flow tube steady-state experiments and chambers with continuous dilution. The absolute OA concentrations in each reactor could also play a role in the observed differences, with lower concentrations leading to volatilization of compounds with higher saturation vapor concentrations. The reasons for these discrepancies are not completely clear and require further study.

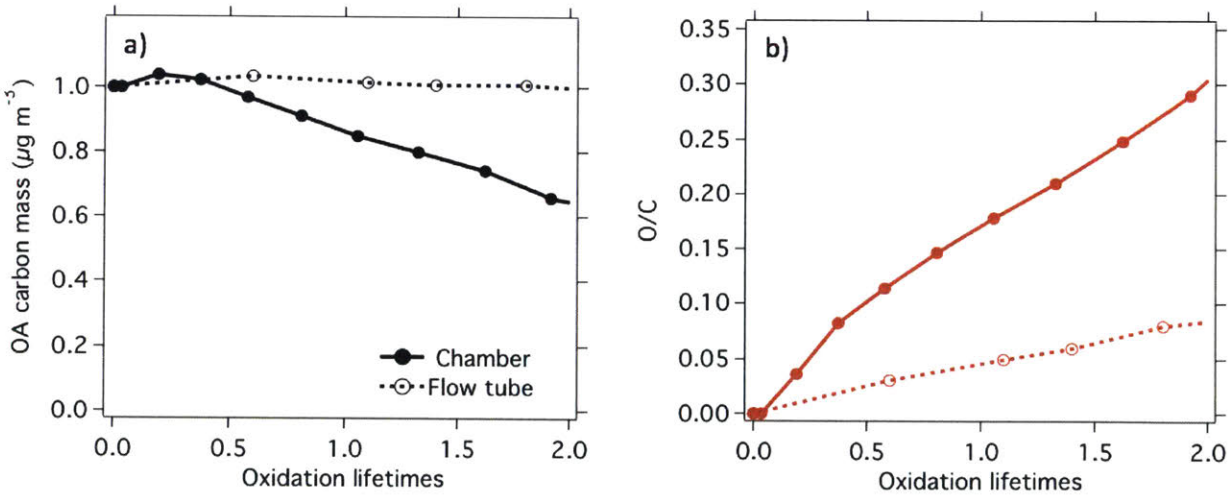

Figure 4-4. Comparison of **(a)** carbon mass and **(b)** O/C between chamber squalane oxidation (present study, solid lines and markers) and previous flow tube studies (dashed lines and open markers) (Kroll et al., 2009; Smith et al., 2009). Data are only shown for lifetimes less than or equal to 2, where a significant concentration of squalane still exists in the particle phase.

4.3.2 Products of oxidation

The loss of carbon mass seen in the particle phase indicates the formation of products more volatile than squalane that are lost to the gas phase. In terms of carbon mass, the two most abundant ions

observed in the gas phase during oxidation are $C_3H_6OH^+$ (nominal mass 59.050) and $C_{11}H_{24}OH^+$ (nominal mass 173.191). These two ions correspond to a C_3 carbonyl (C_3H_6O, acetone or propionaldehyde) and a C_{11} alcohol ($C_{11}H_{24}O$, undecanol), respectively.

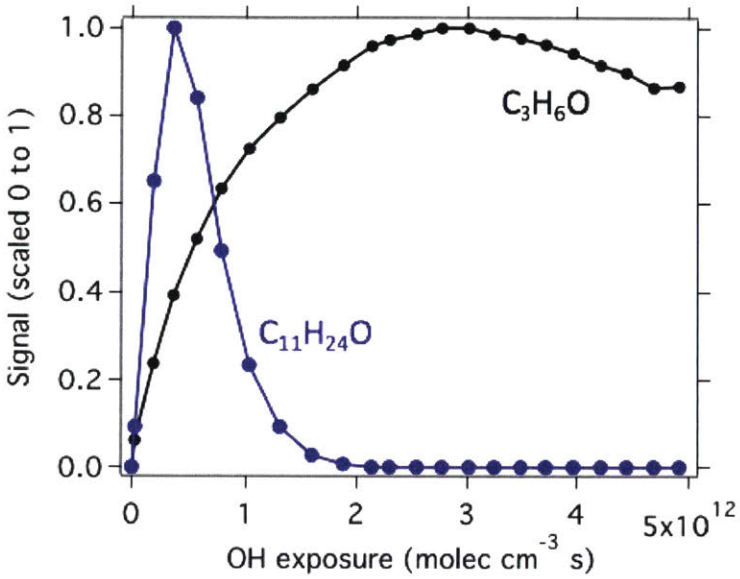

Figure 4-5. C_3H_6O (black) and $C_{11}H_{24}O$ (blue) formation observed in the gas phase. Data are corrected for chamber dilution, background subtracted, and scaled from 0 to 1 for comparison. Maximum concentration of C_3H_6O corresponds to 6.3 μg C m^{-3} and maximum in $C_{11}H_{24}O$ corresponds to 3.6 μg C m^{-3} in the chamber.

The maximum concentrations of these two ions reach 6.3 μg C m^{-3} for C_3H_6O and 3.6 μg C m^{-3} for $C_{11}H_{24}O$ (Fig. 4-5) – no other ions show a concentration greater than 0.7 μg C m^{-3} in the chamber. The concentrations of C_3H_6O and $C_{11}H_{24}O$ evolve very differently in the chamber. C_3H_6O grows in with increasing OH exposure, levels off, then shows a slight decrease. In contrast, $C_{11}H_{24}O$ grows in more quickly, reaches a maximum, then decays back to zero. The differences between the observed concentrations of these two ions are indicative of secondary chemistry; in other words, these two products are still susceptible to reaction and loss by OH. The effect of subsequent OH reaction on the formation of an oxidation product can be corrected for by fitting a line to the initial formation of the product as a function of squalane loss (Fig. 4-6), assuming the product is a first-generation product (Atkinson et al., 1982). Product yield corrections for C_3H_6O and $C_{11}H_{24}O$ indicate that the true amounts of these species formed over the course of the experiment are 6.6 μg C m^{-3} and 9.7 μg C m^{-3}, respectively. The small correction in C_3H_6O implies

a long-lived species, meaning that this product is likely to be acetone (k_{OH} = 2.19 x 10^{-13} cm^3 $molec^{-1}$ s^{-1}, Demore et al., 1997) rather than propionaldehyde (k_{OH} = 1.99 x 10^{-11} cm^3 $molec^{-1}$ s^{-1}, Atkinson et al., 2006). The much larger correction calculated for $C_{11}H_{24}O$ is consistent with the OH reaction rate coefficient of a long-chain alcohol (k_{OH} (octanol) = 1.44 x 10^{-11} cm^3 $molec^{-1}$ s^{-1}, Nelson et al., 1990).

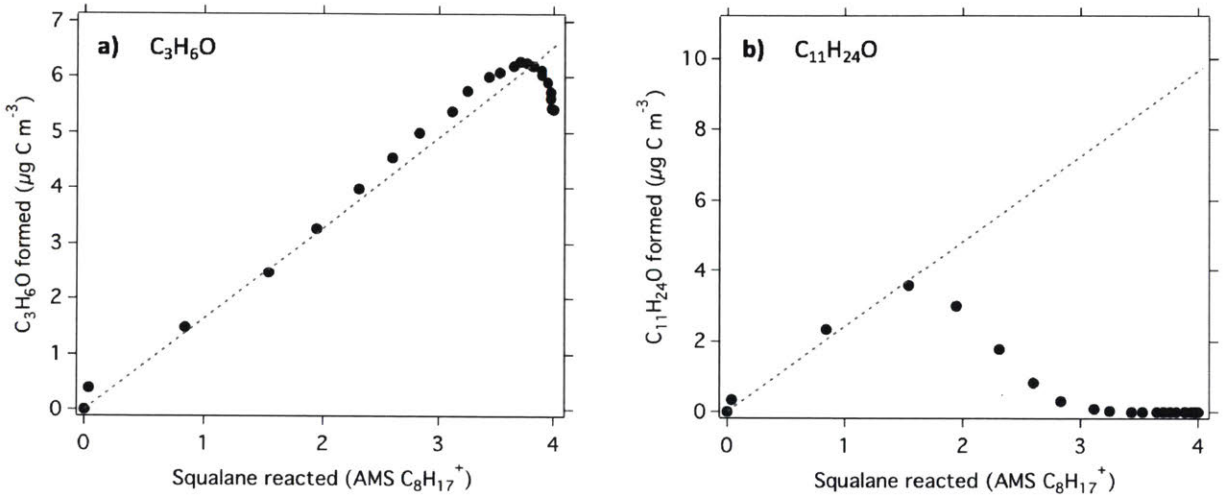

Figure 4-6. Two major gas phase products of heterogeneous oxidation of squalane, **(a)** C_3H_6O and **(b)** $C_{11}H_{24}O$, plotted against squalane reacted. Dotted lines are linear fits (least-squares) to the first 4 data points indicating integrated formation of these two products after correcting for OH-product reaction. C_3H_6O shows a minor correction indicating a product with slow OH reaction rate coefficient; slight increase in measured concentration (circles) over corrected concentration (fit) suggests some secondary formation. $C_{11}H_{24}O$ shows a large correction indicating significant reactive loss due to OH.

The observed oxidation products can also provide information about the reaction mechanism of heterogeneous squalane oxidation. Since C_3H_6O (acetone) and $C_{11}H_{24}O$ (undecanol) formation are linear with squalane loss, they are primary products (i.e., formed from a single reaction of squalane with OH) and reasonable formation mechanisms can be described that follow the known possible reaction pathways for OH oxidation of saturated organic compounds (Fig. 4-7). Acetone formation is proposed to come from H-abstraction from a tertiary carbon to form an alkyl radical (Atkinson, 1997). O_2 rapidly reacts with this radical to form a tertiary peroxy radical (RO_2). Due to the lack of α-hydrogens (hydrogen associated with the carbon atom directly bonded to oxygen) for tertiary peroxy radical species, RO_2 most likely forms an alkoxy radical (RO) which then undergoes carbon-carbon bond breakage to give acetone and a C_{27} alkyl radical which will react further.

Formation of undecanol is likely initiated by a similar reaction mechanism, H-abstraction from a tertiary carbon then C-C bond breakage to form a C_{11} alkyl radical (Fig. 4-7b). The C_{11} alkyl radical then forms RO_2, then RO, which subsequently abstracts a hydrogen from a neighboring molecule to give the C_{11} alcohol species and propagating the radical chain. In addition to the proposed reaction pathways, acetone and undecanol could also potentially be formed from RO_2 + RO_2 reactions of primary or secondary peroxy radicals (Russell, 1957; Bennett & Summers, 1974)

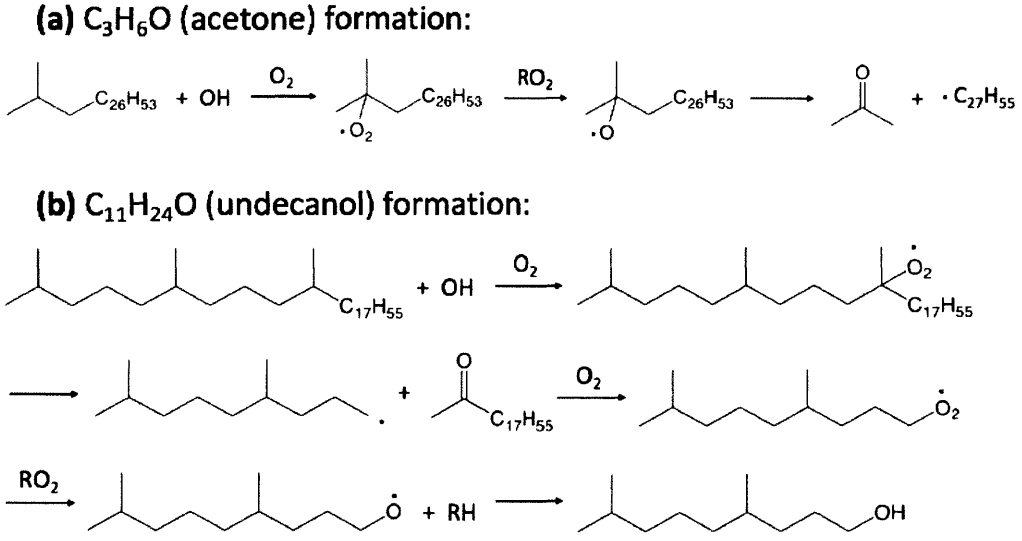

Figure 4-7. Proposed reaction mechanisms for formation of **(a)** acetone and **(b)** undecanol.

Observations of a higher abundance of ketones than alcohols in the particle phase in previous studies have suggested that the Russell mechanism is not dominant, as it is in the bulk condensed phase, and that Bennett-Summers or O_2 reactions play major roles at particle surfaces (George et al., 2007; Hearn et al., 2007). These mechanisms are supported by the observation of H_2O_2 in the gas phase, a byproduct of the Bennett-Summers reaction, and the dependence of ketone formation on O_2 concentration. Likewise, in the present experiment, acetone is likely generated from one of these two pathways. While we do not measure the H_2O_2 or examine the dependence of acetone formation with O_2 concentration, acetone generation by the Russell mechanism would also form a C_3 alcohol which is not observed. However, although we do not see evidence for RO_2 self-reaction, we cannot rule out the reaction between two different RO_2 species (cross-reaction) to form acetone (Madronich & Calvert, 1990). In the formation of undecanol, as in the case of acetone, we do not observe significant yield of the partner product (C_{11} carbonyl) that would be expected if a Russell

mechanism was operational. We take this as evidence that the formation of undecanol goes through an alkoxy radical intermediate which abstracts a hydrogen from another molecule (bottom reaction in Fig 4-7). This secondary oxidation of RH by RO is further supported by the fast oxidation observed (more than 1 oxygen added per oxidation of squalane). Regardless of the exact reaction pathway, fragmentation from alkoxy radical formation is central to the evolution of OA composition in this system and occurs even at low O/C.

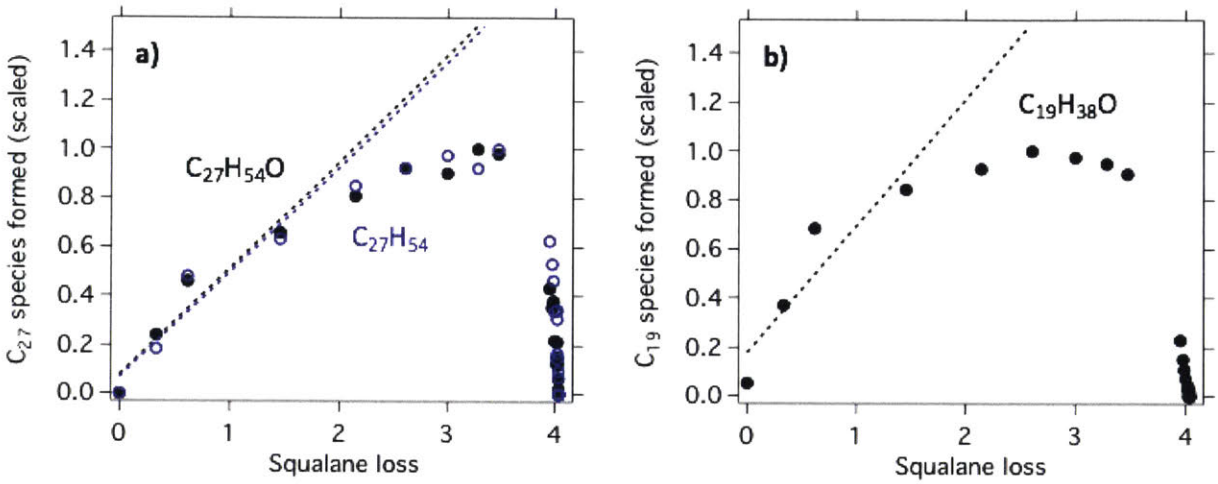

Figure 4-8. Particle phase measurements of selected **(a)** C_{27} and **(b)** C_{19} species as a function of squalane loss. Both $C_{27}H_{54}$, $C_{27}H_{54}O$, and other species (not shown) are identified for compounds with $n_C = 27$, while only $C_{19}H_{38}O$ is identified for $n_C = 19$. Lines are fits to initial formation of ion vs. squalane loss indicating they are first generation species. Both CHARON and AMS data are not corrected for dilution or wall loss here.

The products of fragmentation reactions are also seen in the particle phase and can further support the proposed mechanisms. For example, first-generation acetone formation simultaneously forms C_{27} radical species which can react to form stable products and likely remain in the particle phase due the size and low vapor pressure of potential products. Similarly, a C_{19} ketone should be formed from the fragmentation of the squalane backbone to give the C_{11} alcohol product observed in the gas phase. Indeed, we do observe multiple C_{27} species in the particle phase that are formed with oxidation (Fig. 4-8a). $C_{27}H_{54}$ (potential alcohol dehydration product formed in the CHARON inlet, $C_{27}H_{56}O - H_2O$), $C_{27}H_{54}O$ (carbonyl), and other ions are identified with $n_C = 27$. The observation of alcohol and carbonyl products is not surprising as the formation of the C_{27} alkyl radical (pathway 2) gives a peroxy radical that can potentially react via multiple RO_2 pathways described above. If

all acetone formation was via pathway 1, then only the aldehyde product would be observed. In contrast, in the previously described mechanism for formation of undecanol, the C_{19} carbonyl is a direct product from the fragmentation of squalane and is supported by the lack of C_{19} alcohol formation (Fig. 4-8b).

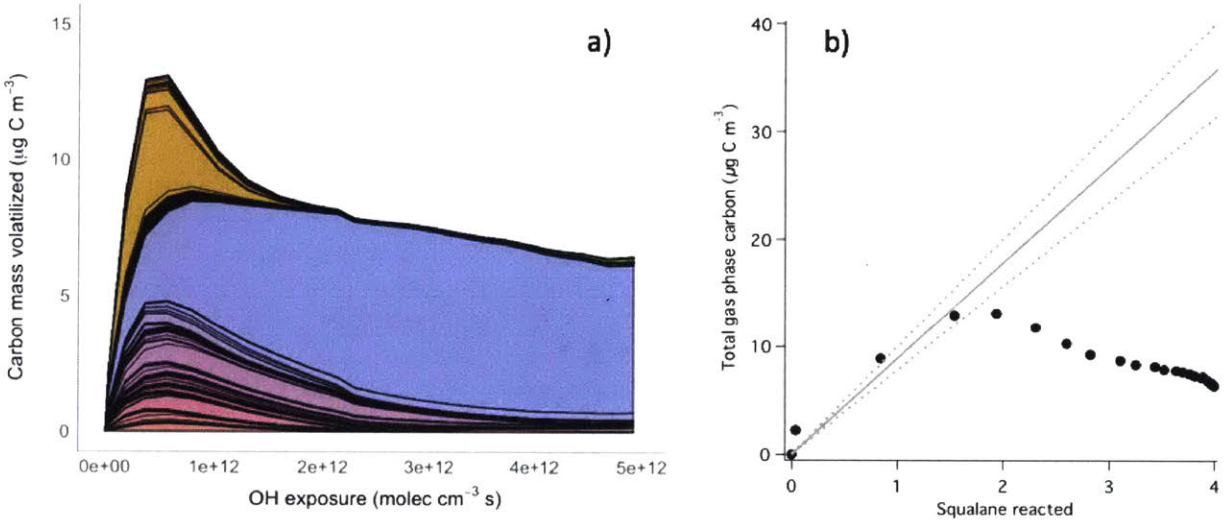

Figure 4-9. (a) Total gas phase carbon measured in the chamber (colors are arbitrary). **(b)** Yield correction for total gas phase carbon produced as a function of squalane reacted. Solid line is linear fit to the first 4 data points (through origin). Dashed lines are +/- 1 the standard error in the fit slope.

Thus far, we have described the formation of the major species in the gas phase (acetone and undecanol) and mechanistically related ions in the particle phase. However, many more ions were measured and identified amounting to a substantial amount of carbon. In the chamber, the concentration of gas phase carbon peaks at ~13 μg C m^{-3} then decays and levels off to ~8 μg C. m^{-3} (Fig. 4-9a). Using the approach for corrected the gas phase yield of acetone and undecanol for OH reaction, the total amount of gas phase carbon is corrected for reaction to determine the total gas phase carbon yield from the heterogeneous oxidation of squalane (Fig. 4-9b). This leads to large correction in the gas phase carbon yield, likely because most VOCs react with OH much more quickly than acetone. After correction, 36 ± 7 μg C m^{-3} ($\pm 1\sigma$) is volatilized from the squalane particles over the course of the experiment (Fig. 4-10). Using the acetone sensitivity for all ions, the estimate accounts for 57% of the 63 μg C m^{-3} lost from the particle phase. However, the estimate for carbon volatilized based on gas phase measurements is likely a lower limit because

the PTR3 can have lower sensitivity to other ions relative to acetone and CO and CO_2 were not measured.

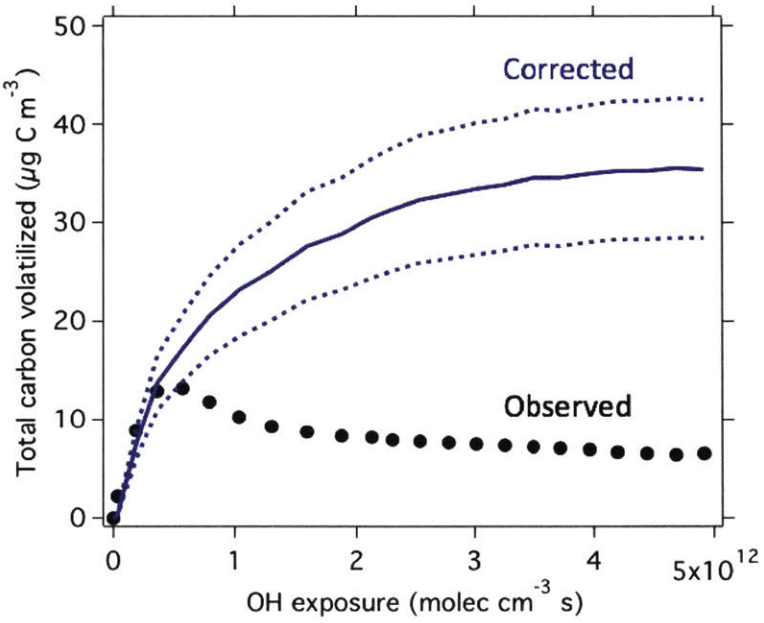

Figure 4-10. Total gas phase carbon measured by PTR-MS as a function of OH exposure. Black markers are concentrations observed in the chamber. All identified ions were summed to get total observed signal. Solid blue line is the gas phase carbon concentration corrected for reaction with OH (see Fig. 4-9b) and dashed lines correspond to $\pm 1\sigma$ in the linear fit slope between total carbon and squalane loss.

4.4 Conclusions

In this work we observe the rapid oxidation of squalane particles resulting in the loss of 77% (63 μg C m^{-3} loss) of the carbon mass and an O/C of +1.4 after an OH exposure equivalent to 38 days of atmospheric aging. Under these experimental conditions, this corresponds to a carbon lifetime due to volatilization of 24 days. The changes in composition and mass loss seen here are in contrast with previous squalane aging studies using flow tube reactors and suggests that fragmentation reactions are much more important under the reaction conditions probed in this study. The reason for this difference is unclear, but may be related to differences in experimental conditions such as the difference in OH concentrations or differences between steady-state flow reactors and semi-batch chamber experiments. Future careful studies of heterogeneous oxidation using a wider variety of precursors and experimental conditions will be necessary to understand the

discrepancies between flow tube heterogeneous oxidation studies and those performed in chambers.

Speciated gas phase measurements identified acetone and undecanol as the major volatilized products of oxidation; these products account for nearly half of the observed gas phase carbon. This suggests that although there are many possibilities for reaction and many ions are detected, the product distribution is relatively simple. Identification of first-generation C_{27} and C_{19} species in the particle phase confirms that these VOCs are first-generation products resulting from the fragmentation of squalane. Summing the total observed gas phase carbon and correcting for reactive OH loss gives a total gas phase carbon yield of 36 μg C m^{-3} over the course of the experiment. Over half (57%) of the carbon lost from the particle phase is accounted for by speciated gas phase measurements, but small, highly oxygenated products (as well as CO and CO_2) are unlikely to be detected in this experiment and may preclude the possibility of measuring carbon closure if those are significant products from squalane oxidation. Importantly, the method used for correcting VOC concentration for OH reaction is based on correcting primary products of OH and squalane. Thus, these yields reflect primary products and may not be representative of the end products of squalane oxidation that involve secondary gas phase chemistry (e.g., undecanol + OH).

Although previous results have suggested that fragmentation reactions only become important for compounds with moderately high oxygenation (O/C ~ 0.4) (Kroll et al., 2009), the results from this experiment show that fragmentation reactions can be important for organic compounds that do not have any oxygen-containing functional groups. In particular, molecules with tertiary carbons that are not contained in a ring structure are highly susceptible to fragmentation and subsequent volatilization of carbon mass. Furthermore, peroxy radicals at tertiary carbons are likely to form alkoxy radicals which, in addition to fragmentation, can propagate radical chain chemistry leading to enhanced oxidation rates. These results suggest that heterogeneous oxidation can be important to the overall lifetime time of OA and can serve as an efficient source of OVOCs, especially for particles with in remote regions of the atmosphere or those with long depositional lifetimes (i.e., in the free troposphere). Aircraft studies specifically targeting long-term aging of OA would be useful to help constrain the effect of heterogeneous oxidation on ambient particles.

4.5 Acknowledgements

The author would like to acknowledge Martin Breitenlechner, Alexander Zaytsev, and Abigail Koss for assistance with PTR-MS operation and analysis.

4.6 References

Atkinson, R. (1997). Gas-Phase Tropospheric Chemistry of Volatile Organic Compounds: 1. Alkanes and Alkenes. *Journal of Physical and Chemical Reference Data*, *26*(2), 215–277. Retrieved from http://scitation.aip.org/content/aip/journal/jpcrd/26/2/10.1063/1.556012

Atkinson, R. (2007). Rate constants for the atmospheric reactions of alkoxy radicals: An updated estimation method. *Atmospheric Environment*, *41*(38), 8468–8485. Retrieved from http://linkinghub.elsevier.com/retrieve/pii/S1352231007006152

Atkinson, R., Aschmann, S. M., Carter, W. P. L., Winer, A. M., & Pitts, J. N. (1982). Alkyl nitrate formation from the nitrogen oxide (NOx)-air photooxidations of C2-C8 n-alkanes. *The Journal of Physical Chemistry*, *86*(23), 4563–4569. https://doi.org/10.1021/j100220a022

Atkinson, R., Baulch, D. L., Cox, R. A., Crowley, J. N., Hampson, R. F., Hynes, R. G., et al. (2006). Evaluated kinetic and photochemical data for atmospheric chemistry: Volume II – gas phase reactions of organic species. *Atmospheric Chemistry and Physics*, *6*(11), 3625–4055. https://doi.org/10.5194/acp-6-3625-2006

Balkanski, Y. J., Jacob, D. J., Gardner, G. M., Graustein, W. C., & Turekian, K. K. (1993). Transport and residence times of tropospheric aerosols inferred from a global three-dimensional simulation of 210Pb. *Journal of Geophysical Research*, *98*(D11), 20573. Retrieved from http://doi.wiley.com/10.1029/93JD02456

Barmet, P., Dommen, J., DeCarlo, P. F., Tritscher, T., Praplan, A. P., Platt, S. M., et al. (2012). OH clock determination by proton transfer reaction mass spectrometry at an environmental chamber. *Atmospheric Measurement Techniques*, *5*(3), 647–656. https://doi.org/10.5194/amt-5-647-2012

Bennett, J. E., & Summers, R. (1974). Product Studies of Mutual Termination Reactions of Sec-Alkylperoxy Radicals - Evidence for Non-Cyclic Termination. *Can. J. Chem.*, *52*, 1377–1379. https://doi.org/10.1139/v74-209

Breitenlechner, M., Fischer, L., Hainer, M., Heinritzi, M., Curtius, J., & Hansel, A. (2017). PTR3: An Instrument for Studying the Lifecycle of Reactive Organic Carbon in the Atmosphere. *Analytical Chemistry*, *89*(11), 5824–5831. https://doi.org/10.1021/acs.analchem.6b05110

Canagaratna, M. R., Jimenez, J. L., Kroll, J. H., Chen, Q., Kessler, S. H., Massoli, P., et al. (2015). Elemental ratio measurements of organic compounds using aerosol mass

spectrometry: characterization, improved calibration, and implications. *Atmospheric Chemistry and Physics*, *15*(1), 253–272. Retrieved from http://www.atmos-chem-phys.net/15/253/2015/

Chan, M. N., Zhang, H., Goldstein, A. H., & Wilson, K. R. (2014). Role of Water and Phase in the Heterogeneous Oxidation of Solid and Aqueous Succinic Acid Aerosol by Hydroxyl Radicals. *The Journal of Physical Chemistry C*, *118*(50), 28978–28992. Retrieved from http://pubs.acs.org/doi/abs/10.1021/jp5012022

Che, D. L., Smith, J. D., Leone, S. R., Ahmed, M., & Wilson, K. R. (2009). Quantifying the reactive uptake of OH by organic aerosols in a continuous flow stirred tank reactor. *Physical Chemistry Chemical Physics*, *11*(36), 7813–7885. Retrieved from http://xlink.rsc.org/?DOI=b904418c

Chim, M. M., Lim, C. Y., Kroll, J. H., & Chan, M. N. (2018). Evolution in the Reactivity of Citric Acid toward Heterogeneous Oxidation by Gas-Phase OH Radicals. *ACS Earth and Space Chemistry*, acsearthspacechem.8b00118, .https://doi.org/10.1021/acsearthspacechem.8b00118

DeCarlo, P. F., Kimmel, J. R., Trimborn, A., Northway, M. J., Jayne, J. T., Aiken, A. C., et al. (2006). Field-Deployable, High-Resolution, Time-of-Flight Aerosol Mass Spectrometer. *Analytical Chemistry*, *78*(24), 8281–8289. Retrieved from http://pubs.acs.org/doi/abs/10.1021/ac061249n

Demore, W. B., Howard, C. J., Sander, S. P., Ravishankara, A. R., Golden, D. M., Kolb, C. E., et al. (1997). Chemical Kinetics and Photochemical Data for Use in Stratospheric Modeling Evaluation Number 12 NASA Panel for Data Evaluation, (12). Retrieved from https://jpldataeval.jpl.nasa.gov/pdf/Atmos97_Anotated.pdf

George, I. J., & Abbatt, J. P. D. (2010). Heterogeneous oxidation of atmospheric aerosol particles by gas-phase radicals. *Nature Publishing Group*, *2*(9), 713–722. Retrieved from http://dx.doi.org/10.1038/nchem.806

George, I. J., Vlasenko, A., Slowik, J. G., Broekhuizen, K., & Abbatt, J. P. D. (2007). Heterogeneous oxidation of saturated organic aerosols by hydroxyl radicals: uptake kinetics, condensed-phase products, and particle size change. *Atmospheric Chemistry and Physics*, *7*(16), 4187–4201. Retrieved from http://www.atmos-chem-phys.net/7/4187/2007/

Hallquist, M., Wenger, J. C., Baltensperger, U., Rudich, Y., Simpson, D., Claeys, M., et al. (2009). The formation, properties and impact of secondary organic aerosol: current and emerging issues. *Atmospheric Chemistry and Physics Discussions*, *9*(1), 3555–3762. Retrieved from http://www.atmos-chem-phys-discuss.net/9/3555/2009/

Heald, C. L., Coe, H., Jimenez, J. L., Weber, R. J., Bahreini, R., Middlebrook, A. M., et al. (2011). Exploring the vertical profile of atmospheric organic aerosol: Comparing 17 aircraft field campaigns with a global model. *Atmospheric Chemistry and Physics*, *11*(24), 12676–12696. https://doi.org/10.5194/acp-11-12673-2011

Hearn, J. D., & Smith, G. D. (2006). A mixed-phase relative rates technique for measuring aerosol reaction kinetics. *Geophysical Research Letters*, *33*(17), 3–7. https://doi.org/10.1029/2006GL026963

Hearn, J. D., Renbaum, L. H., Wang, X., & Smith, G. D. (2007). Kinetics and products from reaction of Cl radicals with dioctyl sebacate (DOS) particles in O2: A model for radical-initiated oxidation of organic aerosols. *Physical Chemistry Chemical Physics*, *9*(34), 4803–4813. https://doi.org/10.1039/b707523e

Hildebrandt, L., Donahue, N. M., & Pandis, S. N. (2009). High formation of secondary organic aerosol from the photo-oxidation of toluene. *Atmospheric Chemistry and Physics Discussions*, *9*(1), 693–733. Retrieved from http://www.atmos-chem-phys-discuss.net/9/693/2009/

Kessler, S. H., Smith, J. D., Che, D. L., Worsnop, D. R., Wilson, K. R., & Kroll, J. H. (2010). Chemical Sinks of Organic Aerosol: Kinetics and Products of the Heterogeneous Oxidation of Erythritol and Levoglucosan. *Environmental Science & Technology*, *44*(18), 7005–7010. Retrieved from http://pubs.acs.org/doi/abs/10.1021/es101465m

Kessler, S. H., Nah, T., Daumit, K. E., Smith, J. D., Leone, S. R., Kolb, C. E., et al. (2012). OH-Initiated Heterogeneous Aging of Highly Oxidized Organic Aerosol. *The Journal of Physical Chemistry A*, *116*(24), 6358–6365. Retrieved from http://pubs.acs.org/doi/abs/10.1021/jp212131m

Kroll, J. H., & Seinfeld, J. H. (2008). Chemistry of secondary organic aerosol: Formation and evolution of low-volatility organics in the atmosphere. *Atmospheric Environment*, *42*(16), 3593–3624. Retrieved from http://linkinghub.elsevier.com/retrieve/pii/S1352231008000253

Kroll, J. H., Smith, J. D., Che, D. L., Kessler, S. H., Worsnop, D. R., & Wilson, K. R. (2009). Measurement of fragmentation and functionalization pathways in the heterogeneous oxidation of oxidized organic aerosol. *Physical Chemistry Chemical Physics*, *11*(36), 8005. Retrieved from http://xlink.rsc.org/?DOI=b905289e

Kroll, J. H., Donahue, N. M., Jimenez, J. L., Kessler, S. H., Canagaratna, M. R., Wilson, K. R., et al. (2011). Carbon oxidation state as a metric for describing the chemistry of atmospheric organic aerosol. *Nature Chemistry*, *3*(2), 133–139. https://doi.org/10.1038/nchem.948

Kroll, J. H., Lim, C. Y., Kessler, S. H., & Wilson, K. R. (2015). Heterogeneous Oxidation of Atmospheric Organic Aerosol: Kinetics of Changes to the Amount and Oxidation State of Particle-Phase Organic Carbon. *The Journal of Physical Chemistry A*, *119*(44), 10767–10783. Retrieved from http://pubs.acs.org/doi/10.1021/acs.jpca.5b06946

Kwan, A. J., Crounse, J. D., Clarke, A. D., Shinozuka, Y., Anderson, B. E., Crawford, J. H., et al. (2006). On the flux of oxygenated volatile organic compounds from organic aerosol oxidation. *Geophysical Research Letters*, *33*(15), 1–5. https://doi.org/10.1029/2006GL026144

Lambe, A. T., Zhang, J., Sage, A. M., & Donahue, N. M. (2007). Controlled OH Radical

Production via Ozone Alkene Reactions for Use in Aerosol Aging Studies. *Environmental Science and Technology*, *41*(7), 2357–2363. https://doi.org/10.1021/es061878e

Lambe, A. T., Miracolo, M. a, Hennigan, C. J., Robinson, A. L., & Donahue, N. M. (2009). Effective Rate Constants and Uptake Organic Molecular Markers in Motor Oil and Diesel Primary Radicals. *Environmental Science & Technology*, *43*(23), 8794–8800. https://doi.org/10.1021/es901745h

Lim, C. Y., Browne, E. C., Sugrue, R. A., & Kroll, J. H. (2017). Rapid heterogeneous oxidation of organic coatings on submicron aerosols. *Geophysical Research Letters*, *44*(6), 2949–2957. https://doi.org/10.1002/2017GL072585

Madronich, S., & Calvert, J. G. (1990). Permutation reactions of organic peroxy radicals in the troposphere. *Journal of Geophysical Research*, *95*(D5), 5697–5715. https://doi.org/10.1029/JD095iD05p05697

McNeill, V. F., Yatavelli, R. L. N., Thornton, J. a., Stipe, C. B., & Landgrebe, O. (2008, March 17). The heterogeneous OH oxidation of palmitic acid in single component and internally mixed aerosol particles: vaporization, secondary chemistry, and the role of particle phase. *Atmospheric Chemistry and Physics Discussions*. https://doi.org/10.5194/acpd-8-6035-2008

Molina, M. J., Ivanov, A. V, Trakhtenberg, S., & Molina, L. T. (2004). Atmospheric evolution of organic aerosol. *Geophysical Research Letters*, *31*(22), L22104-5. Retrieved from http://doi.wiley.com/10.1029/2004GL020910

Müller, M., Eichler, P., D'Anna, B., Tan, W., & Wisthaler, A. (2017). Direct Sampling and Analysis of Atmospheric Particulate Organic Matter by Proton-Transfer-Reaction Mass Spectrometry. *Analytical Chemistry*, *89*(20), 10889–10897. https://doi.org/10.1021/acs.analchem.7b02582

Nah, T., Kessler, S. H., Daumit, K. E., Kroll, J. H., Leone, S. R., & Wilson, K. R. (2014). Influence of Molecular Structure and Chemical Functionality on the Heterogeneous OH-Initiated Oxidation of Unsaturated Organic Particles. *The Journal of Physical Chemistry A*, *118*(23), 4106–4119. Retrieved from http://pubs.acs.org/doi/abs/10.1021/jp502666g

Nelson, L., Rattigan, O., Neavyn, R., Sidebottom, H., Treacy, J., & Nielsen, O. J. (1990). Absolute and relative rate constants for the reactions of hydroxyl radicals and chlorine atoms with a series of aliphatic alcohols and ethers at 298 K. *Int. J. Chem. Kin.*, *22*(11), 1111. https://doi.org/10.1002/kin.550221102

Renbaum, L. H., & Smith, G. D. (2009). The importance of phase in the radical-initiated oxidation of model organic aerosols: reactions of solid and liquid brassidic acid particles. *Physical Chemistry Chemical Physics*, *11*(14), 2411–2441. Retrieved from http://xlink.rsc.org/?DOI=b816799k

Renbaum, L. H., & Smith, G. D. (2011). Artifacts in measuring aerosol uptake kinetics: The roles of time, concentration and adsorption. *Atmospheric Chemistry and Physics*, *11*(14), 6881–6893. https://doi.org/10.5194/acp-11-6881-2011

Ruehl, C. R., Nah, T., Isaacman, G., Worton, D. R., Chan, A. W. H., Kolesar, K. R., et al. (2013). The influence of molecular structure and aerosol phase on the heterogeneous oxidation of normal and branched alkanes by OH. *Journal of Physical Chemistry A*, *117*(19), 3990–4000. https://doi.org/10.1021/jp401888q

Russell, G. A. (1957). Deuterium-isotope Effects in the Autoxidation of Aralkyl Hydrocarbons. Mechanism of the Interaction of PEroxy Radicals 1. *Journal of the American Chemical Society*, *79*(14), 3871–3877. https://doi.org/10.1021/ja01571a068

Slade, J. H., & Knopf, D. A. (2013). Heterogeneous OH oxidation of biomass burning organic aerosol surrogate compounds: Assessment of volatilisation products and the role of OH concentration on the reactive uptake kinetics. *Physical Chemistry Chemical Physics*, *15*(16), 5898–5915. https://doi.org/10.1039/c3cp44695f

Slade, J. H., & Knopf, D. A. (2014). Multiphase OH oxidation kinetics of organic aerosol: The role of particle phase state and relative humidity. *Geophysical Research Letters*, *41*(14), 5297–5306. https://doi.org/10.1002/2014GL060582

Smith, J. D., Kroll, J. H., Cappa, C. D., Che, D. L., Liu, C. L., Ahmed, M., et al. (2009b). The heterogeneous reaction of hydroxyl radicals with sub-micron squalane particles: A model system for understanding the oxidative aging of ambient aerosols. *Atmospheric Chemistry and Physics*, *9*(9), 3209–3222. https://doi.org/10.5194/acp-9-3209-2009

Vlasenko, A., George, I. J., & Abbatt, J. P. D. (2008). Formation of volatile organic compounds in the heterogeneous oxidation of condensed-phase organic films by gas-phase OH. *Journal of Physical Chemistry A*, *112*(7), 1552–1560. https://doi.org/10.1021/jp0772979

Worsnop, D. R. (2002). A chemical kinetic model for reactive transformations of aerosol particles. *Geophysical Research Letters*, *29*(20), 19–22. https://doi.org/10.1029/2002GL015542

Zhang, Q., Jimenez, J. L., Canagaratna, M. R., Allan, J. D., Coe, H., Ulbrich, I., et al. (2007). Ubiquity and dominance of oxygenated species in organic aerosols in anthropogenically-influenced Northern Hemisphere midlatitudes. *Geophysical Research Letters*, *34*(13). Retrieved from http://doi.wiley.com/10.1029/2007GL029979

4.7 Appendix

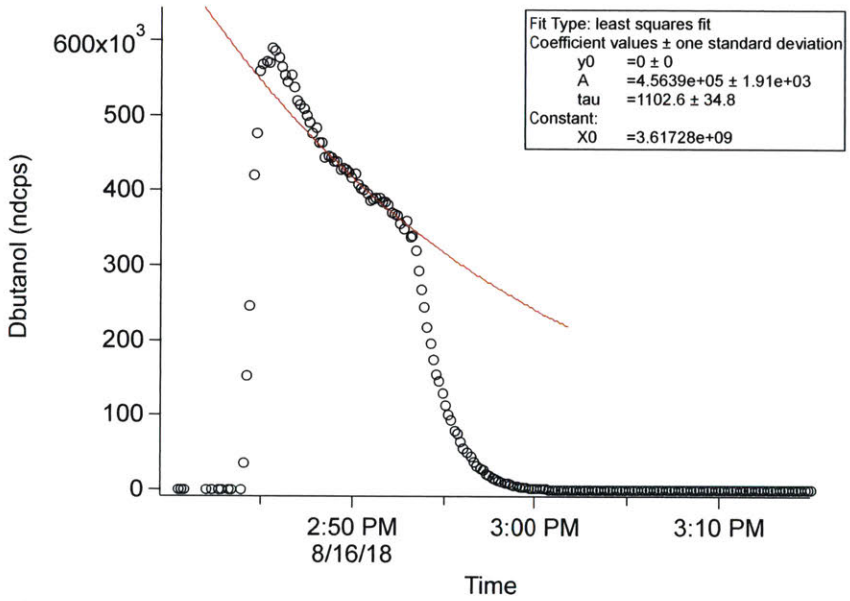

Figure A4-1. Dilution time constant fit using deuterated butanol signal before oxidation is initiated. Initial five minutes are not fit to allow tracer to equilibrate in the chamber. Calculated dilution time constant (18 minutes) agrees with flow rates and chamber volume.

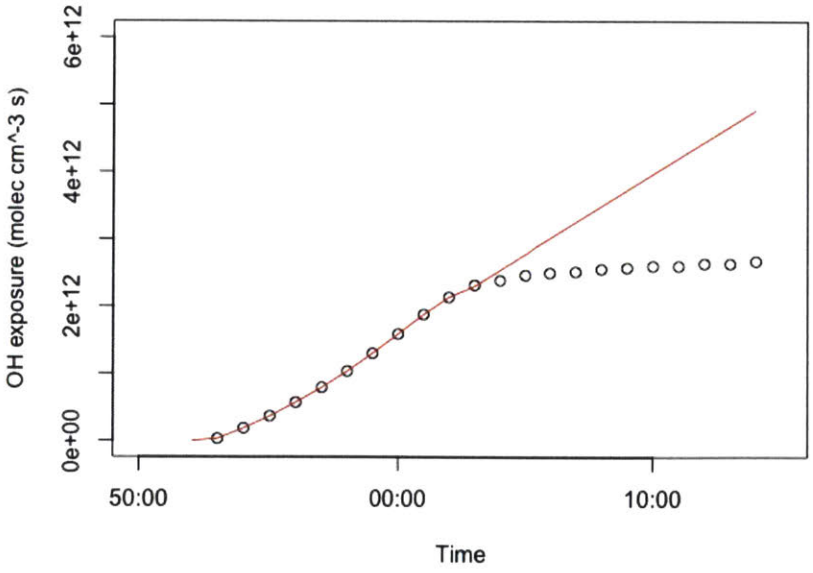

Figure A4-2. OH exposure calculated from deuterated butanol decay (black circles). Tracer is depleted in the middle of the experiment and OH exposure is extrapolated (red line) using an exponential fit to the data.

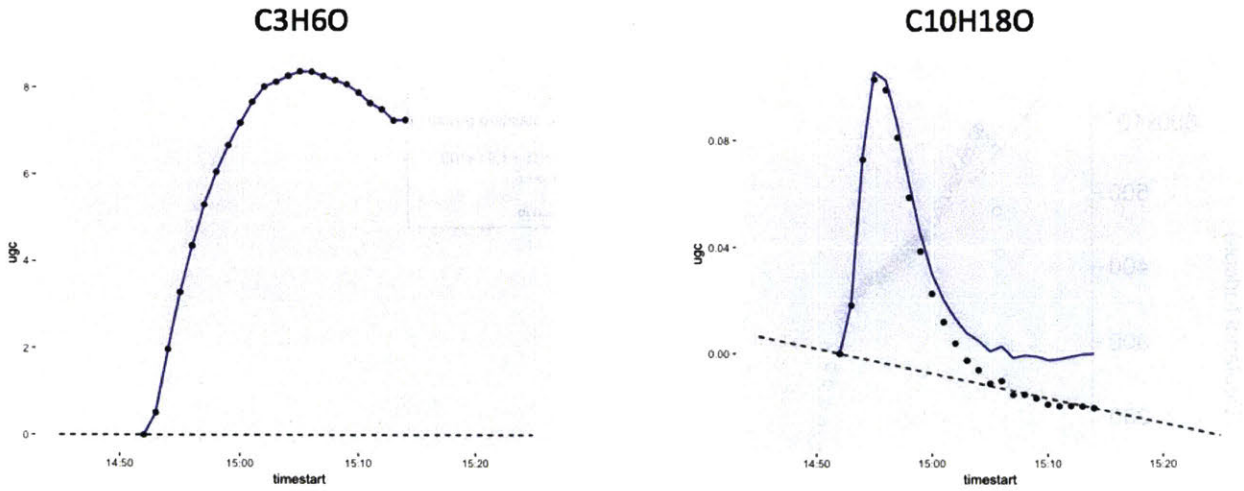

Figure A4-3. Measurements (black markers), background subtraction (dotted line), and corrected concentration (blue line).

Chapter 5

Conclusion

5.1 Summary of results

A more complete understanding of the chemistry that underlies the formation and evolution of organic aerosol mass and composition is important to assess the impacts of atmospheric particulate matter on human health and climate. From previous studies, it is clear that the composition of OA continues to change after its initial emission (POA) or formation (SOA). However, the processes that give rise to these changes over longer timescales are not constrained well by experimental data and thus are often not included, or only crudely included, in chemical transport models. The goal of this thesis is to better quantify the effects of two important aging processes, condensation and heterogeneous oxidation, on the evolution of OA loading and composition over multiple days.

In *Chapter 2*, the photochemical (OH) aging of biomass burning emissions from a variety of fuels was studied in a set of chamber experiments as part of the FIREX 2016 campaign. The results showed that all fuels also showed significant oxidation (increase in average carbon oxidation state) and condensation of SOA mass over the aging times investigated (0.25 – 4 days of equivalent atmospheric aging), but the amount of OA mass formed was highly variable. This variability in SOA formation could not be explained in terms of the OA enhancement ratio, but could be explained in terms of the absolute mass of OA formed. The differences in aging time and the total concentration of non-methane organic gases (NMOGs) measured before oxidation are able to account for the differences in SOA formation between experiments. After accounting for the loss of organic gases in the chamber due to dilution, the effective SOA carbon yield (fraction of gas-phase carbon converted to particle-phase carbon) is calculated to be 24% after 6 hours of aging and increases to 56% after 4 days. This relationship provides a simple parameterization for the inclusion of SOA formation from biomass burning in chemical transport models which is currently unconstrained.

The role of morphology on heterogeneous oxidation kinetics was explored in *Chapter 3* in a set of flow tube oxidation experiments. Squalane coated onto inorganic seed particles was used as a

proxy for phase-separated or mixing-limited organic particles and oxidized by OH. Over aging times equivalent to approximately just 3 days, rapid increases in the average carbon oxidation state (up to +1.3) and loss of carbon mass (40%) was observed for the coated particles. A linear relationship between the organic surface area to volume ratio (SA/V) of the particles and the measured second-order rate coefficient of OH with squalane was found. Consequently, the changes in composition observed were much greater for the oxidation of coated particles compared to pure squalane particles. When compared on the basis of oxidation lifetimes, the changes in composition between the pure and coated particles were essentially identical, suggesting that the more rapid changes in composition were solely due to the differences in organic SA/V and not due to any differences in chemical reaction mechanisms. When the results were applied to the heterogeneous oxidation of typical ambient OA particles, the composition of pure particles (200 nm) and thick coatings (greater than 50 nm) showed relatively slow changes with regards to tracer concentration, average carbon oxidation state, and fraction of carbon remaining. Conversely, the composition of thin organic coatings (1 – 20 nm) showed very rapid changes, indicating that morphology can play an important role in the rate of heterogeneous oxidation of ambient particles.

In *Chapter 4*, products of the heterogeneous oxidation of squalane were measured over long timescales equivalent to weeks of OH aging in an environmental chamber. Changes in the mass loading and composition observed, 77% carbon loss and O/C increase of 1.4 after 38 days of equivalent atmospheric aging. These changes were much greater than previous flow tube oxidation studies when compared on an oxidation lifetime basis. This discrepancy between flow tube and chamber heterogeneous oxidation studies cannot be currently explained, but is critically important to understanding heterogeneous oxidation kinetics in the atmosphere. Two newly developed proton transfer reaction mass spectrometers (PTR3 and CHARON PTR3) were used to identify and quantify products from heterogeneous oxidation in the chamber. Total gas phase carbon measured accounted for 57% of the carbon lost from the particle phase. First-generation formation of acetone (C_3H_6O) and undecanol ($C_{11}H_{24}O$) were observed in large quantities accounting for about half of the total gas phase carbon formed. C_{27} and C_{19} species were identified in the particle phase, supporting the evidence for the importance of fragmentation reactions in the heterogeneous oxidation of squalane. Potential reaction mechanisms for the formation of acetone and undecanol were described, both of which are initiated by the abstraction of a hydrogen from a tertiary carbon

and subsequent formation of an alkoxy radical. Evidence for secondary condensed phase chemistry (RO + RH) was observed, related to the formation of undecanol.

5.2 Current state of instrumentation and future needs

Much of the work presented in this thesis is the direct result of advancements in instrument development. Quantitative measurements of bulk OA from an aerosol mass spectrometer (AMS) have been available for over 10 years now; however, speciated measurements of organics from chemical ionization mass spectrometers (e.g., PTR-MS) have typically been used to identify products, while quantification has been lacking. New inlet designs that minimize loss of semivolatile and intermediate volatility compounds and new chemical ionization techniques now allow for the measurement of a wide array of organic compounds that are nearly comprehensive, able to measure the majority of organic carbon species present in the atmosphere in both the particle and gas phases. This is likely key to the correlation between non-methane organic gases (measured by PTR-ToF-MS) and SOA formation found in *Chapter 2*, a relationship which has not been observed in previous studies. However, challenges with the quantification of organic species remain, limiting the chemical insight provided by these measurements. For example in *Chapter 4*, acetone sensitivity is used to estimate the concentration of all gas-phase species measured by PTR3. While this is a reasonable estimate for the sensitivity of many species, sensitivities can vary significantly by a factor of 2 or more. The number of organic species present in the atmosphere and produced in laboratory oxidation experiments is large and precludes the direct calibration of all individual species detected. Furthermore, instrument sensitivities can change with environmental conditions (e.g., relative humidity) and have matrix effects depending on the instrument used. Robust methods to estimate sensitivities of species under a variety of conditions and without direct calibration will be crucially important to enable better measurements of total carbon in the atmosphere.

Although, bulk measurements of OA are considered quantitative, measurements of aged particles depend greatly on the collection efficiency (CE) of particles in the AMS. In *Chapter 2*, AMS CE is calculated for a subset of the data by first calculating the effective average density for OA by comparing size distributions measured by AMS particle time-of-flight (PToF) measurements and a scanning electrical mobility spectrometer (SEMS). The effective density is then used to calculate

total OA mass from SEMS total volume, then compared to AMS OA mass to calculate CE. To estimate the CE for all data, the relationship between CE and a measure of the volatility of the OA (mass fraction remaining after passing through a thermal denuder) is parameterized. The CE correction changes the SOA carbon yields calculated in *Chapter 2* by around a factor of 4, but this correction is often not included in other laboratory studies and thus represents a major uncertainty in studies where it is not included. In addition, although CE was corrected for in *Chapter 2,* the correction itself contains a significant amount of uncertainty, as there is uncertainty in the parameterization between CE and mass fraction remaining. Newly developed capture vaporizer technology for the AMS should eliminate the need for CE correction (CE = 1 for all particles using the capture vaporizer), although few published studies using this technology exist. A working capture vaporizer will be key to the robust quantification of OA mass in future studies and should be used to validate or reassess previous results from AMS measurements.

Development of new measurement techniques are also needed in the area of particle morphology. Currently used techniques to probe the shape and structure of aerosol particles depend on the collection of particles onto a substrate before they can be used for microscopy (e.g., tunneling electron microscopy). This collection step has the potential to alter the morphology of particles as they impact and reside on the collection substrate. In *Chapter 3*, knowledge of the particle generation technique was used to inform the structure of the particles (i.e., organic coated onto seed particles), but ultimately must be assumed without direct measurements of particle morphology. In-situ techniques for measuring particle morphology would be useful to determine in what regions of the atmosphere particle morphology plays an important role in oxidation kinetics as seen in *Chapter 3*.

The capabilities of particle and gas phase measurements in the atmosphere have progressed significantly and are now capable of measuring a major number of species of varying molecular weight, oxidation state, and structure. However, there is clearly room for continued instrument development, particularly improved quantification techniques in both the particle phase and gas phase. In-situ measurements of particle morphology are also sorely needed to determine the importance of morphological effects (e.g., enhanced oxidation rates and surface composition change) in the atmosphere. Improvements in these areas will allow for more accurate

characterization of atmospheric composition and also improved insights into the chemical mechanisms of atmospheric oxidation.

5.3 Implications and future directions

The results from this work have major implications for our understanding of how aging impacts OA mass and composition. In the biomass burning experiments, OA mass is observed to condense rapidly with the onset of oxidation for all experiments; however, OA continues to grow with continued oxidation. For example, after 1 day of aging 37% of the NMOG carbon has converted to OA. This increases to 45% after 2 days, then 51% after 3 days, and finally 56% after 4 days of aging. The SOA yields calculated show that multiday aging must be included in order to account for the total amount of SOA formed from biomass burning emissions. Future work in this area should include modeling studies that incorporate the SOA yields described here. However, before this can be done, accurate measurements of emission factors for various fuel types are needed to improve emission inventories for modeling purposes. Future aircraft campaigns with PTR-ToF-MS measurements should prioritize characterizing emissions, but also must be made alongside accurate measurements of BBOA age since BBOA composition is likely to change quickly after emission. In addition, pseudo-Lagrangian studies tracking smoke plumes downwind of fires, or at least making several plume transects, would be useful for verifying the SOA yields described in this thesis. The inclusion of these SOA yields in models likely requires the accurate representation of BBOA volatility distributions in models; measurements of the volatility of biomass burning POA should be prioritized in future biomass burning aircraft campaigns are laboratory studies. Finally, there is still work to characterize the total amount of carbon from biomass burning, but this is within reach with recent development of novel chemical ionization mass spectrometers.

The heterogeneous oxidation studies also have important implications for the evolution of OA composition and loading. The relationship between organic SA/V and the second-order rate coefficient of oxidation imply that for morphologically complex particles (i.e., non-spherical), heterogeneous oxidation can be faster than typically assumed. In addition, for highly viscous or glassy OA, the particle surfaces can be rapidly oxidized while the bulk of the particle remains relatively unreacted. This means that OA properties that depend on surface composition might evolve very rapidly for mixing-limited particles. In-situ measurements of particle morphology and

the surface composition of ambient particles will be important for determining the importance of surface effects on heterogeneous oxidation kinetics in the atmosphere. More specifically, accurate estimates of the fraction of particles that are glassy/highly-viscous and average organic coating thickness (or organic SA/V) are needed for different particle types (e.g., pure biogenic, SOA on mineral dust, anthropogenic POA, etc.) and under varying atmospheric conditions (e.g., boundary layer, free troposphere, high vs. low relative humidity). For the second set of heterogeneous squalane experiments, the rapid oxidation observed suggests that the experimental conditions used can play a major role in the observed oxidation rates. Also, the high yields of acetone and undecanol imply that OA might be an efficient source of OVOCs to the upper or remote atmosphere. Future heterogeneous oxidation experiments should focus on the quantification of gas phase products from a wider variety of OA proxies with different structures and oxidation states, as well as ambient OA and lab-generated SOA. Of particular concern is the discrepancy between flow tube and chamber heterogeneous oxidation studies seen in the work presented here. Future work should prioritize investigating the cause of these differences by running experiments under varied experimental conditions, for example, varied OA concentration, dilution rate, and oxidant concentration. Heterogeneous oxidation might play an even more important role in the evolution of particles if the chamber experiments in *Chapter 4* are a better representation of heterogeneous oxidation in the atmosphere than previous flow tube oxidation experiments.

The work presented in this thesis presents the general picture of OA aging over two distinct timescales – one shorter timescale (1 – 2 days) and the other long (beyond 2 days). As seen in the aging of biomass burning emissions, over the course of 1-2 days of aging there are large and rapid changes to the loading of OA due to the oxidation of reactive organic gases that lead to condensation of SOA. This condensation of SOA also drives rapid increases to the average carbon oxidation state of particles. After particles have left the near-field close to the source of emissions, most organic gases have reacted; however, oxidation of longer-lived gases can still contribute to changes in OA composition and loading. In addition to the oxidation of longer-lived gases, direct reaction of oxidants with particles can alter the composition and loading of OA through heterogeneous oxidation over a longer timescale until particles are deposited to the surface through wet or dry deposition. Other aging processes such as aqueous processing in cloud droplets and photolysis will also contribute to the evolution of OA in the atmosphere and should receive

continued attention in future studies. A key determinant to the importance of these longer-term aging processes is the lifetime of particles in the atmosphere before deposition. Ultimately, the work presented in this thesis show that aging processes over two different timescale regimes (short and long term) are important to the evolution of OA loading and composition and that this understanding can help inform chemical transport models and measurements.